AN INVESTIGATION OF AMBIENT DRYING OF EUCALYPTUS GRANDIS WOOD

A THESIS SUBMITTED TO THE GRADUATE DIVISION OF THE
UNIVERSITY OF HAWAI'I AT MĀNOA IN PARTIAL FULFILLMENT
OF THE REQUIREMENTS FOR THE DEGREE OF
MASTER OF SCIENCE

IN

MOLECULAR BIOSCIENCES AND BIOENGINEERING

MAY 2016

By

David H. Harris

Thesis Committee:

Scott Turn, Chairperson

Marcelo Kobayashi

Samir Khanal

Charles Kinoshita

Acknowledgments

This thesis was done in coordination with many individuals. I would like to personally thank all those involved. I would like to thank Terry Kai for his time and skill in fabricating the A-frame test stands that were used in this project. I also appreciate the time from Ryan Kurasaki for training me to use the machinery in the shop.

I would also like to thank Mary Kaheiki, Roy Ishizu, Marla Fergerstrom, and Angel Magno, and all others employed by the College of Tropical Agriculture and Human Resources to maintain the research stations at Lalamilo and Waiakea for their assistance in installing the test stands.

I would also like to thank Willie Rice from Forest Solutions Inc., for his efforts in locating and harvesting the trees used in this experiment. I would also like to thank him for providing valuable data from the Public Utilities Commission that were used in the scenario analysis.

I would also like to thank Dr. Scott Turn, my main mentor on this project. I greatly appreciate his patience, advice and guidance in this thesis.

Abstract

Eucalyptus has a high growth rate and material density which makes it an attractive biomass source for alternative fuel in Hawai'i. A challenge to implementing biomass-based energy systems is managing the moisture content using low cost methods. Ambient air drying may be an ideal option. This thesis reports results of natural-environment wood drying experiments and the development of both empirical and finite element models to describe moisture content over time as a function of solar insolation, ambient temperature, precipitation, and relative humidity.

Hawai'i has at least 10 climate zones, making it an ideal location to conduct drying experiments under varied environmental conditions. For this project, logs were placed in two locations on the island of Hawai'i; Lalamilo to represent dry climates, and Waiakea to represent wet climates. The change in mass as water evaporated from the logs was monitored on an hourly basis for a period of nine months and the results were compared with model prediction.

The drying curves and constant parameters derived from the empirical model were then used in a scenario analysis. The scenario analysis determined 1) the best time of year to harvest logs, 2) the length of time needed to dry logs at different locations, and 3) whether the extra cost to transport logs to a dry site was justified.

0 Table of Contents

0.1 List of Figures

0.2 List of Tables

0.3 Nomenclature

A-Cross sectional area [m^2]

B- Hydraulic Conductivity [m/s]

c/c_m-Concentration [mol/m^3]/[kg/m^3]

C_p-Heat capacity [J/kg K]

D- Effective diffusion coefficient [m^2/s]

E- Energy [kJ or btu]

G-Volumetric flow rate [m^3/s]

ΔH_{vap}-Latent Heat of Vaporization [$kJ/kmol_{H2O}$]

H- Head [m]

h- Convective heat transfer coefficient-[W/m^2K]*J**-diffusive flux [mol/m^2s]

K-rate constant [s^{-1}]

k- Thermal conductivity [W/mK]

I-Inertial Force [N]

l- Length [m]

m- Mass [kg]

M or MC-Moisture content

N-Matrix of directional cosines

P-Pressure [Pa]

Q-Energy transferred [kJ/h]

q- Total energy flux per unit area [kW/m^2]

r- Radius [m]

R- Universal Gas constant [8.314 J/molK]

S-Saturation

SG-Specific Gravity

T-Temperature[C, F or Kelvin]

u- Velocity vector [m/s]

U-Overall heat transfer coefficient-[W/m^2K]

V-Volume [m^3]

W- Molecular Weight [kg/kmol]

X-Concentration [kg/kg of solution]

y- Hydraulic head-[m]

z- Length in z direction [m]

Greek symbols

α-Directional permeability [m^2]

β- Magnus value of 17.62

γ- incident solar radiation [MJ/m^2]

δ- Determined gas Constant

ε-Sample porosity [m^3 of empty space/ m^3 of solid]

ϵ -Emissivity

κ- Directional Permeability [m^2]

λ - Magnus value

μ-Dynamic viscosity [$N*s/m^2$]

ξ- surface vapor transfer coefficient [s/m]

ρ Density [kg/m^3]

σ- Stefan-Boltzmann Constant [W/m^2K^4]

$\emptyset$-Angle

τ- Tortuosity

φ-relative humidity

ψ- Magnus Parameter [516 K]

1 Introduction:

1.1 Eucalyptus in Hawai'i

Hawai'i is an isolated island chain with limited energy sources. Much of Hawai'i is powered by oil and coal which are imported at high costs. To reduce energy costs, natural fuel sources that are grown in Hawai'i are being investigated. This study has particular interest in eucalyptus, a fast growing hardwood tree that has existed in Hawai'i for approximately 150 years (HARC, 2012).

Since the majority of sugar production ceased on Hawai'i Island, commercial hardwood operations utilizing *Eucalyptus spp.* have been planted on former sugarcane land. The Hawai'i Agricultural Research Center, HARC, reported that approximately 25,000 acres were scheduled for planting as of 2011 . Eucalyptus was being planted for the anticipated production of wood chips, paper pulp, and dimensional lumber.

Experiments have been conducted to test the viability of eucalyptus as an energy source. In 2010, Hawai'ian Commercial & Sugar Co. co-fired three trailer loads of eucalyptus woodchips with bagasse to assess impacts on boiler operations. In 2011, AES Hawai'i, Inc. the only dedicated coal-burning power plant in Hawai'i added eucalyptus chips to its coal supply at a rate of 10% of fuel mass in a test burn. The AES power plant electric output during the tests ranged from 180 to 185 MW (Britt, 2011).

There are several characteristics that make eucalyptus a potentially viable energy source, including its growth rate. Eucalyptus trees grow quickly and regenerate rapidly, producing a high yield of wood in a short amount of time. The Brazilian Eucalyptus Potential Productivity Study, BEPP, recorded an average of 40 m^3/ha/year of wood in Brazil, making it among the

fastest growing hardwood species in the world (Binkley, 2012). Other benefits of eucalyptus is that it burns freely, leaves very little ash after it burns, produces good charcoal and is drought and frost hardy (Britt, 2011).

The limiting factors for growing eucalypts have been considered. Stape et al. (2004) determined that abundant rainfall is essential for eucalyptus growth. In northeastern Brazil, a gradient study using clonal *E. grandis* by *E. urophylla* identified the main environmental factors controlling growth as water, light, and associated resource use, nitrogen. After characterizing fourteen stands with the Above Ground Net Primary Production (AGNPP), of 9 to 35 Mg/ha/yr, they determined that water was the limiting resource. The AGNPP increased 2.3 Mg/ha/yr for each additional 100 mm/yr of rainfall (Stape *et al.*, 2004). The reference did not cite the point at which additional rainfall would become detrimental to growth. High precipitation on the windward coasts of the Hawai'ian Islands makes them suitable for growing eucalyptus.

To determine the best locations for growing and harvesting eucalyptus, a 10 year study was conducted on Hawai'i Island by the USDA Forest Service's Pacific Southwest Research Station and the C. Brewer Co. Ltd. The study concluded that out of the 600,000 acres of commercial forest land on the island, approximately 230,000 acres were suitable for short term crop rotation. Suitable sites include ranch lands and abandoned sugar cane fields, from sea level to 914.4 meters, with rainfall of 1,016 to 6,350 mm annually, usually well distributed with a dry season of no longer than 3 months (Whitesell *et al.*, 1992).

Of the 500 known species of eucalyptus, 100 were introduced to Hawai'i for evaluation. In Hawai'i, *E. urophylla* has a particularly high biomass yield of 11.6 tons of dry matter per acre (Dudley & Osgood, 1996). A study conducted from 1990 to 1996 demonstrated the potential for

improvement of *E. urophylla* by introduction of provenances from native ranges (Dudley & Osgood, 1996). Several provenances *of E. urophylla* from Indonesia as well as hybrids of *E. grandis* by *E. urophylla* were introduced for the trial. The seeds were planted in Pepeekeo, Hawai'i. After four years, the tree diameters were measured and selected trees were felled and weighed. Weights of the trees ranged from 96 kg/tree to 170 kg/tree. The volumes of selected trees ranged from 2 to 8 times the average volume of the provenance. In conclusion, it is possible to improve eucalyptus yield through the selection of the best adapted provenance for a specific site (Dudley & Osgood, 1996).

Ten species trials were established between 1979 and 1984 to determine potential growth for fuel wood trees. The two species of eucalypts that performed the best were *E. grandis* and *E. saligna*, outperforming other species in diameter, height and survival rates (Whitesell *et al.*, 1992).

Past research has shown that eucalypts grow well in Hawai'i, and there are suitable lands available for them. The species *E. grandis, E. urophylla,* and *E. saligna* have better potential than most species. With land available, these species have potential to be one of the resources to displace fossil fuels in Hawai'i.

1.2 Industrial wood drying

1.2.1 Diffusion

Lumber drying is an important industrial process since wood has to be nearly completely dry before it can be used for construction or furniture. Drying enhances performance in systems using wood as fuel, since less energy is required to evaporate water before it burns. Dry wood also costs less to ship, is less likely to stain or decay, is more resistant to insect damage, has better hold for nails and screws, and accepts surface finishes better than wet wood (Reeb, 1997).

For use in construction and furniture, kilns are often used. They offer an environment with high enough temperatures to release bound or hygroscopic water from wood, and they are also controlled to prevent the wood from deforming. In the case of this study, the wood is to be used as fuel, so surface checks and deformation are not an issue. The main issue however, is energy input, and depending on the source of energy, a controlled kiln may not be economically viable.

Usually when wood is kiln or air dried, it is stacked. Stacked boards are usually uniform in length, since over hanging lumber in the stacks are subject to warping. Stickers, or small uniformly-sized boards, provide spaces for air to move across the lumber surfaces (Reeb, 1997). In air drying, a protective roof is often placed over the stack. This project will differ from the traditional methods, since un-sawn logs will be used.

Wood is considered a hygroscopic material, a material in which the equilibrium pressure of water vapor changes with moisture content and temperature. Examples of hygroscopic materials include some foods, soils, and wood (J. Zhang & Datta, 2004). Like most hygroscopic

materials, the moisture content in wood will change until it reaches equilibrium with the surrounding environment (Reeb, 1997).

Initially, water is present in wood in three forms, free water, water vapor, and hygroscopic water (bound water). The free water is present in the cell cavities or lumens of the wood. This water can be in the form of vapor or liquid. As wet wood dries, it is the free water and vapor that leaves first. The fiber saturation point (FSP) is the point where all free water has left and only hygroscopic water remains. Hygroscopic water is present within the cell walls and does not diffuse until the FSP is reached. When this point is reached the wood may start to shrink or crack (Reeb, 1997).

The drying of wood consists of two phases that can be illustrated with a graph as shown in Figure 1.1. The first phase of drying is when the free (unbound water) liquid water moves by capillary forces to the surface at the same rate that moisture evaporates from the surface. The second phase begins when capillary flow decreases, and the moisture content reaches the FSP (Jankowsky & dos Santos, 2004).

The hygroscopic water, or water below the FSP, does not diffuse readily. The diffusion of hygroscopic water is affected by specific gravity of the wood, the moisture content gradient, and by internal resistance to diffusion. Jankowsky and Santos found a characteristic drying curve that represents the drying phases for *Eucalyptus grandis* shown in Figure 1.1(Jankowsky & dos Santos, 2004).

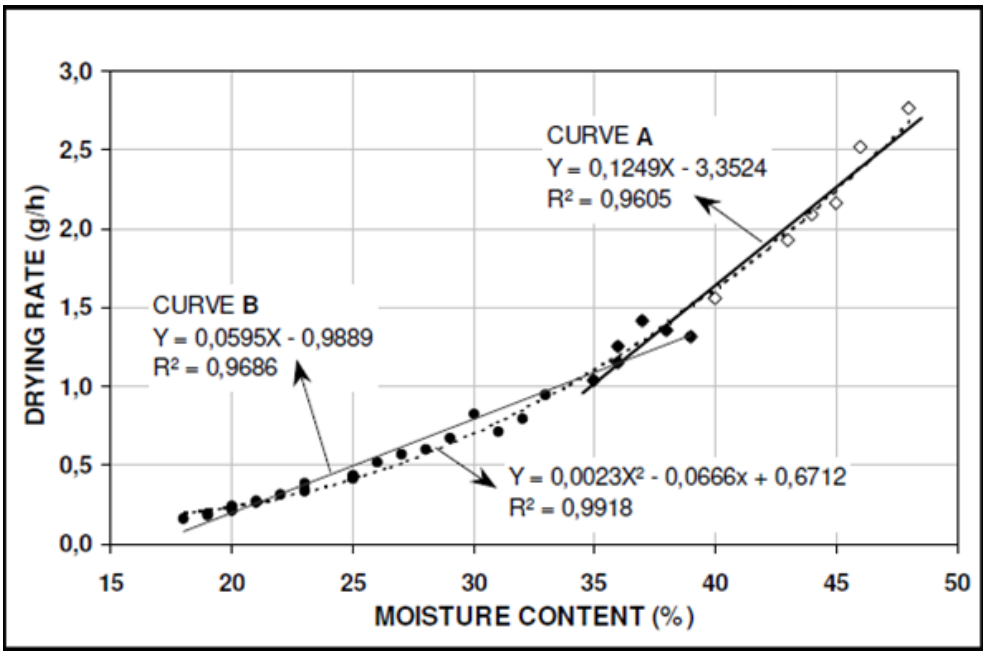

Figure 1.1 Drying curve showing the increase in drying rates with increased moisture content (Jankowsky & dos Santos, 2004)

Wood is different from other porous and hygroscopic materials in that it is an orthotropic material; heat conduction and diffusive properties are not consistent in all three dimensions. Hunter (1995) compared two experiments on capillary pressure by Spolek and Plumb (1981) and Vougt and Shaussm (1940). Spolek and Plumb centrifuged and weighed the wood (Spolek & Plumb, 1981). Voigt and Shaussm collected and measured the mass of wood after it was dried (Voigt *et al.*, 1940). Both studies produced similar results showing that capillary diffusion was the main driving force of water transport in wood (Hunter, 1995). Experimental results have shown that water can diffuse at a rate 15 times higher in the longitudinal direction, (along the

length of the log) than in the radial direction (from the center to the edge of the log) (Reeb, 1997).

1.2.2 - Calculating moisture content

The two primary methods for describing moisture content are the wet basis method and the dry basis method. Equations 1 and 2 describe the wet basis and dry basis method.

$$M_{wb} = \frac{m_{water}}{m_{water} + m_{dry\ matter}} \quad (1)$$

$$M_{db} = \frac{m_{water}}{m_{dry\ matter}} \quad (2)$$

Where m is mass and MC_{wb} and MC_{db} are wet basis moisture content and dry basis moisture content, respectively (Reeb, 1997).

Green wood, wood that has been freshly cut, can have a moisture content up to 250% on a dry basis which is 71% on a wet basis (Bousquet, 2000).

1.2.3 Benefits of dry wood

Wood with lower moisture content will produce heat more efficiently, since less energy is needed to evaporate water. In a study conducted by the Hawai'i Natural Energy Institute, heating values of different species of wood were determined. The heating value for bone dry *E. grandis* was 19.2 MJ/kg, meaning that complete oxidation of 1 kg of completely dry wood to CO_2 and H_2O will release 19.2 MJ of heat (Turn *et al.*, 2005).

Moisture content reduces efficiency. The latent heat of vaporization, the amount of energy required to evaporate 1 kg of water is 2.26 MJ at 25 °C and 1 atm. This amount of energy is subtracted from the initial heating value of the wood. The total heating value of 1 kg of wet wood can be found using equation 3.

$$NHV = HHV(1 - M_{wb}) - 2.26M_{wb} \quad (3)$$

Where *HHV* is the higher heating value of dry wood (MJ/kg), *NHV* is the net heating value or the heating value of the biomass with moisture present (MJ/kg), and M_{wb} is previously defined (Sokhansanj, 2011). In the case of *E. grandis*, the average initial moisture content is 51.1% (wet basis) so M_{wb} is 0.511 and the *HHV* is 19.2 MJ/kg. The net heating value with 51.1% wet basis moisture content is 8.23 MJ/kg. By drying the wood to 15% moisture content, wet basis, the *NHV* will be 15.16 MJ/kg which is an increase of 84% relative to the initial heating value.

1.2.4 - Air drying

A benefit of air drying is the reduced cost. To use a natural gas drying kiln to reduce the moisture content of *E. grandis* (specific gravity of 0.413), from 56% to 15% moisture content (wet basis), it is estimated it will cost $24 per m^3 with a natural gas price of $17.78 per GJ. With the more recent price of $5.21 per GJ, kiln drying could cost $7.01 per m^3. In industrial processes, drying 590,000 m^3 per year will have an annual cost of $4,154,417 (Reeb, 2011). Air drying is essentially free, and has the potential to save millions of dollars. Heat recovery and use for drying at a biomass energy conversion facility could also provide a lower cost energy source.

Hawai'i Island has ten climate zones making it an ideal location for ambient air drying experiments (Juvik *et al.*, 1978).

Experimentation of large scale air drying of eucalyptus has been done to determine the best location and time of year for drying. The Pacific Southwest Forest and Range Experimental Station conducted a study in Hilo, HI involving boards of *E. robusta* that were 25 mm thick with random widths from 152 to 406 mm. Each board was approximately 2.44 meters long. There were 13 piles in the study, arranged side by side in a single row. The piles were set at increasing spacing and consisted of stacked boards separated by stickers. All the piles were covered with metal corrugated roofs. The study showed that *E. robusta* lumber could be dried to below 20 percent moisture content in 2 ½ months during typical summer weather) (Skolmen, 1964). This shows that large scale air drying is possible even in humid conditions.

1.3 Modeling water movement in wood

A model of logs drying in the surrounding environment could be useful to determine the cost effectiveness of wood drying for large scale fuel usage. Since weather conditions will be different for different locations and seasons, the model could be used to predict the best location and time of the year to harvest the logs and start the drying process. It can also be used to determine if it is cost effective to transport logs to drier areas to enhance drying or if it is better to dry them on site.

When modeling moisture movement in wood, it is important to consider the properties of different kinds of wood. Diffusion and heat conduction coefficients vary between species, between different samples of the same species, and different parts within the same tree (Siau, 1995). Water in heartwood will diffuse at a slower rate than the softer wood near the exterior. Diffusion rates also differ in regions where there are branches or knots (Kamke, 2014).

Models found in the literature use different approaches and assumptions. Models may vary depending on the geometry of the sample, the surrounding environment, and the number of boards or logs, their orientation to one another, and the air flow between logs or boards in a stack.

In ambient conditions, moisture transport in wood is governed by transient energy and mass conservation equations with boundary conditions being: temperature, relative humidity, solar insolation and wind speed. Through the boundary conditions, the drying process can include diurnal and seasonal cycles.

2 Objectives

The goals of this research are outlined as follows:

1. Create models to estimate the moisture content of *Eucalyptus grandis* logs as a function of time under ambient conditions.

   The two types of models are:

   -A phenomenological model constructed in COMSOL Multiphysics™

   -An empirical model constructed in Microsoft Excel™

2. Design and conduct outdoor experiments to measure changes in moisture content to validate models

3. Use the models to conduct scenario analysis to evaluate enhanced ambient wood drying practices.

3 - Literature review

Drying wood is considered one of the oldest problems in chemical and agricultural engineering, so literature on wood drying and modeling is abundant. Predictions have been made and verified using two and three dimensional models with varying accuracy. In order to better improve model prediction across a variety of tree species, experiments have been performed to determine relevant wood material properties.

This literature review is presented in five sections. Section 3.1 discusses the relevant equations necessary for the model. Section 3.2 summarizes data sources and material properties that are relevant to the model. Section 3.3 reviews past models and validation. This section is divided into two sub-sections. Section A will review phenomenological models and section B will review empirical models. Section 3.4 reviews a paper that conducted a scenario analysis study concerning transportation costs. Section 3.5 summarizes methods that are consistently used in most models and have proven to be accurate.

3.1 - Equations

Relevant modeling studies in the literature utilize different equations and solution techniques, but the common elements in most are Darcy's Law, Fick's Law of Diffusion and the energy and mass balance equations.

The movement of fluid via capillary action is calculated most commonly using Darcy's Law as shown in equation 4.

$$u = -\left(\frac{\kappa}{\mu}\right)\nabla(P) \quad (4)$$

In the case of a liquid, capillary pressure, P_C, is applied to Darcy's Law equation. The difference of gas and capillary pressure is the liquid pressure. An expression for capillary pressure, P_C, is presented in equation 5.

$$P_C = 56.75 * 10^3(1 - S_L)e^{\frac{1.062}{S_L}} \quad (5)$$

Where S_L is the degree of saturation of liquid water (Sandoval-Torres *et al.*, 2012).

S_L is found with equation 6.

$$S_L = \frac{C_{m,L}}{(\varepsilon * \rho_{H2O})} \quad (6)$$

Where $c_{m,L}$ is liquid mass concentration (Datta, 2014).

The difference between P_G and P_C is liquid pressure or P_L. P_L can be calculated using equation 7.

$$P_L = P_G - P_C \quad (7)$$

The modified version of Darcy's Law for liquid pressure is found in most water diffusion models, equation 8 is Darcy's Law equation for liquid according to the Pinheiro model.

$$u_L = -\left(\frac{\kappa_L}{\mu_L}\right)\nabla(P_L) \quad (8)$$

Both Darcy's Law for gas and for liquid are also incorporated in most models. In this case κ_L is the directional permeability of the liquid (Pinheiro *et al.*, 1998).

The velocity vector of gas is found in equation 9.

$$u_G = -\left(\frac{\kappa_L}{\mu_L}\right)\nabla(P_G) \tag{9}$$

Diffusion is also an important mechanism of mass transfer in porous media. In the case of porous media, fluid will not move linearly since will follow the path of empty pores and void spaces. Instead it will take a tortuous path of an unknown length that is greater than the length of the porous domain. The ratio between the actual length and the tortuous length is reffered to as tortuosity, τ (Geankoplis, 1993). See equation 10.

$$D_{A,eff} = \frac{\varepsilon}{\tau} D_{AB} \tag{10}$$

Where $D_{A,eff}$is the effective diffusivity of the liquid, and D_{AB} is the diffusivity of substance *A* in *B* (m^2/s), most commonly the diffusivity of water vapor in air (Geankoplis, 1993).

In open air, drying simulations, rain fall may have to be taken into consideration. The flux of liquid water moving through the surface of the log depends on the concentration of rain and the momentum of rain, and pressure head for cases in which stagnant water is involved. To model rain fall infiltration in a porous media, particularly soils, Richard's Equation is used. Richard's equation describes the change in diffusivity and permeability with respect to change in moisture content. See equation 11.

$$\frac{\partial M}{\partial t} = \frac{\partial}{\partial z}[D(M)]\frac{\partial M}{\partial z} - \frac{\partial \kappa(M)}{\partial M}\frac{\partial M}{\partial z} \tag{11}$$

Where *M* is moisture content, *D(M)* is diffusivity with respect to *M*, *κ(M)* is permeability with respect to *M*, and *z* is depth in material (Salvucci, 1996).

A model was developed by, Van den Brande, Blocken, and Roels (2013) to depict the infiltration of wind driven rain on wooden facades. In this model, wind driven rain (*wdr*) was treated as a mass source term *q*, in kg/m^{2}s. See equation 12.

$$q_{ext} = q_{wdr} + \xi\left(p_{vap,atm} - p_{vap,surf}\right) \quad (12)$$

Where q_{ext}, is the mass of moisture from the environment, and q_{wdr} is the mass source from rain and ξ is the surface vapor transfer coefficient (s/m), $p_{vap,atm}$ is atmospheric vapor pressure and $p_{vap,surf}$ is vapor pressure at the surface (Van den Brande *et al.*, 2013).

The model that best accounts for the height of rain per unit of time was found in the model published by Chui, and Freyburg in 2007. This model calculated the flux with respect to permeability, pressure and the amount of rain in mm per second. See equation 13.

$$n\frac{\kappa_s}{\mu}\kappa_r\nabla\left(p + \rho_f g z\right) = \dot{y} + R_{ext}(H_{ext} - H_{tot}) \quad (13)$$

Where n is normal to the surface, κ_s and κ_r are intrinsic (m^2) and relative permeabilities respectively, *z* is the height of rain (m), *y* is non head dependent flux (m/s), μ is viscosity (Pa*s), and H_{ext} is external total head (m), and H_{tot} is total head (m) (Chui & Freyburg, 2007).

According to a study published by Tschernitz in 2001 the most useful formula for predicting energy transfer rates in wood is Fourier's law of heat conduction. See equation 14.

$$Q = \frac{kA\Delta T}{l} \quad (14)$$

Where Q is the rate of energy transferred (kJ/s), ΔT is the temperature difference (K), A is surface area (m^2), l is thickness (m), and k is thermal conductivity (kW/m K) (Tschernitz, 2001).

To account for energy transfer from a gaseous or liquid medium to a solid surface, convective heat transfer, equation 15, is used. See equation 15.

$$Q = UA(T_s - T_a) \quad (15)$$

U is the overall heat transfer coefficient (kW/m^2 K), T_s is the temperature of the surface of the solid object in (K), and T_a is the temperature (K) of the surrounding environment (Tschernitz, 2001).

Since much of the energy in this study's drying system will come from the sun, it is important to consider radiative heat transfer. See equation 16.

$$q = \in \sigma\left({T_s}^4 - {T_a}^4\right) \quad (16)$$

Where q is heat flux (kW/m^2), ϵ is dimensionless emissivity, and σ is the Stefan-Boltzmann Constant, 5.677x10^{-8} (kW/(m^2K^4)) (Geankoplis, 1993).

Latent heat determined by the volume of wood, specific gravity of bone dry wood, and expected change in moisture content as shown in equation 17 (Tschernitz, 2001).

$$E_a = V(SG)\left(\rho_{H_2O}\right)\Delta H_{vap}\left(M_i - M_f\right) \quad (17)$$

Where E_a is the sensible enthalpy (kJ) required to evaporate water from the wood substance, ρ_{H2O} is the density of water (kg/m^3), V is volume of the wood (m^3), ΔH_{vap} is latent heat

of vaporization for liquid water (kJ/kg), *SG* is specific gravity of oven dry green wood, and M_i and M_f are initial and final moisture contents (wet basis), respectively (Tschernitz, 2001).

Temperature and pressure play an important role in the diffusion of moisture through wood. The Clausius-Clapeyron equation determines the vapor pressure of a liquid as a function of temperature (Chieh, 2008). See equation 18.

$$P = \delta \exp\left(\frac{-\Delta H_{vap}}{R\,T}\right) \tag{18}$$

Where *P* is pressure (kPa), δ is a determined gas constant, *R* is the universal gas constant (8.314 kJ/kmol K), ΔH_{vap} is the latent heat of vaporization (kJ/kmol) and *T* is temperature (K) (Chieh, 1999). If P_1 and P_2 are different pressures at different temperatures the equation has the form of equation 19.

$$ln\frac{P_1}{P_2} = \left(\frac{-\Delta H_{vap}}{R}\right)\left(\frac{1}{T_2} - \frac{1}{T_1}\right) \tag{19}$$

These formulas can be used to determine the fraction of the water in a gas phase or liquid phase.

Baronas et al. (2001) classified water movement in wood into inter gas diffusion and bound water diffusion. The former is water diffusion in the pore gas volume of the wood. The latter is the diffusion of water within the cell walls. The transverse diffusion coefficient *D*, is dependent on both forms of diffusion and porosity as shown in equation 20 (Baronas et al., 2001) (Baronas *et al.*, 2001).

$$D = \frac{\sqrt{\varepsilon_a} D_{bt} D_{vap}}{(1-\varepsilon_a)(\sqrt{v\varepsilon_a} D_{bt} + (1-\sqrt{\varepsilon_a}) D_{vap}} \quad (20)$$

D_{bt} is the bound water diffusion coefficient, ε_a is porosity, and D_{vap} is the vapor diffusion coefficient of the lumens. D_{vap} is defined in equation 21 (Baronas *et al.*, 2001).

$$D_{vap} = \frac{W D_a p_s}{SG \rho_w RT} \cdot \frac{d\varphi}{du} \quad (21)$$

W is the molecular weight of water (kg/kmol), D_a, is the diffusion coefficient of vapor in air, SG is the specific gravity, ρ is the density, R is the gas constant, T is temperature (K) and $d\varphi/du$ is the change in relative humidity with respect to the change in moisture concentration of the wood. In their experiment, the diffusivity, D, was applied to Fick's law of diffusion.

D_{bt} is found using an Arrhenius equation, equation 22.

$$D_{bt} = 7 * 10^{-6} * \exp\left(-\frac{E_b}{RT}\right) \quad (22)$$

Where E_b is the activation energy (kJ/mol) and can be found in equation 23.

$$E_b = \left(40.195 - 71.179 M_{db} + 291 {M_{db}}^2 - 669.93 {M_{db}}^3\right) * 10^6 \quad (23)$$

Where M_{db} dry basis moisture content (Baronas *et al.*, 2001).

When temperature and concentration of vapor and liquid have been calculated, it is possible to determine the mass rate of evaporation, or the rate at which liquid is converted to vapor and vice versa. The mass rate can be found in equation 24.

$$\dot{m} = \mathrm{K} * \left(\mathrm{c}_{\mathrm{Vap,Sat}} - \mathrm{c}_{\mathrm{Vap}}\right) \quad (24)$$

Where $c_{Vap,Sat}$ and c_{Vap} are the vapor saturation concentration and vapor concentration respectively in mol/m^3, and K is the drying rate (1/s) (Datta, 2014).

3.2 Properties of Eucalyptus Wood

In order to create an accurate model, the physical properties of eucalyptus must be considered. A study in 2010 measured the permeability of *E. grandis* and *E. citriodora* samples in a custom built gas analysis chamber. Liquid permeability was measured using a Neen^{TM} oil preservative and gas phase permeability was found using air (Da Silva et al., 2010) (da Silva *et al.*, 2010). They concluded that longitudinal permeability of gas was about twice as much as that of liquid and no radial permeability was found for either wood. In they found that the *E. grandis* permeability of air in heartwood was 28 times less than in sapwood and almost zero permeability in heartwood for *E. citriodora*. The measurements for liquid permeability in heartwood were insignificant in both species. Their results are summarized in Table 3.1.

Table 3.1-Longitudinal permeability measurements of Brazilian eucalyptus (da Silva *et al.*, 2010)

		Permeability cm^3/(cm*atm*s)		
	species	Air	Water	Preservative
Sapwood	*E. grandis*	681	470	349
	E. citriodora	612	365	347
Heartwood	*E. grandis*	25	0.42	0.12
	E. citriodora	0	0	0

Another study was done to determine mass transport properties of different hardwood species in Australia. Redman et al. (2012) characterized the mass transport properties in the radial, tangential, and longitudinal directions for spotted gum (*Corymbia maculata*), blackbutt (*Eucalyptus pilularis*), jarrah (*Eucalyptus marginata*), and messmate (*Eucalyptus obliqua)* wood. For each species, one quarter-sawn board (annual growth rings nearly at right angles to the wide face) and one backsawn board (growth rings parallel to the wide face) with dimensions of 300 x 100 x 8 mm were prepared. Three 74 mm diameter samples were cut from each board using an 80 mm diameter hole saw, producing three radial and three tangential samples for each species (Redman et al, 2012). Also for each species, one 200 x 100 x 28 mm thick sample was prepared. From those boards, three 19 mm diameter, 20 mm long cylinders were cut in the longitudinal symmetry plane to test for longitudinal permeability (Redman *et al.*, 2012). The orientation of the boards and samples are illustrated in Table 3.1.

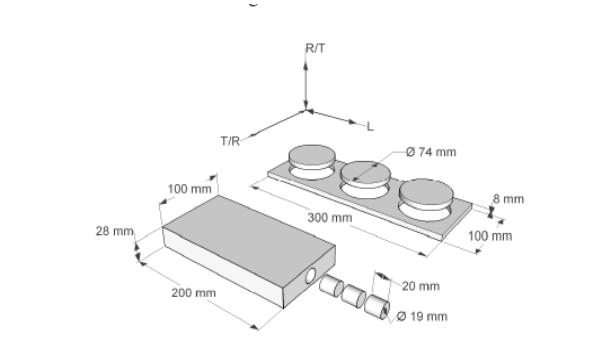

Figure 3.1-Geometry of wood samples of wood used in experiments to determine properties of Australian wood species (Redman *et al.*, 2012)

Custom made gas flux chambers and a custom designed liquid diffusion apparatus were used for this experiment. The results are in Table 3.2 Table 3.3.

Table 3.2-Water permeability for four different woods (L- lengthwised, R-radial, T-Tangential) (Redman *et al.*, 2012)

	Permeability, α (m^2)		
Species	L*10^{-15}	R*10^{-15}	T*10^{-15}
Corymba maculata	0.4	-	0.006
Eucalyptus pilularis	35	0.01	0.02
Eucalyptus marginata	67.4	0.05	0.04
Eucalyptus obliqua	55.5	8.6	0.3

Table 3.3-Water diffusivity for four different woods (L – lengthwise, R – radial, T – tangential) (Redman *et al.*, 2012)

	D (m^2/s)		
	L*10^{-10}	R*10^{-10}	T*10^{-10}
Corymba maculata	0.6	0.1	0.1
Eucalyptus pilularis	2.3	0.3	0.2
Eucalyptus marginata	2.7	0.3	0.4
Eucalyptus obliqua	10.3	0.7	0.4

They concluded that the four species of Australian hardwoods studied were highly impermeable to water in the radial and tangential directions especially in heartwood. For this reason, many models only account for capillary action in the longitudinal direction.

The presence of growth rings in the radial direction presents a challenge in modeling not present in other porous media. A growth ring represents a discontinuity in material properties, resulting in steeper gradients that need smaller elements to prevent instability in the solution (Perré & Turner, 2002)

3.3 Modeling

3.3.1 Phenomenological Models

The finite element method is a numerical method used for finding approximate solutions for a system of differential equations within a closed region. A solution region comprises a mesh (many small, interconnected elements), and gives a piece-wise approximation to the governing equations (Lewis *et al.*, 2004).The mesh can be adaptive to resolve transient regions of steep gradients in material properties and/or solution variables.

In boards, capillary action in the longitudinal direction and diffusion in the tangential direction is considered. Not all papers agree on the best approach to model fluid flow in the tangential direction but Fick's law is often used (Krabbenhøft, 2003). No significant amount of moisture permeates radially in hardwoods so radial diffusion is often ignored. In cylinders or logs, capillary action in the longitudinal direction is often the only mode of transport considered.

An accurate prediction of moisture movement through hygroscopic materials requires a conservation based model in which heat and moisture transport are coupled. This is especially necessary since temperature determines moisture phase change (J. Zhang & Datta, 2004). The governing equations for liquid and vapor phases must also be solved simultaneously.

Water will transport out of each element in both vapor and liquid form. As the partial pressure of water decreases and temperature increases, more liquid will be converted to vapor (J. Zhang & Datta, 2004). A diagram depicting mass movement between elements of wood is shown in Figure 3.3.

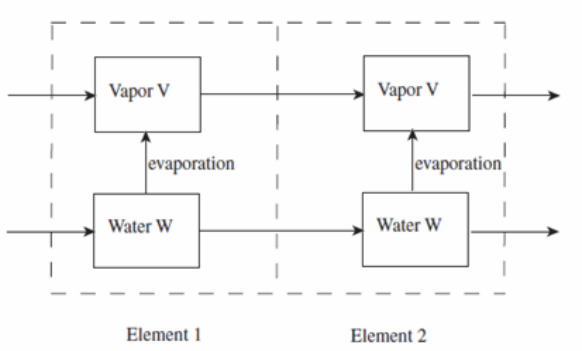

Figure 3.2- Illustration of system with both vapor and liquid water transport (J. Zhang & Datta, 2004)

In Zhang and Datta's study, two different approaches were compared. The first approach, model 1, included the evaporation rate throughout the entire material, whereas model 2 assumes that evaporation only takes place at the surface (J. Zhang & Datta, 2004). Equation 25 was used in the model.

$$\frac{\partial \rho_W}{\partial t} + \frac{\partial \rho_V}{\partial t} = \frac{\partial}{\partial x}\left(D_w \frac{\partial \rho_W}{\partial x}\right) + \frac{\partial}{\partial x}\left(D_v \frac{\partial \rho_V}{\partial x}\right) \quad (25)$$

Where x is position (m), t is time (s), ρ_w is the density of liquid water (kg/m^3), ρ_v is density of vapor (kg/m^3), and D_w and D_v are the diffusivity coefficients of liquid water and vapor respectively (m^2/s).

Total moisture content on a dry basis is found using equation 26.

$$MC = \frac{(\rho_W + \rho_V)}{\rho_s} \quad (26)$$

Where MC is total moisture content (dry basis) and ρ_s is density of the solid or the stationary phase (kg/m^3).

Since liquid diffusivity and vapor diffusivity are different, combining them into one parameter will define a new diffusivity (J. Zhang & Datta, 2004). Equation 17 can be converted to equation 27.

$$\frac{\partial M}{\partial t} = \frac{\partial}{\partial x}\left(D_M \frac{\partial M}{\partial x}\right) \tag{27}$$

Where D_M represents the combined diffusivities of vapor and liquid water (m^2/s).

This method of modeling can be inaccurate in many cases. In the case of high moisture content, as seen in green wood, the pores of hygroscopic materials are unable to hold large amounts of gas. Therefore, vapor transport is negligible within the material and the majority of vaporization takes place at the surface (J. Zhang & Datta, 2004). In this case, accounting for vapor inside the wood can have erroneous results. Model 2 neglects the vapor transport inside the wood and equation 28 is used.

$$\frac{\partial \rho_W}{\partial t} = \frac{\partial}{\partial x}\left(D_W \frac{\partial \rho_W}{\partial x}\right) \tag{28}$$

And total moisture content is found by using equation 29.

$$\rho_s M \approx \rho_W \tag{29}$$

Zhang and Datta concluded that the best model for boards assumes that evaporation only takes place at the surface and the diffusivity of liquid water is the only mode of transport within the material. Even so, many models do include phase change and vapor transport within the wood. This section reviews examples of both kinds of models, see Table 3.4.

In a thesis research project conducted by Adin Berberović, past models were organized into two main groups; single board models and stacked board models. Both single and stacked

models may be applicable to logs as well. Each group was then subdivided into categories. Single-board drying models can be based solely on a drying rate function that describes the movement of the total average moisture content of a board, or based on the movements of each phase of moisture through the board or log (Berberović, 2007).

Common assumptions for water transport in wood are:

- Radial and tangential diffusion are insignificant in cylinders
- The water is in liquid form when it is in the wood, and doesn't evaporate until it reaches the surface
- Wood can be considered isotropic for energy transport but orthotropic for mass transport

The list above shows common assumptions, but not every study agrees on their applicability.

For this literature review, models are classified based on the geometry, the species of wood, the method of drying, if a stack or an individual sample is considered, if ambient air conditions are considered, and whether or not each phase of moisture is considered. Many papers included other porous media besides wood. Since the process for drying other porous media is very similar to that of wood, models with other porous media are included Table 3.4.

Table 3.4 -Summary of past models

Reference	Species Modeled	Other Porous Media	Geometry	Orientation*	Climate Considered	Drying Method	Modeled All Phases of Moisture	Validated
(Alvear *et al.*, 2003)	*Nothofagus dombeyi*		slab	S	no	kiln	yes	
(Awadalla *et al.*, 2004)	spruce		slabs	S		solar kiln		yes
(Baronas *et al.*, 1999)	any		?	?				
(Baronas *et al.*, 2001)	pine		slabs	I	yes	air dried	yes	yes
(Bedane *et al.*, 2011)	*Betula papyrifera*		chips	C & S	yes	kiln and air		yes
(Bekkioui *et al.*, 2011)	*Pinus pinaster*		slabs	S	no	solar kiln	yes	yes
(Berberović, 2007; Bixler, 1985a)	any	x	slabs	I & S		kiln	yes	yes
(Bixler, 1985b)	NA	x	any	NA	no	any method	yes	no
(Bramhall, 1979)	any		any	I	no	kiln	yes	no
(Elustondo & Avramidis, 2005)	any		slab	S	no	kiln		
(Kanevce *et al.*, 2005)	?	x	slab	I	no		yes	
(Khattabi & Steinhagen, 1993)	any		any		no		yes	no
(Krabbenhøft, 2003)	any		any	I & S	yes	kiln and air	yes	yes
(Lamb & Wengert, 1991)	Southern pine		slabs	S	no	kiln	yes	
(Murphy *et al.*, 2012)	*Picea sitchensis*		cylinder	S	yes	air dried	no	yes

Reference	Species Modeled	Other Porous Media	Geometry	Orientation*	Climate Considered	Drying Method	Modeled All Phases of Moisture	Validated
(Noorolahi *et al.*, 2008)	Afra, Roosi, Malach		cube	I	no	air dried	no	yes
(Pang, 1996)	any softwood		slabs	I & S	no	kiln		yes
(Pang, 2007)	*Pinus radiata*		slabs	I	no	kiln	yes	yes
(Perré & Turner, 2002)	any		cylinder	I	no		yes	yes
(Pinheiro *et al.*, 1998)	Eucalyptus		cylinder	I	no	thermo-balance	yes	yes
(Simpson & Hart, 2000)	any		slabs	S	yes	air dried	no	yes
(Time, 1998)	spruce and pine		cylinder	?	yes	kiln and air	yes	yes
(Truscott, 2004)	any softwood		slab	I & S	no	kiln	yes	
(Turner, 1996)	any		slab	I & S	no	kiln		
(Wullschleger *et al.*, 2011)	any		any	I & S	no	kiln and air		yes
(J. Zhang & Datta, 2004)	any	x	any	NA	no	kiln and air	yes	yes
(D. Y. Zhang *et al.*, 2010)	*Quercus mongolica*		any	I & S	no	housed environment	yes	yes

*S= stack, I=individual log or board, ,

Berberović's model simulated the mass and heat transfer process between the surface of the wood and air during the drying of a stack of lumber. General laws of mass and energy conservation were applied. Inputs included the initial conditions of the wood, such as moisture content, temperature, specific gravity, and air properties (Berberović, 2007). The model outputs were surface temperature distribution of the individual boards, temperature of ambient air, absolute humidity surrounding the boards and final moisture content of the wood.

The model was verified by measuring mass after drying and measuring the temperature with thermocouples. It was concluded that this model is good for predicting temperature and moisture content of boards without time consuming experimentation, and it can reveal the best drying schedule for wood collected in different times of the year in Oregon and Washington.

The models previously mentioned primarily dealt with rectangular boards. But it is important to note the models with different geometries. Other geometries included piles of wood chips, or cylindrical logs.

In 1998, a model in cylindrical coordinates was developed for drying *Eucalyptus spp.* in Brazil. This model was based on fundamental heat and mass transfer equations and it was numerically solved using a segregated finite volume method (Pinheiro *et al.*, 1998). Like the Beberovic model, the logs were discretized into smaller portions. An example of a slice of the cylinder and the mesh used in the Pinheiro model is shown in Figure 3.3.

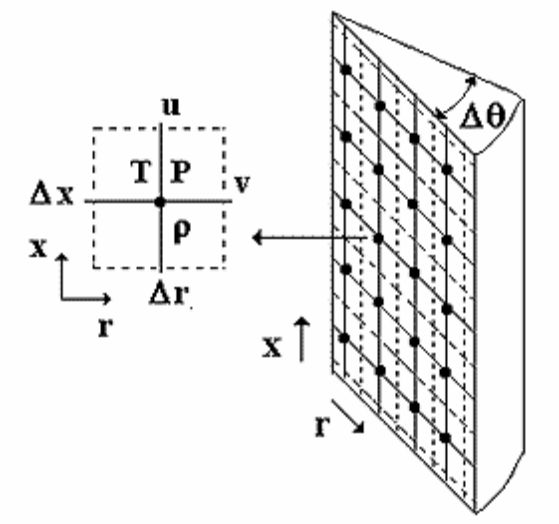

Figure 3.3-Discretized portion of a cylinder with labeled nodes (Pinheiro *et al.*, 1998)

The model proposed in this paper was based on equations describing simultaneous heat and mass transfer in porous media. The equations used were water vapor and air mass balance equations, as well as Darcy's law to describe the movement of the mixture of liquid, vapor and air (Pinheiro *et al.*, 1998). Physical properties of *E. grandis* used in the Pinheiro model are found in Table 3.5

Table 3.5-Physical properties used for Pinheiro's model and their sources (Pinheiro *et al.*, 1998)

Symbol	Parameter	Value	Reference
κ_{g0}	Gas permeability-x direction (single phase)	$1.0*10^{-10}$ m^2	(Alves & Figueiredo, 1989)
	Gas permeability-r direction (single phase)	$1.0*10^{-13}$ m^2	
μ_g	Dynamic viscosity	$2.81*10^{-4}$ $N*s/m^2$	(Gieck & Gieck, 1990)
k_S	Thermal Conductivity of solid	$1.59*10^{-4}$ kW/m K	(Gieck & Gieck, 1990)
δ_V	Vapor equivalent constant	0.462 kJ/kg K	(Gieck & Gieck, 1990)
δ_A	Air equivalent	0.287 kJ/kg K	(Gieck & Gieck, 1990)
ε	Porosity	0.64 m^3air/m^3solid	(Gieck & Gieck, 1990)
ϵ	Emissivity	0.95	(Gieck & Gieck, 1990)
σ	Stephan-Boltzmann Constant	$5.677x10^{-8}$ W/m^2 K^4	(Gieck & Gieck, 1990)

To verify Pinheiro et al.'s model results, recently cut, cylindrical green wood samples of *Eucalyptus spp.* were subjected to isothermal thermogravimetry tests (Pinheiro *et al.*, 1998). The samples were divided into three groups. Groups one and three were cut and group two was carefully debarked. The temperature of the third group was measured by a thermocouple inside

the wood. All groups were dried in a thermobalance. Graphs showing the experimental kiln data versus theoretical data are presented in Figures 3.4 to 3.7:

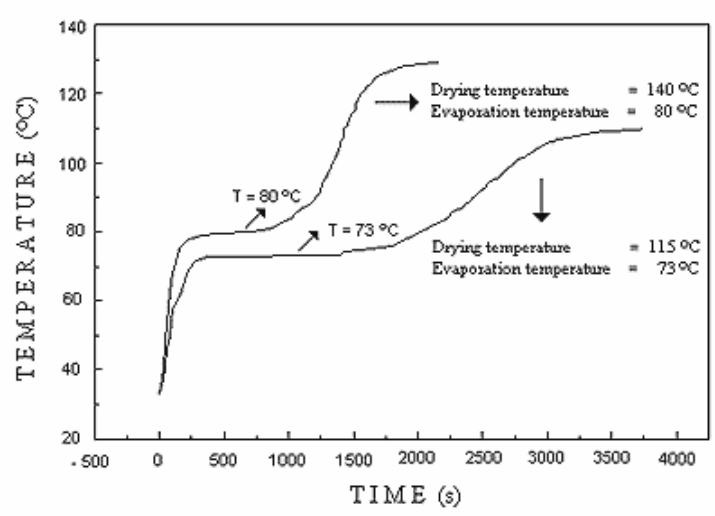

Figure 3.4- Experimental temperature of evaporation for the 3rd sample group (debarked with thermal couple inside) (Pinheiro *et al.*, 1998)

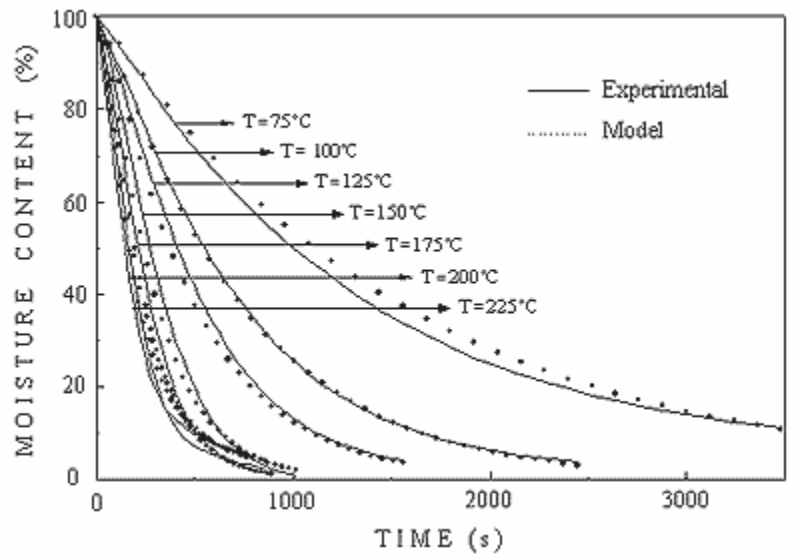

Figure 3.5- Kinetic curve showing the loss of moisture content with respect to time and temperature for group 1 (logs that have been debarked) (Pinheiro *et al.*, 1998)

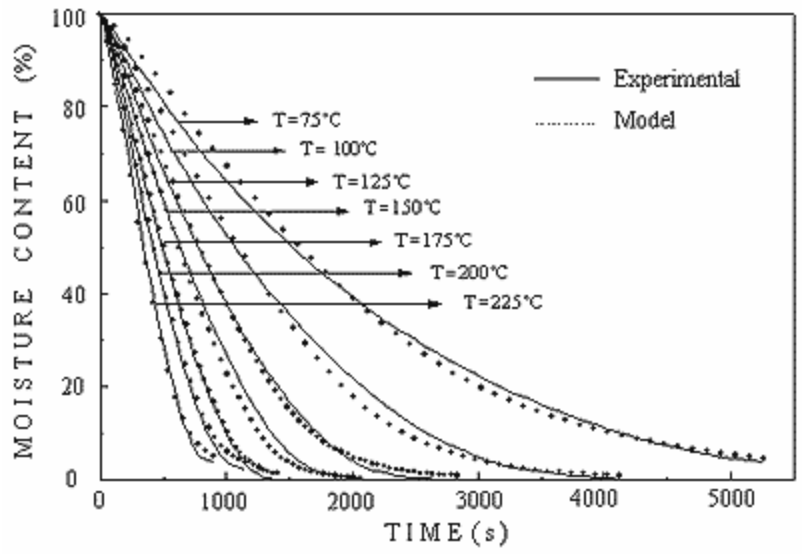

Figure 3.6- Kinetic curve showing the loss of moisture content with respect to time and temperature for group 2 (logs that have not been debarked) (Pinheiro *et al.*, 1998)

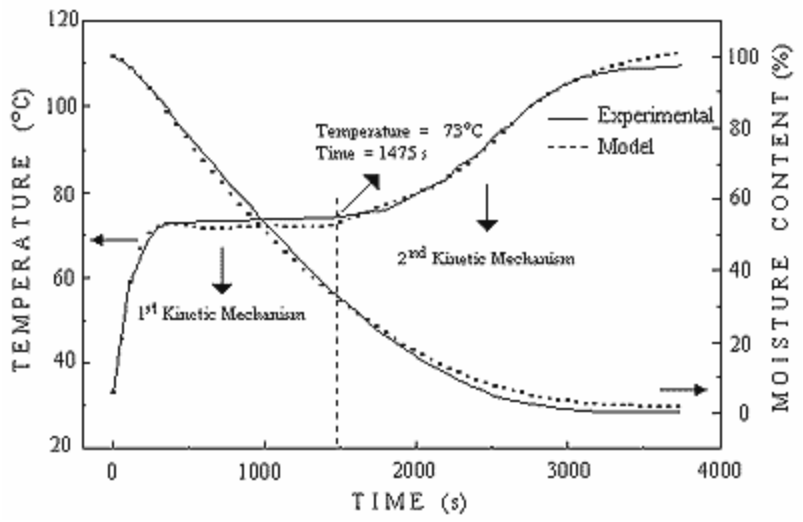

Figure 3.7- Kinetic curve and internal temperature profile for the 3rd sample group (debarked with thermal couple inside) (Pinheiro *et al.*, 1998)

The conclusion was that the model was accurate based on the validation of the isothermal thermogravimetric tests. The simulation of wood drying for a wide range of temperatures could be done with essentially two experimental thermo gravimetric tests, their respective evaporation temperatures and physical properties shown in table 3.5 (Pinheiro *et al.*, 1998).

In 1993, a model was published that described water movement through both cylinders and slabs. The modeling method described three dimensional transient heat conduction in a cylindrical piece of wood assuming it was an orthotropic material (Khattabi & Steinhagen, 1993). The accuracy of the solutions was evaluated by comparing them with established observations. The authors made the assumption that Fourier's law of heat conduction is the dominant mode of heat transfer and other modes can be neglected.

The heat flux vector Q_1 is defined by Cartesian coordinates in matrix form using Fourier's law, equation 30.

$$[Q_1] = -[K_1][G_1] \tag{30}$$

Where $[Q_1]$ and $[G_1]$ are 3x1 column vectors of heat flux and of the temperature gradient (T) along the geometric axes of (*X, Y, Z*), respectively (Khattabi & Steinhagen, 1993). $[K_1]$ is a second order tensor of thermal conductivity. In this case only the diagonal elements are non-zero. This equation is used when the external geometry is properly aligned with orthotropic axes. When it is misaligned, the heat flux vector of interest is Q_2. See equation 31.

$$[Q_2] = -[K_2][Q_2] \tag{31}$$

[Q_2]and [G_2] can be obtained by equations 32 and 33.

$$[Q_2] = [H][\,Q_1] \tag{32}$$

$$[G_2] = [H][G_1] \tag{33}$$

Where [*H*] is the matrix of directional cosines between the new axes, (*X, Y, Z*) and the orthotropic axes, radial, circumferential and axial (*R, C, A*). The matrix [*H*] has the property such that [N^T][*N*]=[*I*]. Here [N^T][*H*] is the transpose of matrix [*N*] and [*I*] is the unit matrix. Using the properties of the above equations, the equation 34 can be obtained.

$$[Q_2] = -[N][K_1][N]^T\{G_2] \tag{34}$$

Thus, using the above equation K_2 can be calculated using equation 35 (Khattabi & Steinhagen, 1993).

$$[K_2] = [N][K_1][N]^T \tag{35}$$

Figure 3.8 from Khattabi and Steinhagen illustrates the geometry of the cylindrical coordinate system. The predicted values using explicit and implicit solution methods are compared to the analytical solution in Figure 3.9**.** They concluded that the explicit technique is sufficient for practical uses.

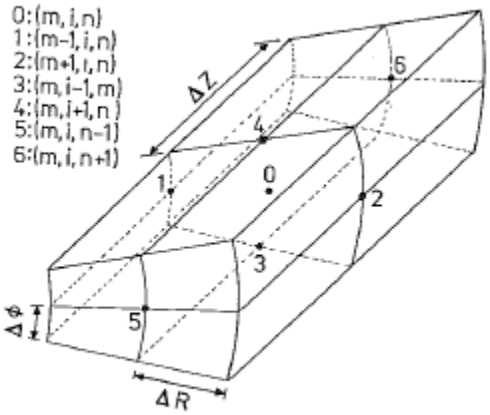

Nodal network of three-dimensional heat conduction in cylindrical coordinates

Figure 3.8 -Discretized portion of cylinder with labeled nodes (Khattabi & Steinhagen, 1993**)**

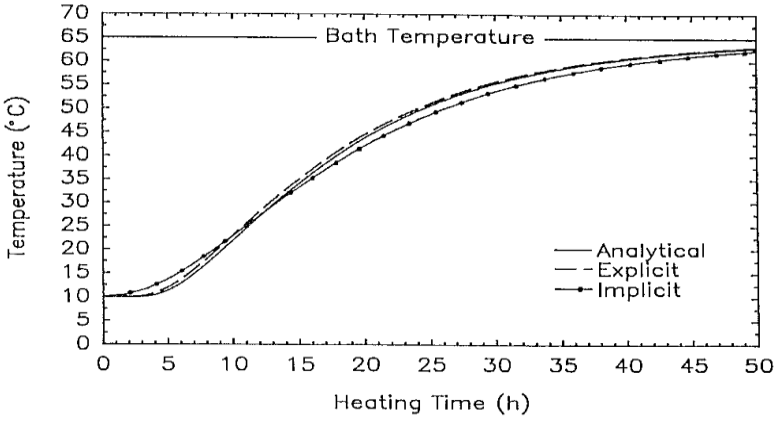

Figure 3.9-Drying curves of theoretical and experimental data (Khattabi & Steinhagen, 1993)

3.3.2 - Empirical Models

Data collected from nearby weather stations (precipitation (mm), solar insolation (MJ/m^2), and temperature (°C) were used to develop an empirical model

The model in this project was largely adapted from the empirical model for lumber drying published by Liang et al (1996). To predict open air drying times of leucaena logs, Liang implemented the Hayhoe and Jackson formula, published in 1974 shown in Equation 36 (Liang *et al.*, 1996). .

$$M_t = M_0 \exp(-a \sum_{i=1}^{t} PE_i + b \sum_{i=1}^{t} P_i + c) \quad (36)$$

Where t is the days after trees were felled, M_t is the moisture content at time t (wet basis), M_0 is the initial moisture content, PE_i is the potential evaporation (mm) of the i^{th} day, P_i is the precipitation (mm) of the i^{th} day, a and b are model parameters (mm^{-1}), and c is a dimensionless constant. The values of a, b, and c, are found using non- linear least squares analysis (Hayhoe & Jackson, 1974). Both the Hayhoe model and the Liang model relied on historical weather data to predict moisture content.

The potential evaporation, PE, was found using the Hargreaves Model shown in equation 37 (Hargreaves & Samani, 1982).

$$PE = \frac{3.214286(T+17.78)\gamma}{(595.5-0.55T)} \quad (37)$$

Where T is temperature (°C), and γ is incident solar insolation (MJ/m^2) (Liang *et al.*, 1996). Equations 36 and 37 are collectively referred to as the Liang model throughout this thesis.

The Liang model was developed from an infield drying experiment using leucaena logs in Waimanalo, HI. Logs cut on January 1 and July 1 were monitored for a 180 day period and their loss in mass was recorded. The experimental results and the model fitted to the drying data are plotted in Figure 3.10.

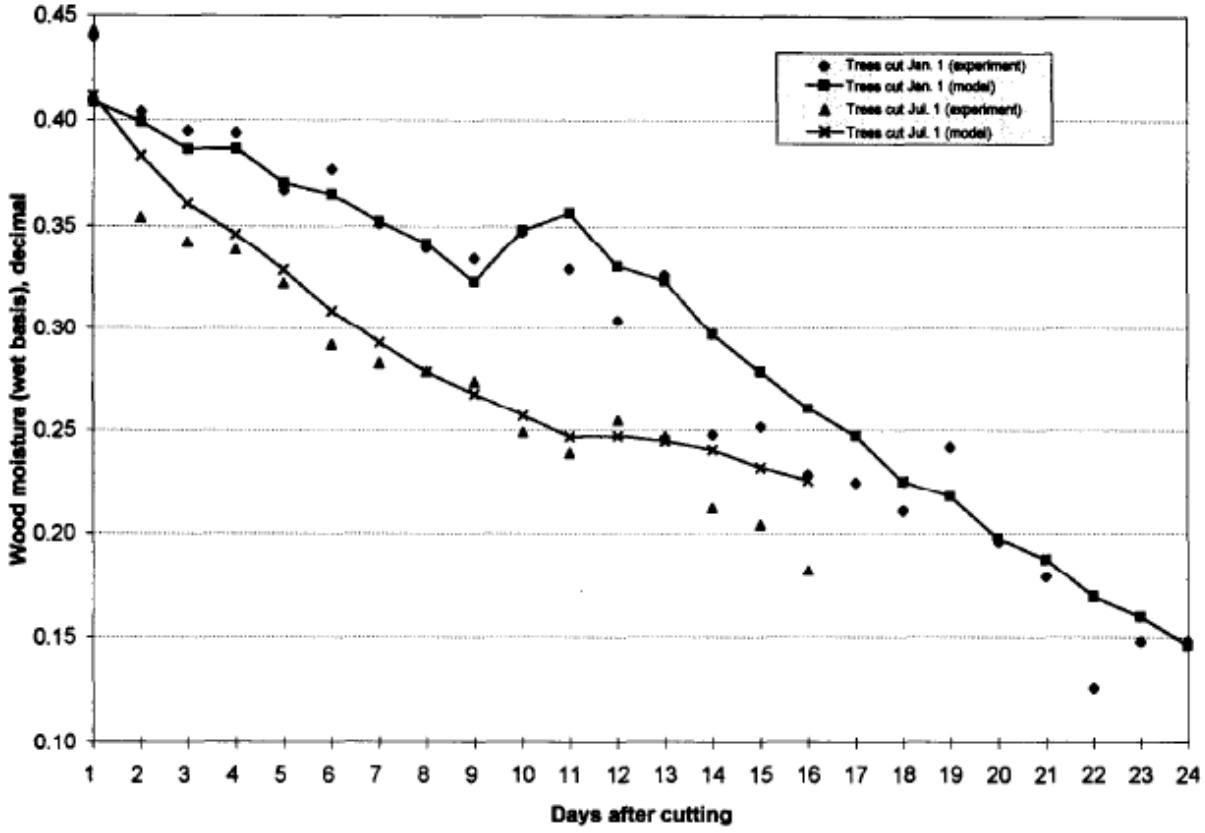

Figure 3.10-Experimental data and fitted model for trees felled on July 1, 1990 and January 1, 1991 (Liang *et al.*, 1996)

The model was then used to predict the drying times of leuceana at two different sites on the island of Kauai. Site 1 had an average annual precipitation rate of 100 mm/yr, and site 2 had an annual precipitation rate of 510 mm/yr. All the trees were assumed to have an initial moisture content of 46%. The predicted results are shown in figure Figure 3.11.

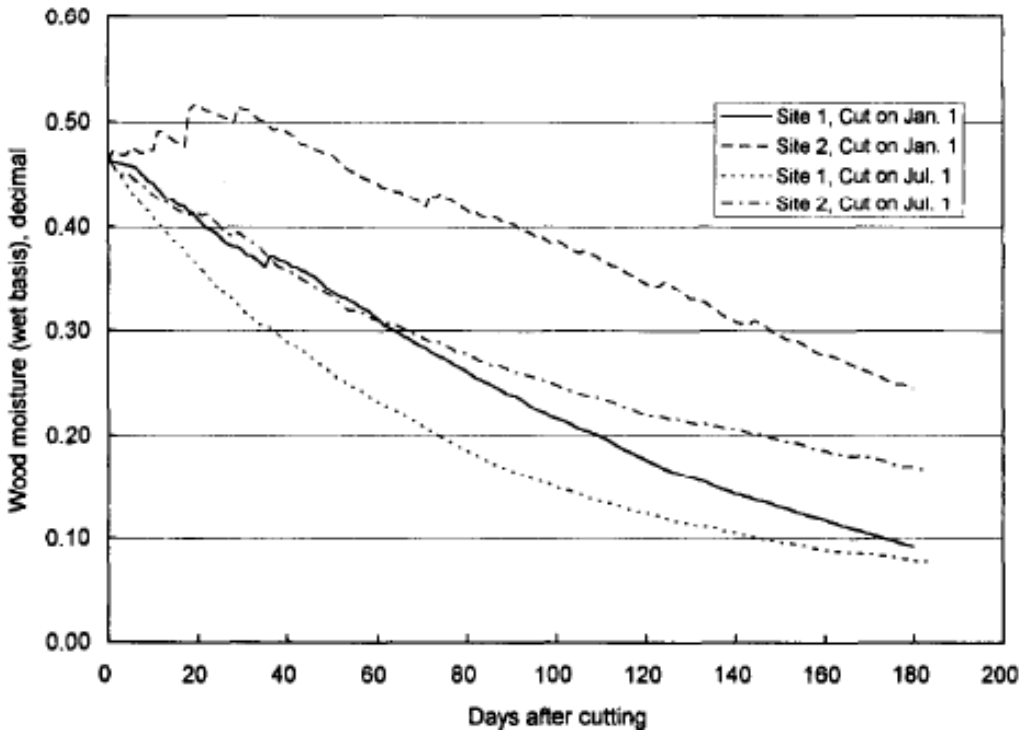

Figure 3.11-The effect of cutting time on wood drying predicted by the model (Liang *et al.*, 1996)

This study also shows that models can be developed using historical data to predict future outcomes. This is important since average historical data is used in the scenario analysis for this thesis.

Another empirical model was developed by Murphy, et al. in 2012. In the Murphy study, an outdoor storage trial was conducted in Derrygreenagh, Ireland to verify the model and assess the drying potential of logs moved from forest locations to drying sites. For this experiment, eight large steel cradles were constructed and placed on load cells connected to a data logger that recorded weights at hourly intervals. Twenty five metric tons of Sitka spruce wood were placed in each cradle and the loss of mass with respect to time was recorded. Murphy's study

determined that a mixed model with a heterogeneous compound symmetry structure, equation 38, was a best fit for the data (Murphy *et al.*, 2012).

$$MC_{10} = B_0 + B_1 * mc_0 + B_2 * {mc_0}^2 + B_3 * rain_{10} + B_4 * ET_{10day} + B_5 * i_2 + B_6 * i_3 + B_7 * i_4 + B_8 * i_5 + B_9 * i_2 * mc_0 + B_{10} * i_3 * mc_0 + B_{11} * i_4 * mc_0 + B_{12} * i_5 * mc_0 + B_{13} * i_2 * {mc_0}^2 + B_{14} * i_3 * {mc_0}^2 + B_{15} * i_2 * {mc_0}^2 + B_{16} * i_5 * {mc_0}^2 \quad (38)$$

Where MC_{10} is the moisture content at the end of a 10 day period, mc_0 is the initial moisture content, $rain_{10}$ is the cumulative rainfall for a 10 day period (mm), ET_{10} is the cumulative evapotranspiration for a 10 day period, i_2 through i_5 are binary variables (0 or 1) for treatments 2 through 5, and B_0 to B_{16} are model coefficients derived from the experiment, listed in Table 3.6 (Murphy *et al.*, 2012).Two types of logs (cleanly delimbed roundwood with an approximate top diameter of 70 mm and smaller, and crudely delimbed energy wood with no minimum top diameter) and three types of log covering schemes (no cover, top covered (T), top and sides covered (T&S)) defined the treatments. Figure 3.12 depicts the drying curves for five different treatments.

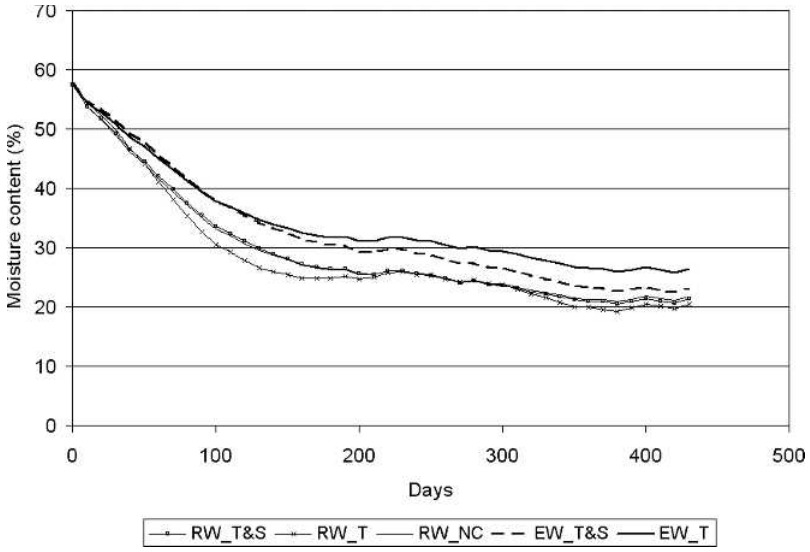

Figure 3.12-The plots of five different treatments for logs drying in Derrygreenagh, Ireland (Murphy *et al.*, 2012). **(RW-round wood, E- energy wood, T-top cover , T&S-top and side cover)**

Table 3.6- Model Coefficients for the Murphy et al model (Murphy *et al.*, 2012)

Coefficient	**Value**
B_0	6.6367
B_1	0.6222
B_2	0.004008
B_3	0.01221
B_4	-0.04933
B_5	-5.9390
B_6	-5.9994
B_7	-6.9249
B_8	-5.9828
B_9	0.3214
B_{10}	0.3345
B_{11}	0.3920
B_{12}	0.3375
B_{13}	-0.00368
B_{14}	-0.00417
B_{15}	-0.00472
B_{16}	-0.00427

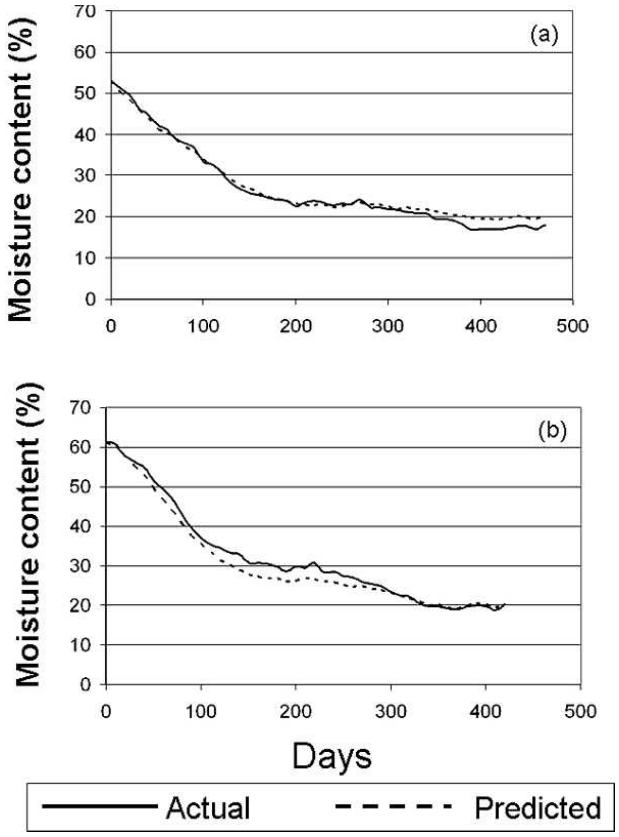

Figure 3.13-Actual and modeled drying times for Sitka spruce, based on number of days to reach 30% moisture content (wet basis) – (a) best fit experiment and (b) worst fit experiment. (Murphy *et al.*, 2012)

The model derived from the experiment was used to predict the number of days to reach moisture content below 30% (wet basis) for four other locations around Ireland, using historical weather data. The sites included Knock, Ballyhaise, Oakpark, and Valentia. The predicted results are shown in Table 3.7.

Table 3.7- The predicted number of days for wood to reach a moisture content below 30% in five locations in Ireland (Murphy *et al.*, 2012)

Location	Season in which drying began			
	Summer	**Autumn**	**Winter**	**Spring**
Starting MC (% wet basis)	**57.5**	**57.5**	**57.5**	**57.5**
Derrygreenagh (days)	104	154	141	103
Knock (days)	98	148	140	98
Ballyhaise (days)	92	125	127	90
Oakpark (days)	91	121	126	93
Valentia (days)	92	140	131	95
Starting MC (% wet basis)	**61.0**	**58.0**	**55.0**	**58.0**
Derrygreenagh (days)	123	157	132	105
Knock (days)	116	150	132	100
Ballyhaise (days)	106	127	119	91
Oakpark (days)	105	125	116	94
Valentia (days)	108	143	122	97

Murphy's study demonstrates the use of historical weather data for drying models, the use of strain gauges and open air storage locations to verify models, and the effectiveness of transporting wood to an off forest location to dry. This thesis reports the verification of eucalyptus drying models in two locations and a scenario analysis in which transporting logs offsite is assessed.

3.4 Scenario Analysis

A scenario analysis that was relevant to this thesis was published in 2008 by Uslu, Faaij, and Berman. Their study described the supply chain for the production of biomass energy

produced in Latin America. It estimated the cost of harvesting, conversion to fuel, trucking to harbor, and shipping from Latin America to Amsterdam.

To determine overall cost of transport, the factors considered included the mass of material transported (kg), lower heating value or LHV of the biomass (MJ/kg), average distance from harbor to plant (km), the fuel input required by the plant (Gg_{dry}/yr), the biomass yield (Mg_{dry},/ha yr), and moisture content (% wb). These variables were used to calculate the net energy gain after transport and the associated cost in €/(kW hr) (Uslu *et al.*, 2008). A generic distance of 100 km to harbor was assumed because possible locations of biomass production were not included in the scope of their research (Uslu *et al.*, 2008). This thesis does have locations for potential biomass harvesting and will have different distance from location to harbor. The other variables used to calculate shipping costs are relevant.

In the case of transporting logs to a dry location, it is important to consider the loading and unloading costs. M. R. Ghaffariyan, et al. published estimated prices of loading and unloading wood in Europe in €/m^3. The estimated cost to load and unload was 3.01 €/m^3 and 2.40 €/m^3, respectively (Ghaffariyan *et al.*, 2012).

3.5 Summary

In summary, there are well-established methods of modeling drying rates of wood in both natural and controlled conditions. Past studies have shown that the finite element method for heat transport and diffusion is reliable. Although equations and assumptions vary in different models, some are used more consistently than others. The most widely accepted assumptions are: wood is a heterogeneous material, liquid mass transport longitudinally in logs via capillary action

is far greater than radial diffusion across growth rings, and hygroscopic materials will lose or gain moisture until it reaches equilibrium with the environment.

Darcy's Law for capillary action, Fick's law of diffusion, water mass conservation and energy conservation laws are used most frequently. These models have been verified in field studies in the literature and some of the methods are adapted for this project. Change in temperature is an important factor to consider since it determines phase change. Most models also agree that the three different phases of moisture content have different properties and each property should be modeled accordingly.

Past studies have shown that empirical models are reliable and historical average weather data can be applied to them. These models require less computation time and have the potential to be used in scenario analysis.

4 -Materials and Methods

This project involved experimental wood drying data collection, the construction of models of the wood drying process, and scenario analysis. The models included a phenomenological model and an empirical model. The phenomenological model was constructed in COMSOL Multiphysics™ and the empirical model was constructed in Microsoft Excel™. The scenario analysis relied on solutions from the empirical model and also utilized Excel™.

The experimental portion included two sites on the island of Hawai'i that were deliberately chosen because of their different climate conditions and their proximity to existing weather stations.

For the empirical model, Liang's method, (see equation 36 in section 3.3 B in literature review), was implemented in a Microsoft Excel™ spreadsheet. Moisture content data derived from experiments were compared with both models.

For the phenomenological model, COMSOL Multiphysics™ was used because of its capability to implement the finite element method in complex shapes. It also has the capability of coupling multiple physical phenomena so heat exchange and moisture transport can be modeled simultaneously. For these reasons, COMSOL Multiphysics™ is often used to create multivariable time dependent models.

4.1 Experimental Methods

E. grandis logs were suspended by load cells in two different locations on the island of Hawai'i to monitor their weight over time exposed to ambient conditions. The sites selected were the University of Hawai'i Agricultural Research Stations at Lalamilo (*20.020 °N, 155.678 °W*), a dry location and Waiakea (*19.633 °N, 155.089 °W*), a wet location. These sites were deliberately selected because of the distinct difference in average rainfall, and their close proximity to weather stations with available hourly data including temperature, rainfall, wind speed, and solar insolation. The Lalamilo Research Station was located an elevation of 762 meters above sea level, with an average annual rainfall of 1270 mm, and average minimum and maximum temperatures of 15 °C and 22.7 °C, respectively (L-CTAHR, 2016). The Waiakea

Research Station was located at an elevation of 233.3 meters above sea level, with an average annual rainfall of 4,318 mm, and average minimum and maximum temperatures of 17.2 °C and 26.1 °C respectively (W-CTAHR, 2016). The monthly average rainfall at each location was also distinctly different as shown in Figure 4.1.

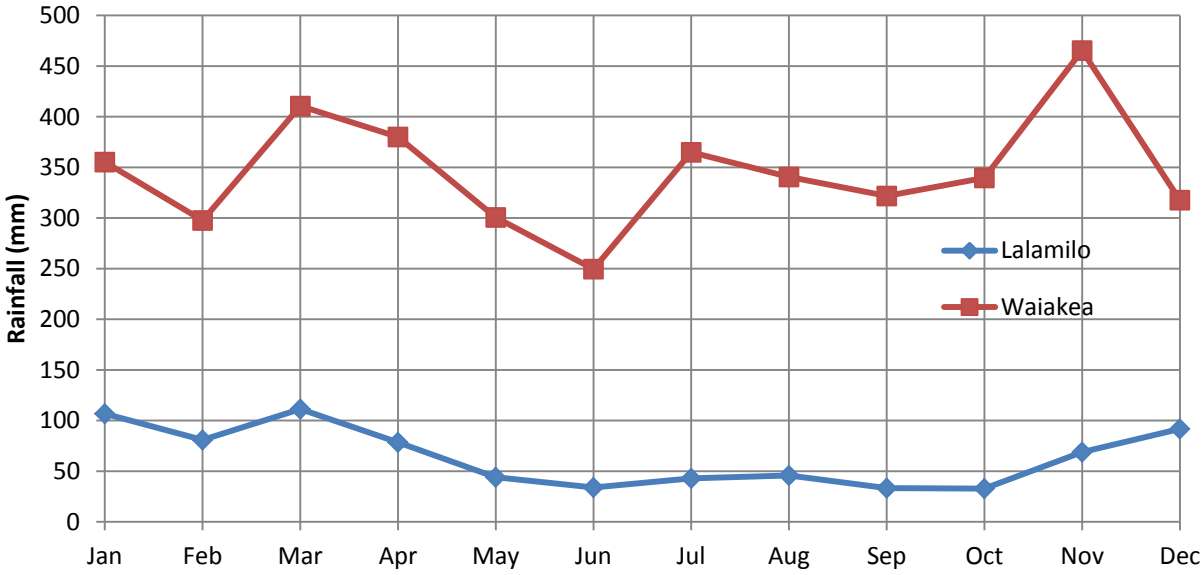

Figure 4.1-Average monthly rainfall distribution at Lalamilo and Waiakea locations (Giambelluca *et al.*, 2014a)

E. grandis logs were provided by Forest Solutions Inc. A tree was felled near Pepeeko, HI (*20.048 °N, 155.458 °W*). Figure 4.2 shows a photo of a stand of eucalyptus trees in the forest where the tree was harvested.The length of the tree from the ground to the first branch was 30.79 meters (101 feet). Seven sections, 2.44 m (8 feet) long, were cut from the base end moving up the trunk. The sections were labeled A-G starting from the cut end (A) to the last section nearest the tree top (G).

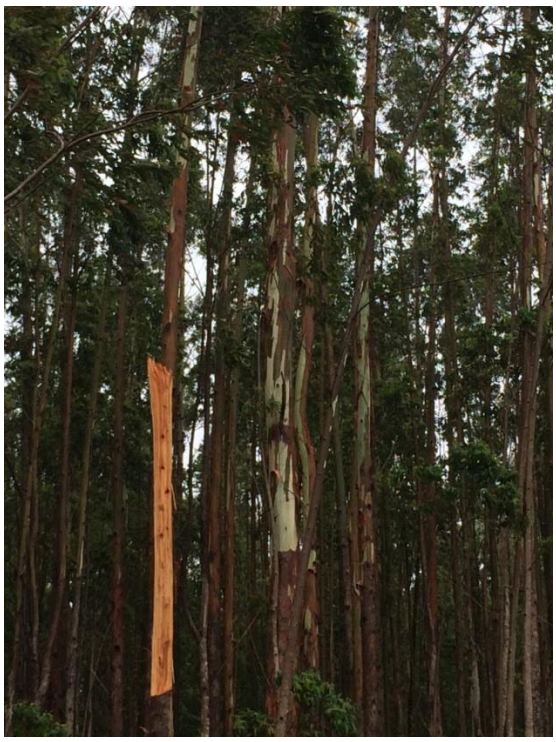

Figure 4.2-*E. grandis* plantation, Pepeeko, HI

To determine the initial moisture content of the tree, disks or cookies, approximately 2.5 centimeters thick, were cut from both ends of each section. Each cookie was immediately placed in a sealed plastic bag and labeled. The total (including bark) diameter and bark-free diameter of each log section was measured at two locations, 90° apart, and recorded. A schematic of the tree, the log sections, and their respective cookies is shown in Figure 4.3.

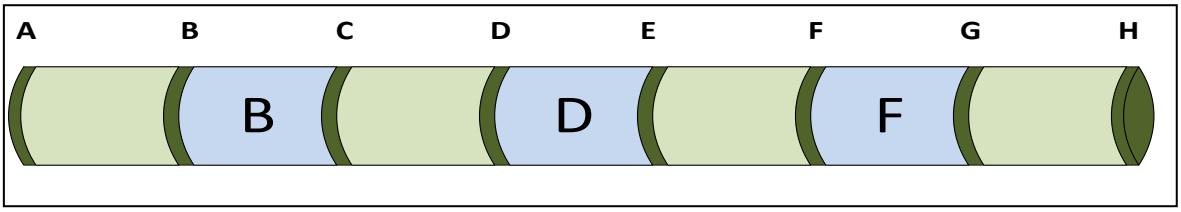

Figure 4.3- The sections and the corresponding cookies. The ones in blue are the sections used in the experiment

The standard ASTM method for determining moisture content of wood and wood based materials was used (ASTM, 2015) . The initial mass of each cookie was recorded, and placed in an oven at 105 °C. Every twenty four hours, the cookies were taken out of the oven and weighed to calculate the loss of mass. This process was repeated until the samples achieved a constant mass for at least three 24 hour periods. The final mass was considered to be the bone dry mass and the difference between the initial mass and bone dry mass was considered the mass of water. The mass of water and the bone dry mass were used to calculate the wet basis moisture content(ASTM, 2015).

Because of the mass of each 2.44 m log, each was cut into two 1.22 m (4 feet) halves in order to fit the load cell capacities. Logs B, D and F were used in the drying experiment. Each drying location used one half of logs B, D, and F. Each 1.44 m log was suspended by steel cables from a steel A-frame support that was 1.22 meters high and 0.914 meters wide. An Interface™ 4-bridge load cell (150 lbf (SSM-150) or 250 lbf (SSM-250) capacities) was placed between the steel cables suspending the log and the steel A-frame support to monitor log mass. This was considered a test stand and three test stands were located at both the Waiakea and Lalamilo sites. Weight data were recorded using a Campbell Scientific™ CR23X datalogger (for Lalamilo) and a CR1000 datalogger (for Waiakea). The mass was recorded every hour. Data were collected from the stations every month for nine months. The experimental set up with three logs installed in three tests stands is shown in Figure 4.4.

Figure 4.4-Test stand apparatus with suspended logs, load cells, and data logger at the Waiakea Research Station

Using Campbell Scientific's proprietary software, Short Cut™, programs were written for each data logger. The scan time, the interval at which electronic signals were sampled, was ten seconds and average values were recorded every hour. The simplified code for each data logger program, as well as the wiring diagrams are presented in Appendix B. The mass data were recovered from the data loggers roughly once a month from May 13, 2015, to January 11, 2016, and were used to determine the moisture content using the wet basis moisture content formula (equation 1). Weather data were recovered from a National Oceanic and Atmospheric Administration website (http://www.ncdc.noaa.gov/crn/station.htm?stationId=1186) for the Waiakea site and from CTAHR weather station at Lalamilo (Diamond *et al.*, 2013) (NOAA, 2016). The latter was not equipped to record solar data so a pyrometer (Li-Cor, Model LI-200R) was mounted on the test stand and data recorded with data logger.

4.2 Empirical Model

The model proposed by Liang et al. (1996) was implemented for the empirical approach to predicting drying of eucalyptus (See section 3.3 B). Solar insolation, precipitation, and ambient air temperature data were collected from nearby weather stations. The solar radiation and temperature data were inserted in equation 39 to calculate the rate of evapotranspiration. Evapotranspiration and precipitation data were substituted into equation 40 to predict log moisture content (See section 3.3 B).

$$PE = \frac{3.214286(T+17.78)\gamma}{(595.5-0.55T)} \tag{39}$$

$$M_t = M_0 \exp(-a\sum_{i=1}^{t} PE_i + b\sum_{i=1}^{t} P_i + c) \tag{40}$$

Using the weight measurements from the load cells, an experimental record of data points was obtained. Starting with guessed values of *a*, *b*, and *c*, Excel spreadsheet, and used to find a theoretical drying curve.

Using the least squares analysis package built into Excel™, the a, b, and c values that gave the closest fit to the measured data points were calculated. The model a, b, and c values were calculated based on the moisture content of each individual log as well as for the three logs combined at each location.

4.3 The Phenomenological Model

The *2-D Moisture Transport V5* model from the COMSOL model gallery was selected for the phenomenological model and is based on work by A.K. Datta from Cornell University (Datta, 2014). The model included formulas for determining liquid and vapor saturations, mass concentration, vapor diffusivity, relative permeability and capillary diffusivity. Datta's model has two domains, one representing the porous material and the other representing the moving air around it, see Figure 4.1. Since the Pinheiro model specifically dealt with *E. grandis* wood, many of the material properties used in this model came from that paper.

The method for finding mass rate of evaporation was also selected from the COMSOL model gallery, *Evaporation in Porous Media with Small Evaporation Rates*, published by A. Halder, A. Dhall, and A.K. Datta. This model was useful because it accounted for the evaporation rate in a porous media low temperatures, whereas other models dealt with elevated temperatures observed in kilns, ovens, or microwaves (Halder *et al.*, 2015).

COMSOL's modules were used extensively. The modules used were Free and Porous Media Flow (fp), Heat Transfer in Fluids (ht), and the Transport of Diluted Species (tds).

4.3.1 Boundary Conditions

Every module required boundary conditions to be set for both the inner and outer domains. The outer domain had the bottom boundary set as a wall to represent the ground and the top boundary was set as an open boundary to represent the atmosphere. The left vertical

boundary for the outer domain was set as the inlet for wind speed, vapor concentration, and ambient air temperature.

Radiation from the sun was included in the heat transfer module and used to account for heat flux at the top boundary of the log. Equation 41 is the standard equation for radiative heat transfer.

$$Q = \in \sigma\left(T_s{}^4 - T_a{}^4\right) \tag{41}$$

Where ϵ is emissivity and σ is the Stefan-Boltzmann Constant,T_s is the temperature of the surface and T_a is the ambient air temperature. (Geankoplis, 1993). The Q (W/m^2) came from data collected by a pyrometer, which was applied to the upper boundary of the log. A value of 0.95 was used for emissivity (Gieck & Gieck, 1990). Ambient air temperature was imposed as the boundary temperature for all four boundaries of the log.

The boundary conditions for the mass transfer module involved the vapor concentrations from the atmosphere. Relative humidity was collected from the weather stations and the vapor concentration at the boundary was found using the Goff-Gratch equation,. (See section 4.1 b domain conditions).

The model assumed atmospheric pressure at all boundaries of the log. Figure 4.5 illustrates the boundary conditions used.

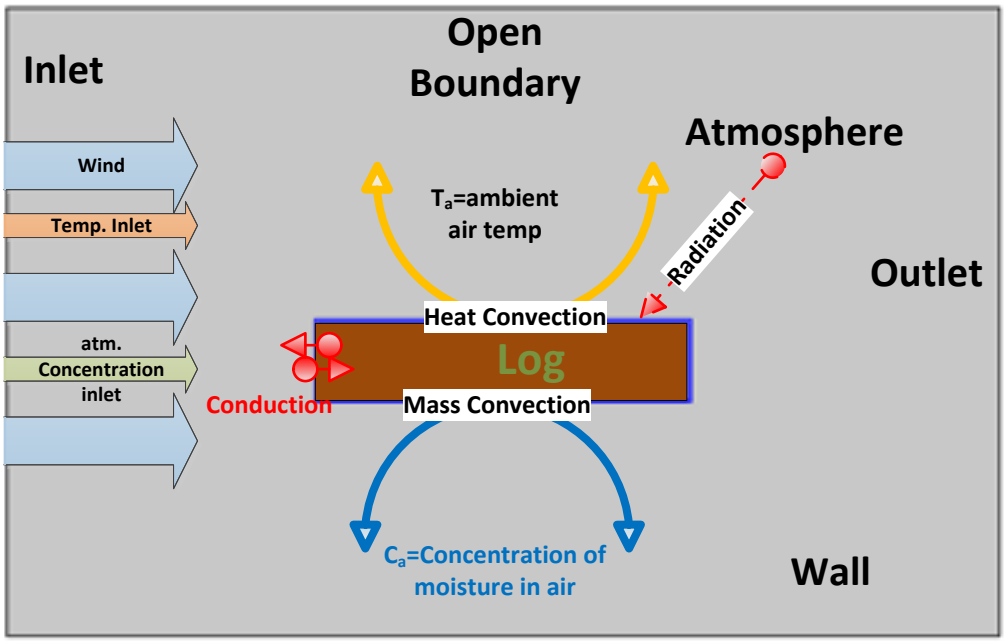

Figure 4.5-Schematic boundary conditions used for the model The log ioncludes the blue outlined rectangle

4.3.2 Domain Conditions

The constant parameters in the model included directional permeability, density of dry wood, and heat capacity of dry wood. Pinheiro, et al. (1998), Silva et al. (2010), and Redman et al. (2012) described the constant thermal and diffusive properties for *E. grandis* and similar species. The physical parameters in their studies are used in this model. (See section 3.2 and Table 3.5 in literature review.)

Because the moving water will carry energy with it, convective heat transport was assumed to occur inside the wood as well as on the surface. Equation 42 shows the standard equation for heat transfer that accounts for both convection and diffusion in porous media as seen in COMSOL Multiphysics™.

$$\left(\rho C_p\right)\frac{\partial T}{\partial t} + \rho C_p \boldsymbol{u} \cdot \nabla \mathrm{T} = \nabla \cdot (k \nabla T) + \mathrm{Q} \tag{42}$$

Convection and diffusion are important phenomena in mass transport. Equation 43 depicts the convection-diffusion equation for fluid flow in porous media as seen in COMSOL Multiphysics™.

$$\frac{\partial c}{\partial t} = \dot{m} + \nabla \cdot (\mathrm{D} \nabla c) - \boldsymbol{u} \cdot \nabla \mathrm{c} \tag{43}$$

Where c is concentration of liquid or vapor (mol/m^3), D is the diffusion coefficient (m^2/s), v is the superficial velocity (m/s), and $\dot{m}$ is the source or sink of the quantity (mol/m^3*s). The $\dot{m}$ term is used to determine how much water was converted from the liquid phase to the vapor phase (COMSOL, 2016).

To find rate of evaporation or $\dot{m}$, equation 44 was used.

$$\dot{m} = \mathrm{K} * \left(\mathrm{c}_{\mathrm{vap,Sat}} - \mathrm{c}_{\mathrm{vap}}\right) \tag{44}$$

This equation is used in both the *2-D Transport of V5* (Datta, 2014),and *Evaporation in Porous Media with Small Evaporation Rates* in the COMSOL model gallery (Halder *et al.*, 2015).

In the case of oven drying for short periods of time, K is often assumed to be a constant value. With varying climate conditions over a long period of time, the K varies with temperature

and vapor concentration. Equation 45 describes the Arrhenius type equation used to determine *K*.

$$K = \alpha * e^{\frac{-E_a}{R*T_{Dew}}} \quad (45)$$

Where α is 3.776*10^5 (1/s), the recommended Arrhenius pre exponential factor for temperatures between 373.15 K to 398.15 K, E_a is 53.78 kJ/mol, the recommended activation energy for the same temperature range, and T_{Dew} is the dew point temperature (K) (Pinheiro *et al.*, 1998).

T_{Dew} was found using equation 46 for dew point temperature (Brown, 2005).

$$T_{Dew} = \frac{\psi*\lambda}{1-\lambda} \quad (46)$$

Where ψ is a Magnus parameter of 516 K (Vömel, 2015) (Sensirion, 2015), and λ was found using equation 47.

$$\lambda = \frac{\log(\frac{\varphi_{wood}}{100}+\frac{\beta*T}{(\psi+T)})}{\beta} \quad (47)$$

Where β is the unitless Magnus value of 17.62, and φ_{wood} is the relative humidity inside the wood (Snyder & Snow, 1984), (UAMN, 2015). The φ_{wood} is a percentage of vapor concentration with respect to saturated vapor concentration found using equation 48.

$$\varphi_{Wood} = \frac{P_{vap}}{P_{sat,vap}} * 100 \quad (48)$$

Where p_{vap}, is vapor pressure and $p_{sat,vap}$ is saturation vapor pressure. p_{vap}, can be found using the ideal gas law, equation 49.

$$p_{vap} = c_{vap} * R * T \quad (49)$$

$p_{sat,vap}$ is found using the more complicated Goff-Gratch equation, equation 50 (Goff & Gratch, 1946)

$$p_{sat,vap} = 101324.6[Pa] * 10^{-7.90298*\left(\frac{T_{amb}}{T}-1\right)} + 5.02808 * \log_{10}\left(\frac{T_{amb}}{T}\right) - 1.3816 * 10^{-7} * \left(10^{\left(11.344*\left(1-\frac{T}{T_{amb}}\right)\right)} - 1\right) + 8.1328 * 10^{-3} * \left(10^{\left(3.49149*\left(1-\frac{T}{T_{amb}}\right)\right)} - 1\right) \quad (50)$$

The Goff-Gratch equation was used in the Datta (2014) model. Figure 4.6 shows the flow chart describing how each equation was used to find mass rate of evaporation in porous media.

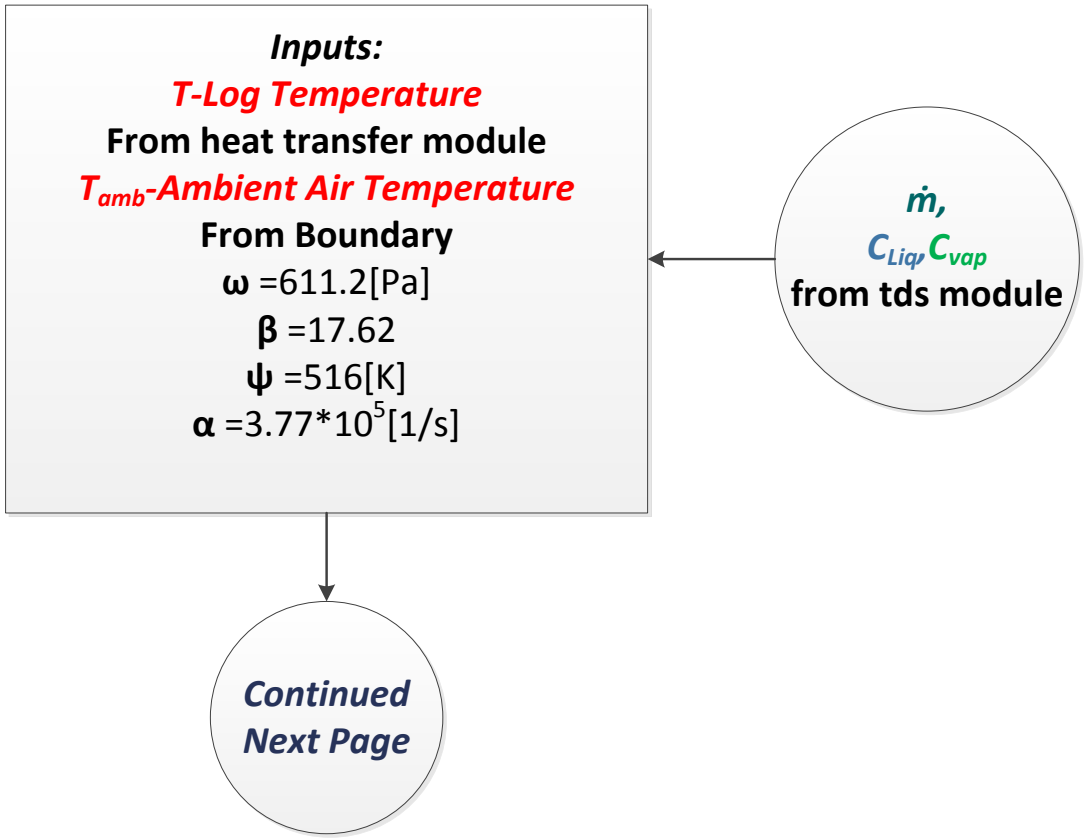

Figure 4.6-Flow chart depicting the equations used to determine the rate of evaporation

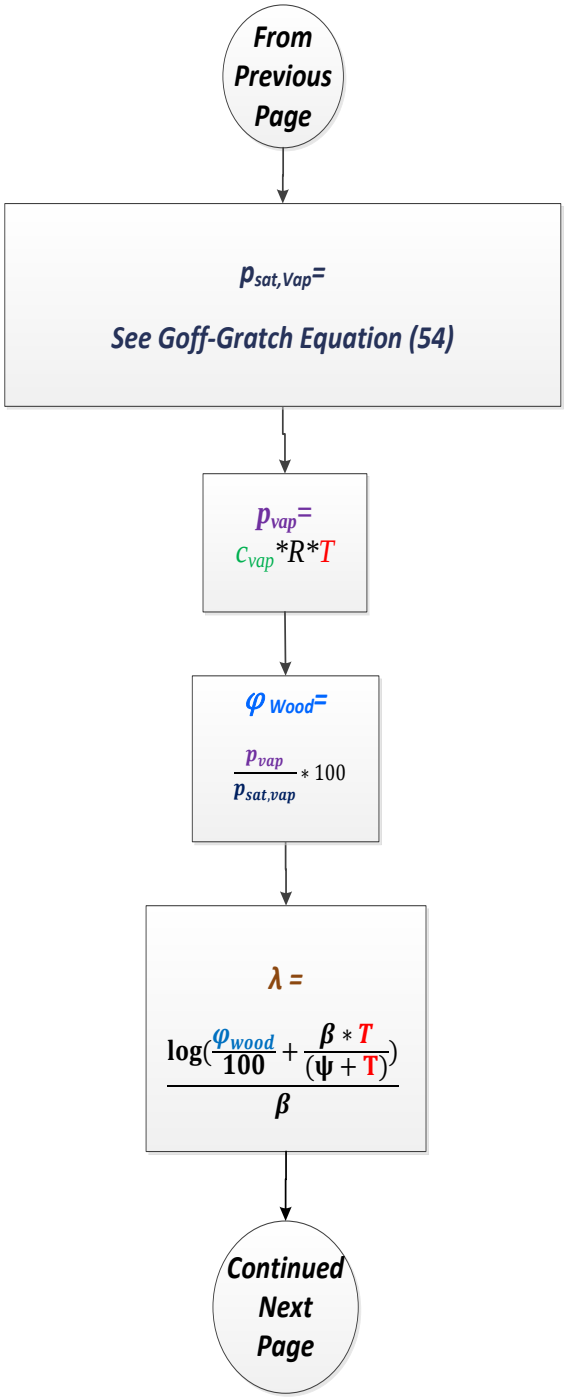

Figure 4.6- Continued

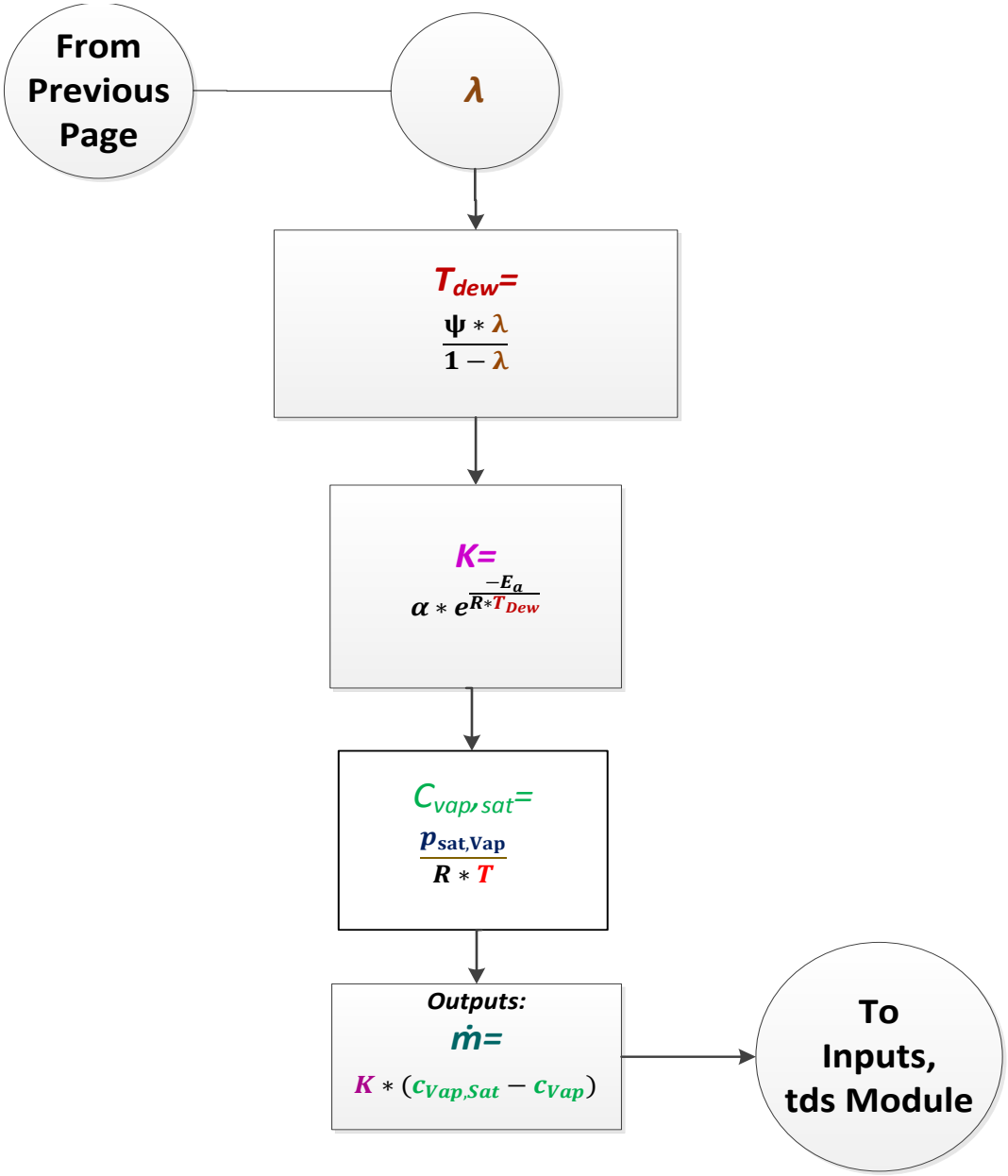

Figure 4.6- Continued

The porous domain was subdivided into two sub-domains; an inner sub-domain and an outer sub-domain that was 1 cm thick. The outer domain relied on the vapor concentration and saturation vapor concentration of in the atmosphere, whereas the inner domain relied on the vapor pressure and saturated vapor pressure of the surrounding elements. See Figure 4.7.

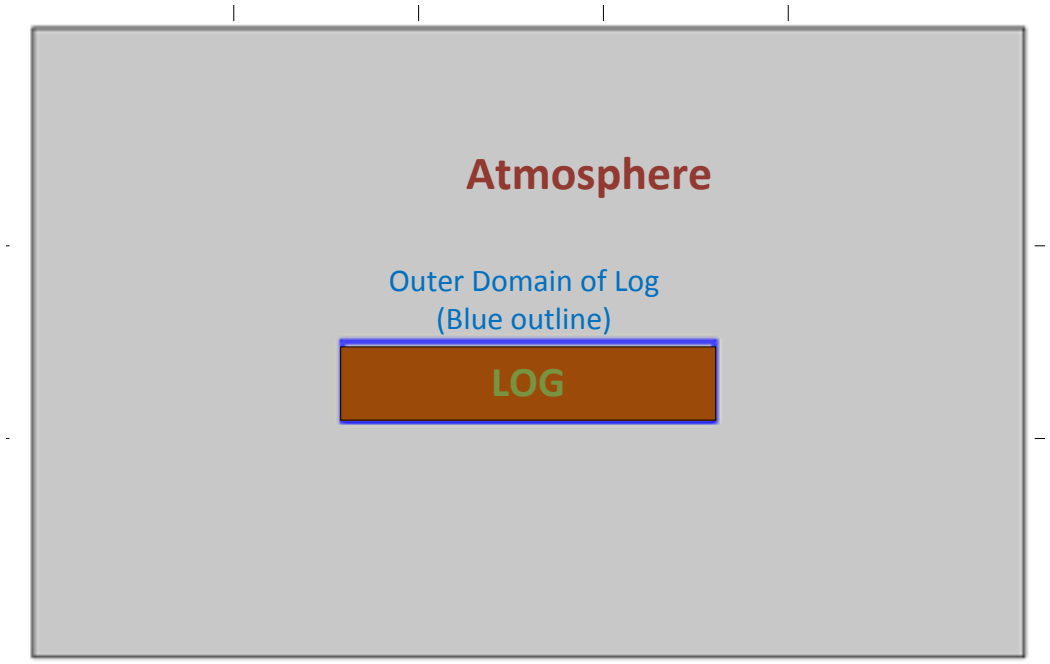

Figure 4.7- The highlighted blue region depicts the outer subdomain in which the mass rate of evaporation depended on atmopsheric conditions

The relative humidity of the atmosphere is used to find atmospheric vapor concentration, the lambda variable (λ_{sur}), dew point temperature ($T_{dew,atm}$),(K) (K_{Sur}) (1/s), and mass rate of evaporation of the wood near the surface of the log ($\dot{m}_{sur}$) (mol/(m^3*s)). Relative humidity data obtained from nearby weather stations was used to find the partial vapor pressure in equation 51.

$$P_{vap,atm} = \frac{\varphi_{atm} * p_{Sat,Vap,atm}}{100} \quad (51)$$

The atmospheric vapor concentration is found using the ideal gas law.

Equation 52 is used for the mass rate of evaporation near the surface.

$$\dot{m}_{sur} = K_{Sur} * \left(c_{Vap,Sat,atm} - c_{Vap,atm}\right) \quad (52)$$

Equations 56-57 is applied to an outer domain, one centimeter thick that surrounded the inner domain. This domain was constructed as a transition zone between the log surface and the greater ambience. See **Error! Reference source not found.**

Interstitial velocity, gas pressure and liquid pressure were inputs that came in the form of a function instead of a constant. The interstitial velocities of liquid and gas were found by equations 53 and 54.

$$u_L = -\left(\frac{\kappa_L}{\mu_L}\right)\nabla(P_G - P_C) \quad (53)$$

$$u_G = -\left(\frac{\kappa_G}{\mu_G}\right) \quad (54)$$

Permeabilities for both liquid and gas were inserted as a property in the domain representing the porous media or the log.

The gas permeabilities for *E. grandis* wood, found in Table 3.5, are the longitudinal and radial permeabilities for a single phase flow. In this model, we have multiple phases diffusing through the wood so the actual permeability was assumed to be a function of both relative permeability and single phase permeability. Equation 55 is used for the permeability accounting for multiphase flow for gas.

$$\kappa_G = \kappa_{G0} * \kappa_{rel,G} \quad (55)$$

Where κ_G is gas permeability, κ_{G0} is single phase gas permeability and $\kappa_{rel,G}$ is relative gas permeability (Datta, 2014).

$\kappa_{rel,G}$ can be found using equation 56.

$$\kappa_{rel,G} = 1 + (2 * S_L - 3) * S_L{}^2 \quad (56)$$

(Perre & Turner, 1999)

κ_G was the value used for permeability in Darcy's Law.

Equation 57, describes fluid through porous media as written in COMSOL.

$$\frac{\partial c}{\partial t} = \dot{m} + \nabla \cdot (\mathrm{D}\nabla c) - \boldsymbol{u} \cdot \nabla \mathrm{c} \quad (57)$$

Where $\dot{m}$ is the mass flow rate, D is diffusivity, u is the velocity vector and c is concentration (COMSOL, 2016).

Diffusion is also considered in this model. Depending on the media in which the water is diffusing, diffusivity can be a function of pressure, temperature, concentration and relative permeability. This model included diffusivity of vapor in air, D_{av}, capillary diffusivity of water in the wood D_{wc}, and an effective vapor diffusivity of vapor through wood, D_{eff}.

D_{av} is shown in equation 58.

$$D_{av} = 2.2 * 10^{-5} \frac{P_0}{P_g} * \frac{T}{T_0}^{1.75} \quad (58)$$

(Pinheiro *et al.*, 1998)

D_{eff} is shown in equation 59.

$$D_{eff} = \kappa_{\text{rel,gas}} * D_{av} * 1 * 10^{-3} \left(\frac{m^2}{s}\right) \quad (59)$$

Where $\kappa_{rel,gas}$ is the relative permeability of gas (Kang *et al.*, 2008).

D_{wc} is the capillary diffusivity in the longitudinal direction found in equation 60 (Datta, 2014).

$$D_{wc} = 1 * 10^{-8} * e^{-2.8+2*M_{db}} \quad (60)$$

Where M_{db} is dry basis moisture content. Most, literature describes the radial liquid diffusivity to be 0.05-0.10 times the longitudinal diffusivity. So for this model radial diffusivity was assumed to be $D_{wc}/10$.

Figure 4.8 depicts the domain conditions used in the model.

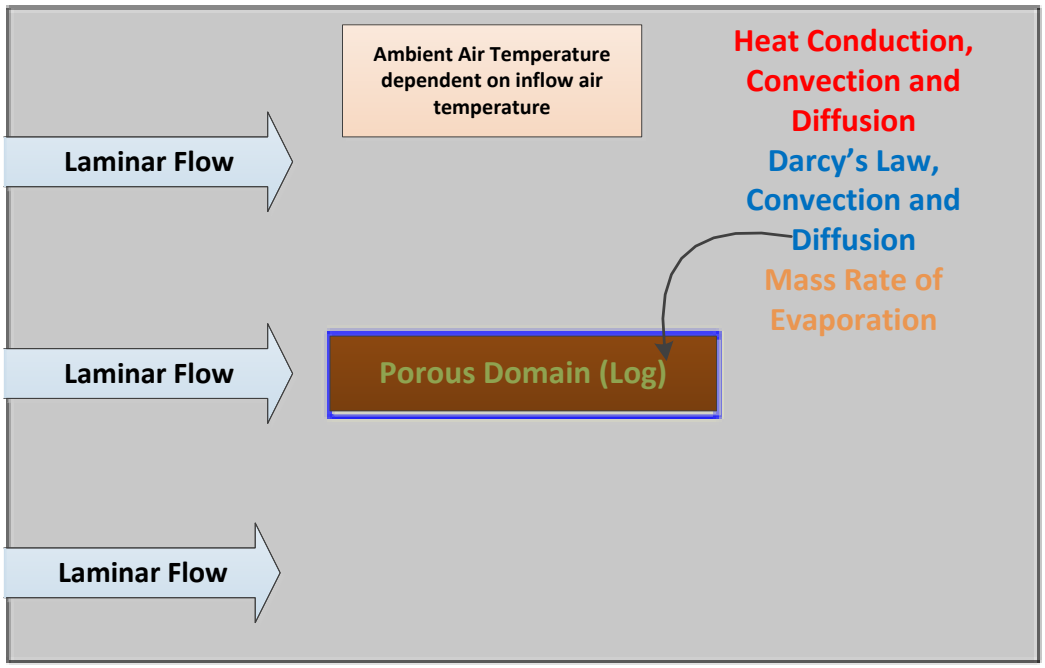

Figure 4.8-Doman conditions for both the atmosphere and wood.

The model used a time dependent solver solving for the times of t=0 hours to t= 4644 hours, the length of time of the experiment when the model was developed. The solver used a time step of 0.1 hours. A course triangular mesh was used for the outer domain representing the atmosphere and the domain representing the outer boundary of the log.. The inner domain used an extremely fine quadrilateral mesh. See Figure 4.9.

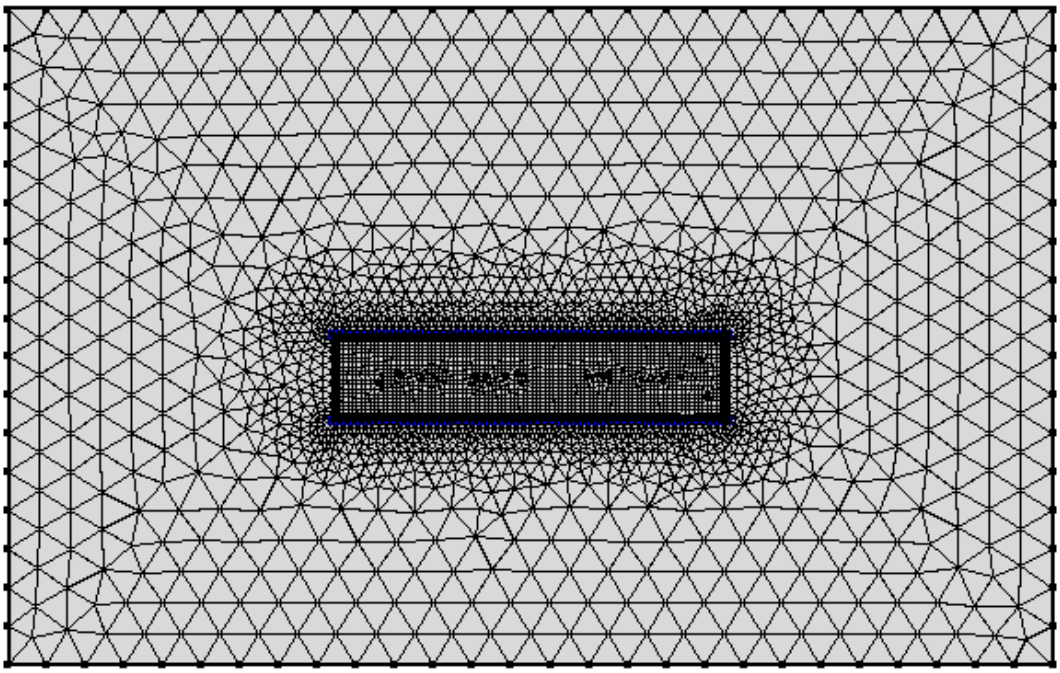

Figure 4.9-Discretization mesh generated by COMSOL. The ambience surrounding the log is discretized in triangular elements (Outer domain) and the log is discretized in quadrilateral elements (inner domain).

Multiple models were formulated, each including or neglecting different aspects of the physical phenomena, i.e. 1) whether to include or neglect ambient wind speed, 2) whether to use hourly wind speed data or average wind speed, 3) whether to include a permeable bark or an impermeable bark, 4) and whether to include or neglect radial diffusion. Results of these investigations and the ensuing model outcomes are described in the Section 5.2.

4.4 Model Application/Scenario Analysis

The empirical models derived from the data from Lalamilo and Waiakea were applied to seven locations on the Island of Hawai'i. This exercise was used to make an initial assessment of whether on-site drying might be effective or if transporting logs to a drier site appeared warranted.

Using Liang's formula and the values derived from the field experiment, the moisture content of logs for seven different locations was predicted. Giambelluca's *Interactive Climate Atlas* was used to find the monthly evapotranspiration and precipitation values for seven eucalyptus plantations as well as for Kawaihae and Lalamilo. The locations of the plantations are labeled in Figure 4.10. The moisture content after six months was predicted assuming the harvest time was the first of January. The process was repeated for every month of the year. It was determined that May is the best time to harvest logs, in any location. The time it took to reach moisture content below 30% wb was also estimated.

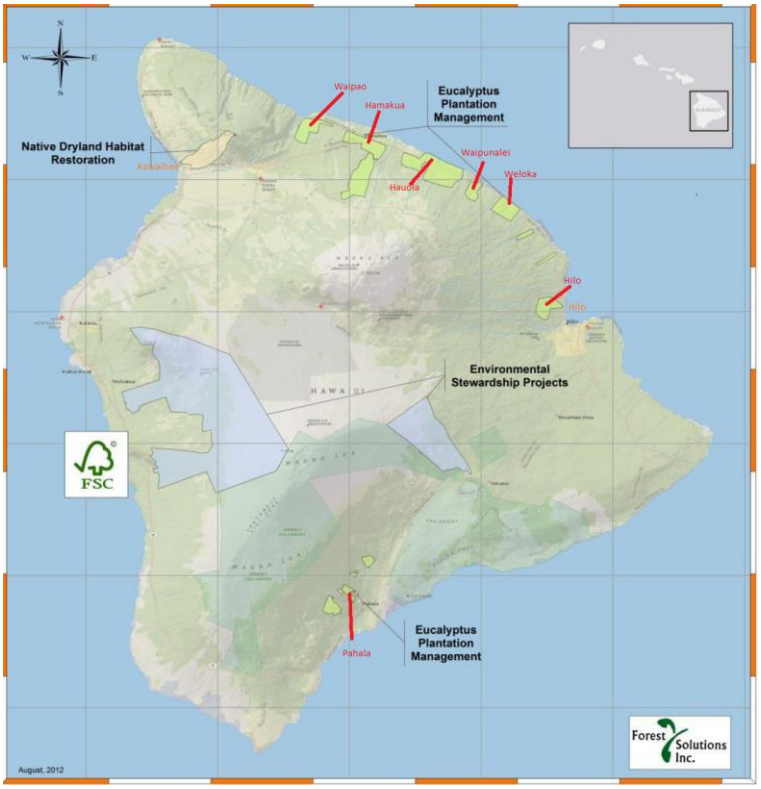

(a)

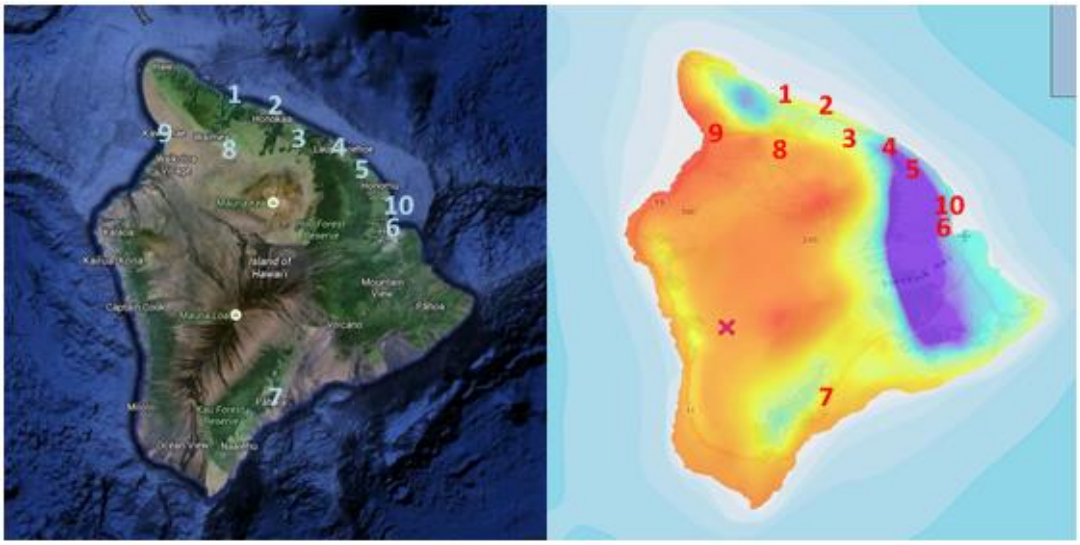

(b)

Figure 4.10- (a) Hawai'i Island with seven identified eucalyptus plantations. (FSI, 2012) *(b) (left) Hawai'i Island as seen from Google Earth™(Google Earth *et al.*, 2016), (right) rainfall map depicting regions with high annual rainfall (purple) and low annual rainfall (red) (Giambelluca *et al.*, 2014a) Lower panel numbering 1-Waipao, 2-Hamakua, 3-Haula, 4-Waipunalei, 5-Weloka, 6-Hilo, 7-Pahala, 8-Lalamilo, 9-Kawaihae Harbor, 10-Hilo Harbor *Source: "Hawai'I, Island." 19.67 N, 155.48 W. **Google Earth.** April 26, 2016

The scenario analysis was done in a similar matter as the Uslu et al. economic analysis in 2008 (See section 3.4 in the Literature Review section). The estimated costs for loading and unloading logs, as well as the Public Utilities Commission, PUC, ratings for transporting lumber were used to estimate the cost of transporting wood that has been dried on site, and transporting wood that has been dried offsite, see Figure 4.11.

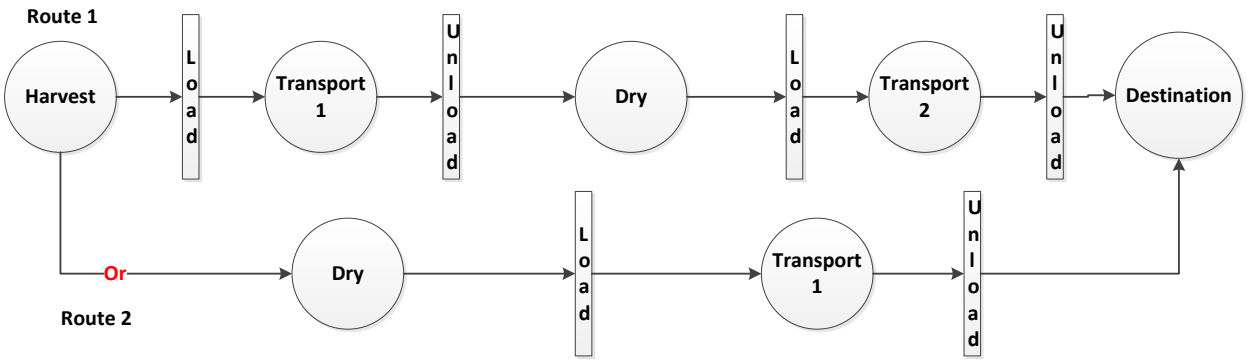

Figure 4.11-Flow chart depicting the process of (1) harvesting logs, loading them, transporting them to a dry location, unloading them, allowing them dry, reloading them, and transporting to a final destination, or (2) harvesting logs, loading them, transporting them to a final destination, and unloading them.

Drying rates were predicted using the Liang model for the scenario analysis. Information concerning loading and unloading costs was estimated from the literature. Ghaffaryian et al. (2013) determined costs of loading and unloading in a cut-to-length harvesting system to be 3.01 €/m^3 and 2.40 €/m^3 ($3.39/$m^3$ and $2.71/$m^3$ based on $1.13/€), respectively, in Iran. The Hawai'i Public Utilities Commission regulates trucking and has a published rate of $120 per hour for activities consistent with log transport. The Google map application was used to calculated transport distances and travel times. Truck loads were defined by weight, 24.5 Mg (27 tons), and differences in log density due to drying were attributed only to moisture loss and

not to changes in log volume due to shrinkage. Differences in net heating value based on differences in moisture content were used to calculate the cost ($/net MJ) of wood delivered at its final destination.

Calculations of $/MJ$_{net}$ are summarized as follows:

$$\rho_{tot,o} = \frac{m_{tot,o}}{V_{log}} \tag{61}$$

Where $\rho_{tot,o}$ is the initial log total density (Mg/m^3), $m_{tot,o}$ is the initial log mass (Mg), and V_{log} is the log volume (m^3).

$$\boldsymbol{\rho_{dm,o}} = \frac{\mathbf{m_{tot,o}(1 - MC_o)}}{\mathbf{V_{log}}} \tag{62}$$

Where $\rho_{dm,o}$ is the initial log dry matter density (Mg/m^3), and MC_o is the initial log moisture fraction.

$$\rho_{tot,t} = \rho_{dm,o}\left(1 + \frac{MC_t}{(1 - MC_t)}\right) \tag{63}$$

Where $\rho_{tot,t}$ is the log total density (Mg/m^3) at time, t, and MC_t is the moisture content at time, t.

The production costs required to produce harvested logs at a loading deck in the forest are assumed to be equal in both scenarios. The incremental cost of delivered wood, C_{tot}, ($/MJ) is defined as:

$$\boldsymbol{C_{tot}} = \left(\sum_{i=1}^{\#\, load} \frac{\boldsymbol{C_{load} m_{TL}}}{\boldsymbol{\rho_{tot}}} + \boldsymbol{C_{trans} T_{trans}} + \sum_{i=1}^{\#\, unload} \frac{\boldsymbol{C_{unload} m_{TL}}}{\boldsymbol{\rho_{tot}}} \right) \left(\frac{\mathbf{1}}{\boldsymbol{HHV}\left(\mathbf{1} - \boldsymbol{MC_f}\right)} \right) \tag{64}$$

where C_{load} is the cost of loading logs ($/m^3), m_{TL} is the mass of logs on a truck (Mg), C_{unload} is the cost of unloading logs ($/m^3), C_{trans} is the log transport cost ($/h), T_{trans} is the total transport time, and MC_f is the final delivered moisture content.

5 Results

This chapter presents experimental results, empirical model results, phenomenological results, and results of the scenario analysis.

5.1 Experimental Methods Results

The dimensions of each cookie and log and the cookie moisture contents (wet basis) are summarized in Table 5.1. Diameters of the logs (including bark) ranged from 28 cm near the base of the tree to 22 cm near the point where the first branch occurred, nearly 20 m away. Bark thicknesses ranged from 0.15 to 1.3 cm. The mass loss in each cookie during oven drying is shown in Figure 5.1. Most of the moisture loss occurred in the first three days of drying. Moisture contents ranged from 52 to 62% (wet basis) with the higher moisture contents recorded in the lower section of the tree. The overall average moisture content of the tree was 54% wet basis. The initial moisture content measurement of the cookies and the initial mass for each log were used to calculate the water mass and bone dry mass. The calculated initial values are in Table 5.2. Logs at each site were one half of 2.44 m sections B, D, and F, of the felled tree. It

was assumed that logs B, D, and F at each drying site had the same initial moisture content and diameter at the beginning of the experiment.

Table 5.1-Summary of dimensions of cookies and logs cut from *E. grandis* tree and cookie moisture contents.

Cookies	A	B	C	D	E	F	G	H (ellipse)
Diameter with bark (cm)	27.9	27.6	26.0	24.9	24.4	23.8	22.1	21.1
Diameter without bark (cm)	27.6	26.0	24.8	24.1	23.5	21.1	21.0	20.3
Bark thickness (cm)	0.15	0.8	0.6	0.4	0.45	1.3	0.55	0.4
MC % wb	62.0	58.2	54.8	54.1	53.8	53.0	52.4	52.3
Logs								
Average log diameter w/ bark(cm)	27.8	26.8	25.6	24.6	24.1	23.0		

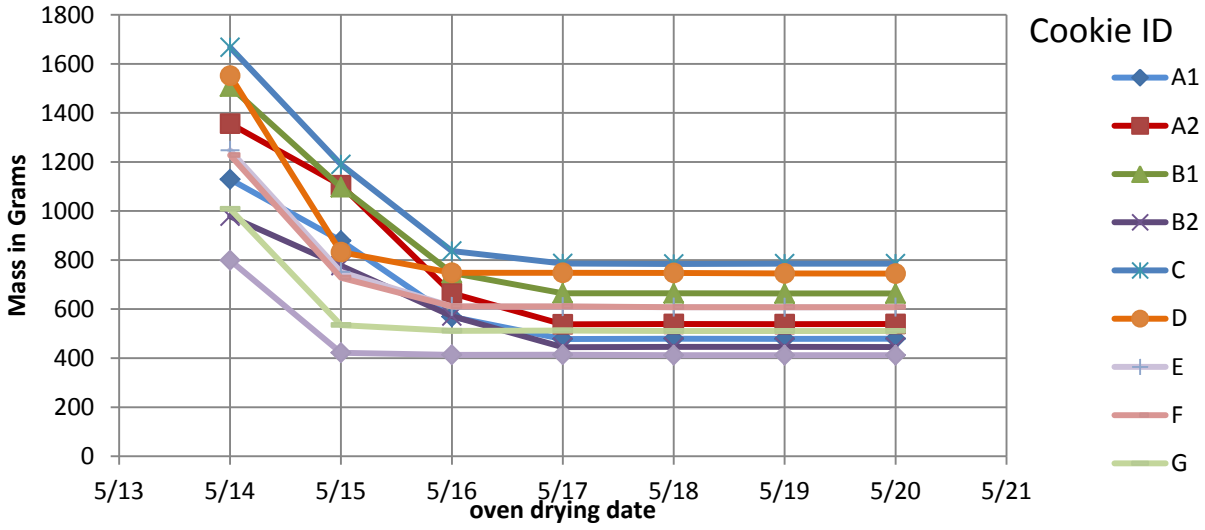

Figure 5.1-Record of *E. grandis* cookie mass during oven drying to determine initial moisture content.

Table 5.2-Initial component masses for logs at Lalamilo and Waiakea.

Lalamilo Logs (Top Half)	B Top	D Top	F top
Initial mass (kg)	53.65	45.30	35.45
Mass of water (kg)	30.31	24.42	18.68
Dry matter mass(kg)	23.34	20.88	16.77
Waiakea Logs (Bottom Half)	B Bottom	D Bottom	F Bottom
Initial total mass (kg)	56.75	38.02	45.50
Mass of water (kg)	32.06	20.49	23.98
Dry matter mass(kg)	24.69	17.53	21.52

Figures 5.2 to 5.4 depict the change in log moisture content, the daily average temperature and total solar insolation, and the cumulative sums of precipitation and evapotranspiration at Waiakea, respectively. Figures 5.5 to 5.7 depict the change in log moisture content, the daily average temperature and total solar insolation, and the cumulative sums of precipitation and evapotranspiration at Lalamilo, respectively.

For each site, every log lost mass at a similar rate (see Figures 5.2 and 5.5). When it rained, each log gained a similar amount of mass as depicted in the log mass curves. Lalamilo logs dried at a faster rate, with the bulk moisture content of the three logs reaching ~21% (wb) after nine months, whereas in Waiakea, the bulk moisture content was ~32 % (wb) over the same time period. There was also more drastic weight gain due to rain events recorded at Waiakea

Differences in precipitation and evapotranspiration at the two locations were significant throughout the experiment. Cumulative precipitation, cumulative evapotranspiration, and average temperature were 4020 mm, 771 mm, and 22.3 °C, respectively, at Waiakea. Lalamilo was drier and cooler, with cumulative precipitation, cumulative evapotranspiration (calculated), and average temperature of 248 mm, 918 mm, and 18.3 °C, respectively.

Figure 5.3 depicts the average daily temperature and solar insolation collected from the nearby NOAA weather station at Waiakea. Solar insolation at Waiakea and Lalamilo totaled 3,454 and 4,257 MJ/m^2, respectively, over the period of the experiment, indicating the Lalamilo received 23.2% more solar energy. This higher solar insolation and less frequent rainfall at Lalamilo explain the higher evapotranspiration rate.

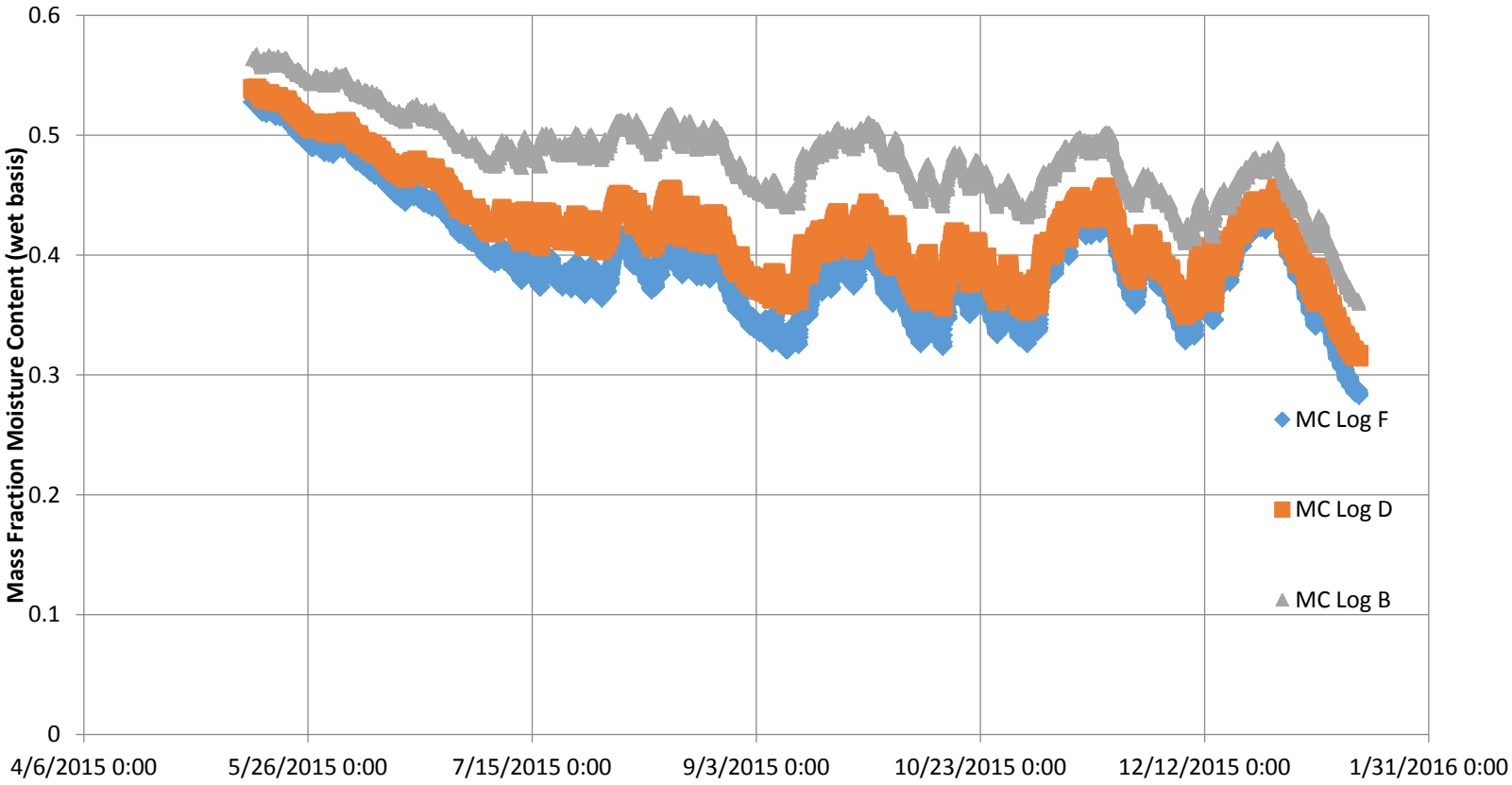

Figure 5.2-Moisture content of the logs at Waiakea from May 15, 2015 to January 14, 2016

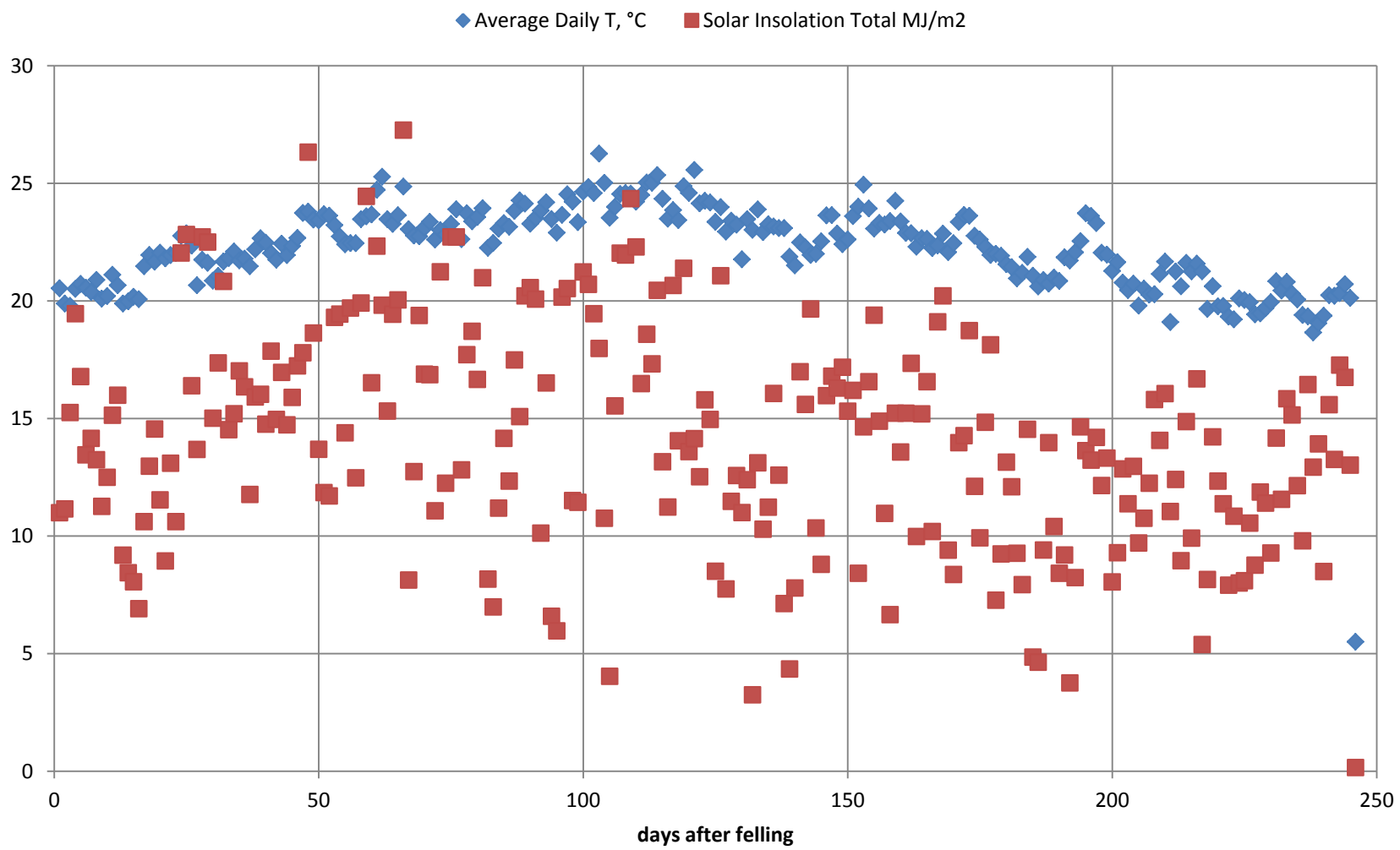

Figure 5.3 - Average daily temperature (°C) and total solar insolation (MJ/m^2) from May 15, 2015 to January 14, 2016, at the Waiakea site.

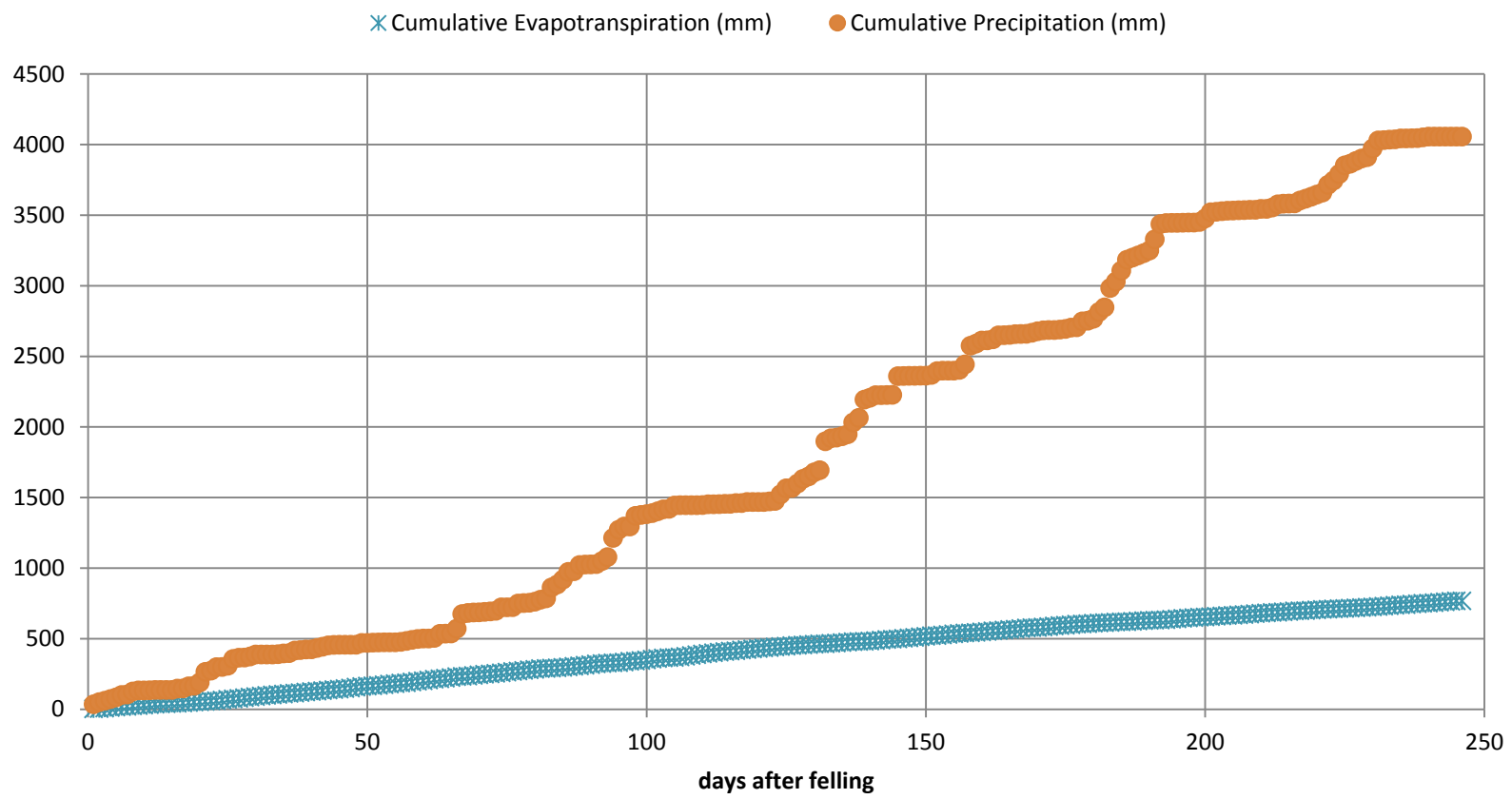

Figure 5.4- Cumulative precipitation and evapotranspiration (mm) from May 15, 2015 to January 14, 2016, at the Waiakea site. Evapotranspiration was calculated using equation 37.

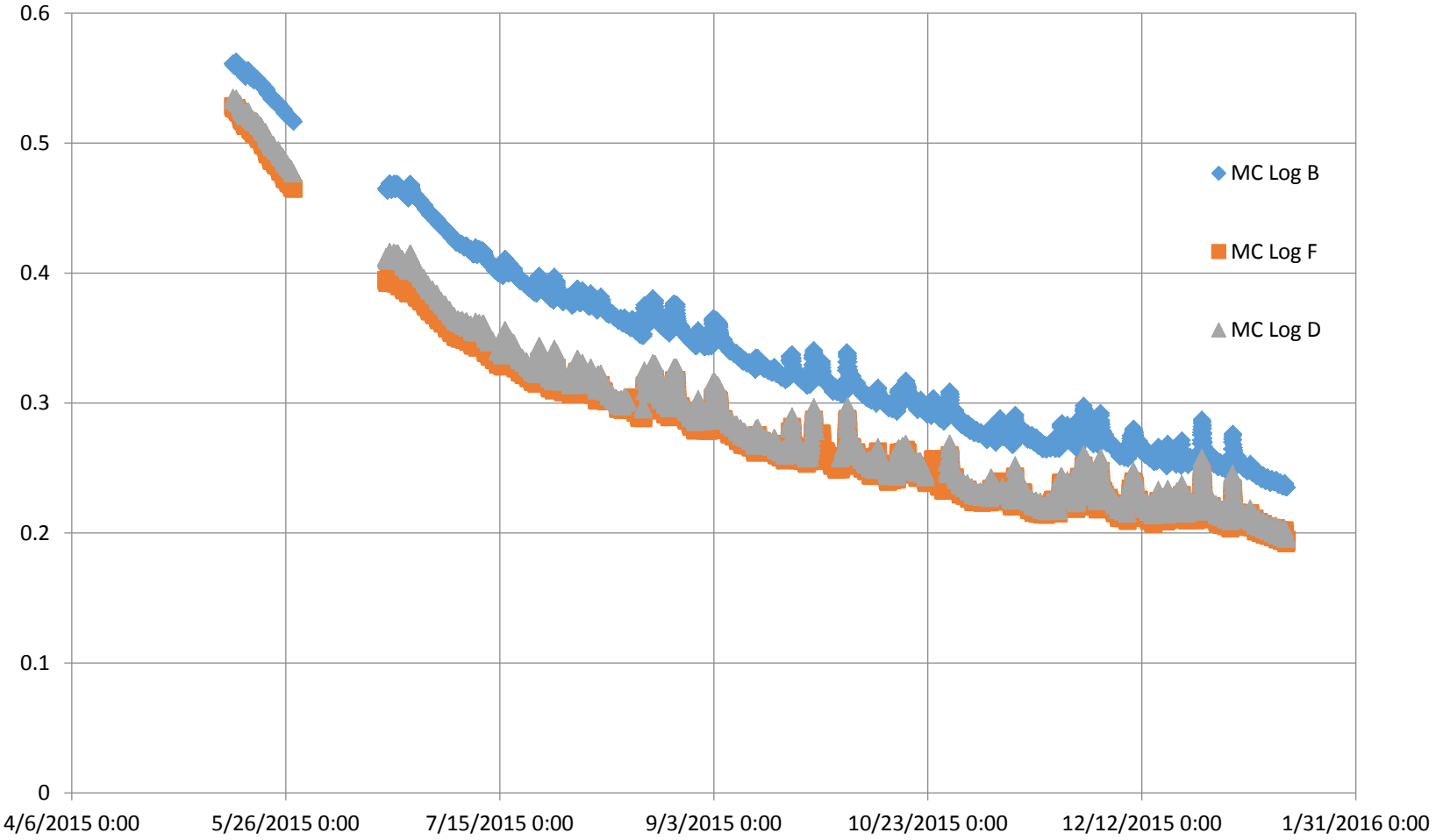

Figure 5.5-Moisture content of the logs at Lalamilo from May 15, 2015 to January 14, 2016

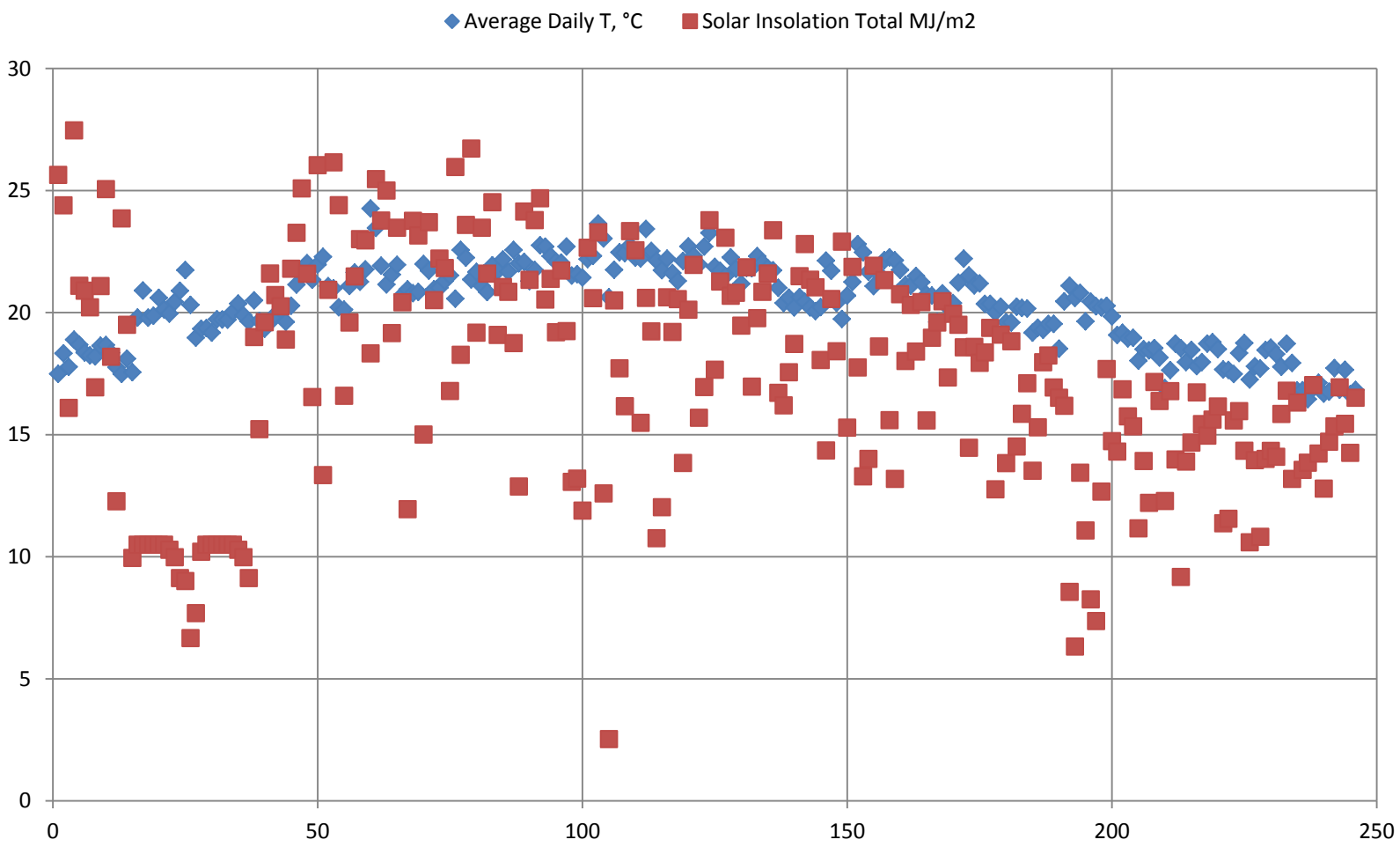

Figure 5.6- Average daily temperature (°C) and total solar insolation (MJ/m^2) from May 15, 2015 to January 14, 2016, at the Lalamilo site.

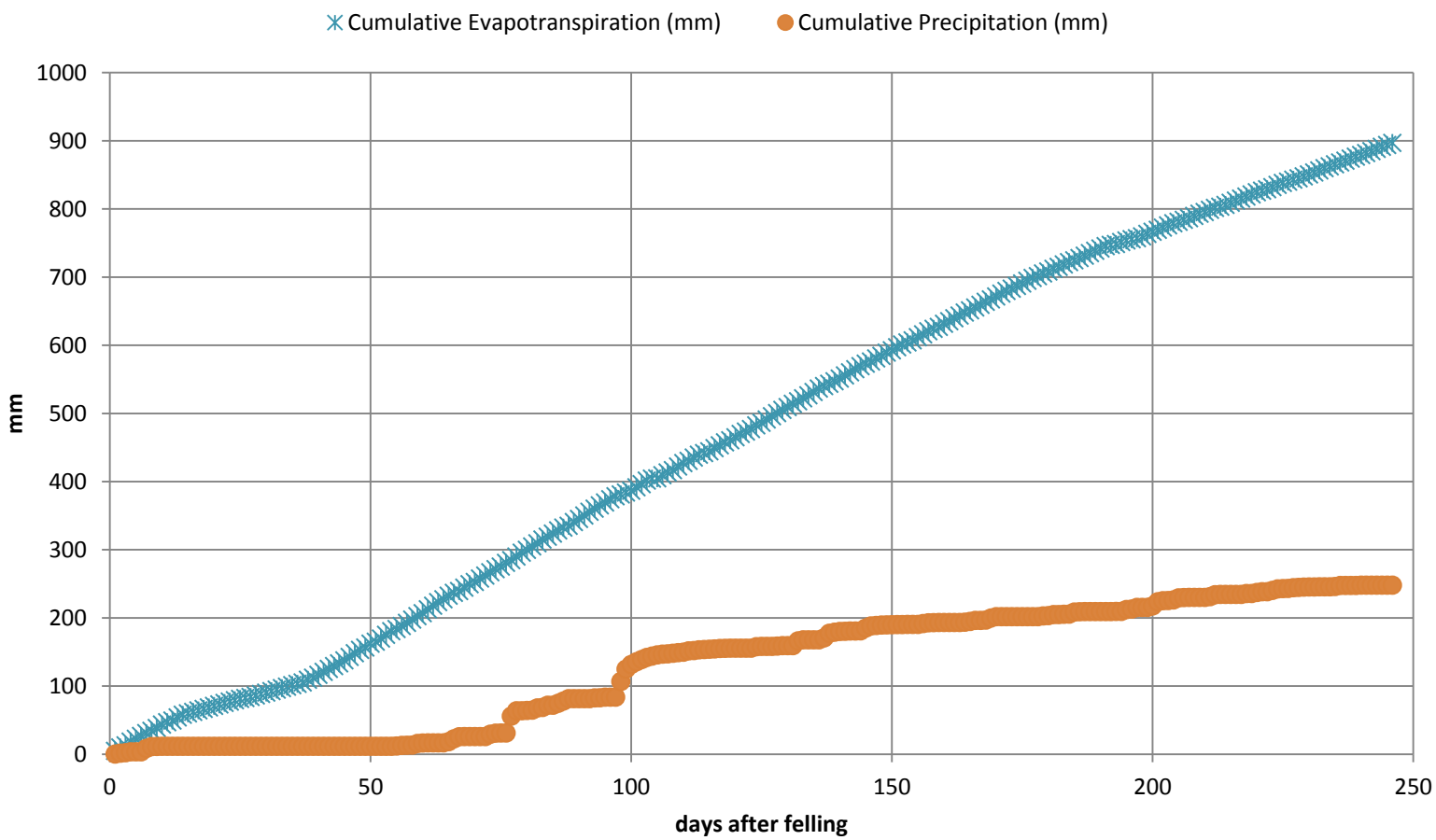

Figure 5.7- Cumulative precipitation and evapotranspiration (mm) from May 15, 2015 to January 14, 2016, at the Lalamilo site. Evapotranspiration was calculated using equation 37.

Photos of the logs at each location after drying are shown in Figures 5.8 through 5.11. The logs at Lalamilo displayed significantly more cracking and checking than those at Waiakea. This may have contributed to faster drying rates displayed by the logs at Lalamilo. Lalamilo logs also displayed a marked color change in the bark and log surface from a white to a dark gray. This may have affected the emissivity and thus the sensible energy available for drying.

Figure 5.8 – Log at Lalamilo displaying a gray color and wood deformation

Figure 5.9- Lalamilo log cross section displaying severe cracking

.

Cracking was apparent in all logs at Waiakea but not as severely as occurred at Lalamilo. The logs in Waiakea also shed a significant amount of bark. See Figures 5.10 to 5.11.

Figure 5.10- Log in Waiakea, showing minimal color change. Bark shedding was observed

Figure 5.11- Waiakea log cross section showing minor cracking

5.2 Empirical Model Results

Table 5.3 summarizes the *a*, *b*, and *c* values derived for the Liang Model (Equation 64) and compares the predicted and experimental final log moisture contents at Waiakea and Lalamilo. Data include values for logs B, D, and F, and for the bulk total of the three logs combined at each location. Values of *a* ranged from 0.00137 to 0.00198 for the three logs at Lalamilo. Similarly, at Waiakea, *a* values ranged from 0.0007 to .00196. The *a* parameter is the coefficient for evapotranspiration. Values of *b*, the cumulative precipitation coefficient, ranged from 0.00140 to 0.00259 at Lalamilo and 7.2×10^{-5} to 0.000287 at Waiakea. The larger *b* value for Lalamilo found in table 5.3 is most likely due to less rainfall. The values of *c* at both locations were zero. The *a* and *b* values were consistently larger for Lalamilo than for Waiakea. The predicted and experimental bulk moisture contents at Lalamilo were 19.6 % wb, and 21.3% wb, respectively, a difference of 1.7% (absolute). The predicted and measured bulk moisture contents at Waiakea were 40.2 % wb and 32.7 % wb, respectively, with a difference of 7.5% (absolute). This larger difference was largely due to the higher degree of variability in the Waiakea data than was displayed at Lalamilo.

Table 5.3-Summary of *a*, *b*, and *c* values for the Liang Model (Equation 64) and comparison of predicted and experimentally-determined final log moisture content at Waiakea and Lalamilo.

Lalamilo	**a**	**b**	**c**	**Experimental MC, t=0 day (wet basis)**	**Experimental MC, t=246 day (wet basis)**	**Liang MC, t=246 days (wet basis)**
Log B	0.00137	0.00140	0	0.565	0.236	0.226
Log D	0.00191	0.00235	0	0.539	0.200	0.168
Log F	0.00198	0.00259	0	0.527	0.197	0.163
Bulk values	0.00165	0.00183	0	0.544	0.213	0.190
Waiakea	**a**	**b**	**c**			
Log B	0.0007	7.2E-05	0	0.565	0.363	0.439
Log D	0.00151	0.000204	0	0.539	0.316	0.383
Log F	0.00196	0.000287	0	0.527	0.286	0.367
Bulk values	0.00122	0.00016	0	0.544	0.327	0.402

Figures 5.12 to 5.14 compares moisture content values determined experimentally and predicted by the Liang model (coefficients derived from the experimental values) for each log at Waiakea corresponding to the data shown in Table 5.3.

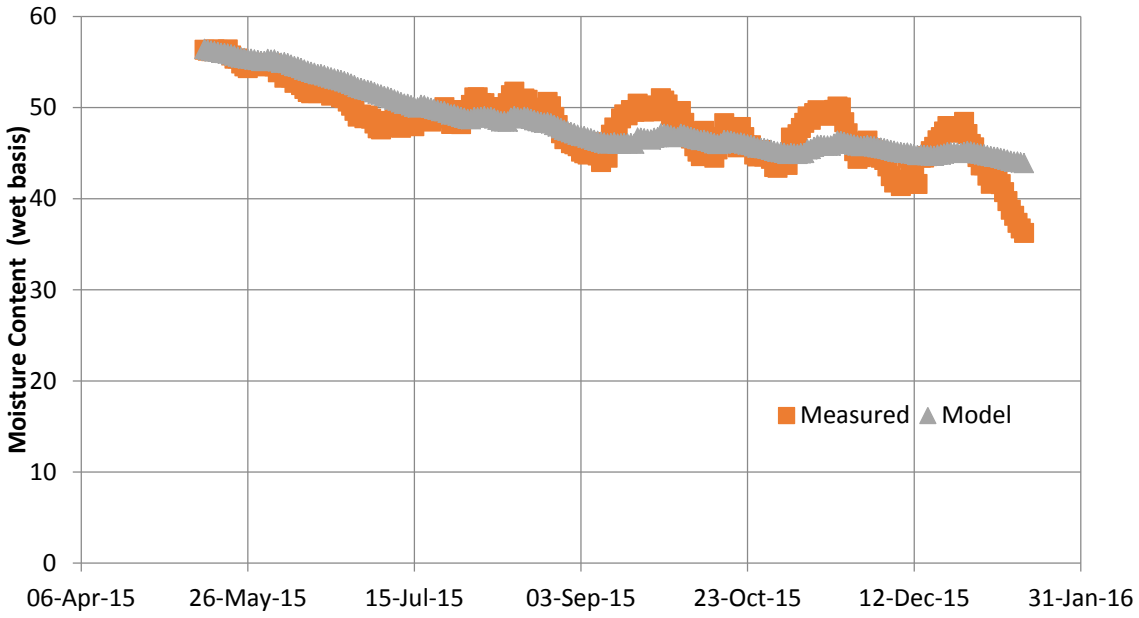

Figure 5.12-Predicted moisture content (Liang model) and experimentally determined moisture content for Waiakea Log B. Note: Liang model coefficients were derived from this experimental data set.

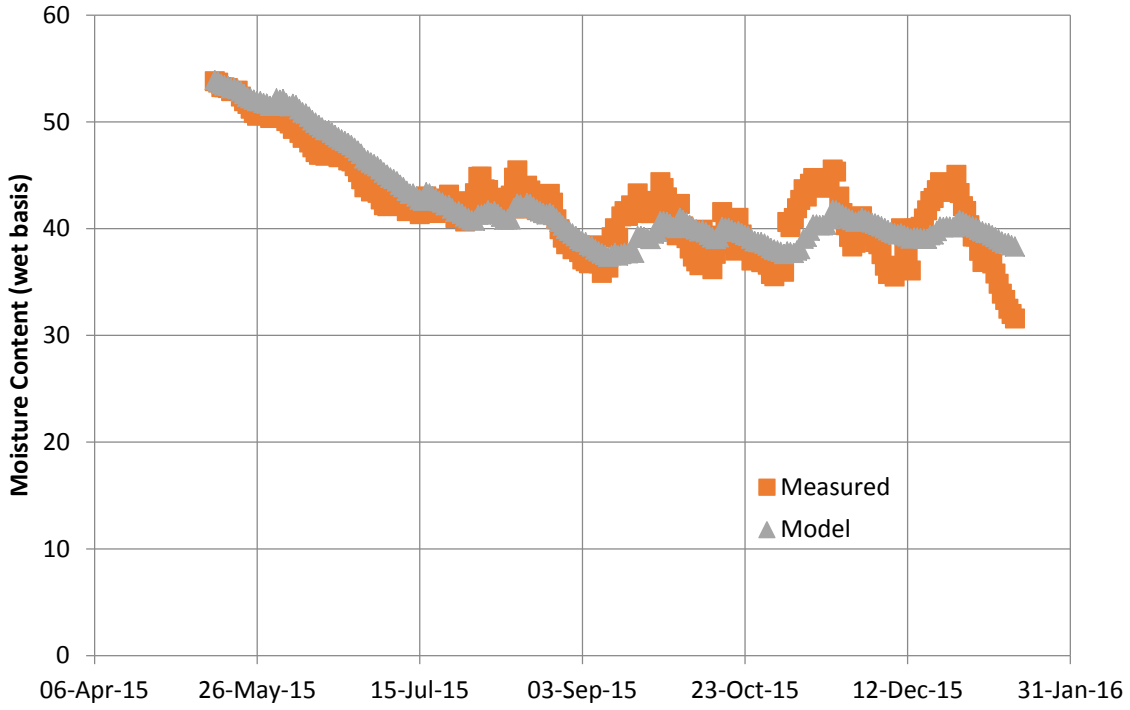

Figure 5.13- Predicted moisture content (Liang model) and experimentally-determined moisture content for Waiakea Log D. Note: Liang model coefficients were derived from this experimental data set.

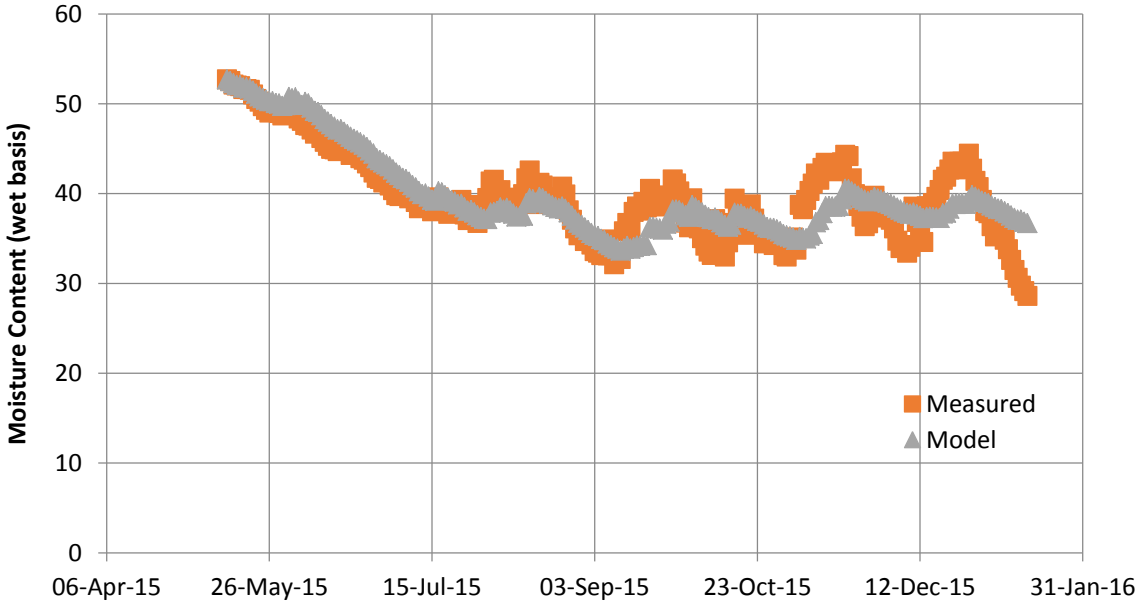

Figure 5.14- Predicted moisture content (Liang model) and experimentally-determined moisture content for Waiakea Log F. Note: Liang model coefficients were derived from this experimental data set.

Figure 5.15 compares moisture content values determined experimentally and predicted by the Liang model (coefficients derived from the experimental values) for the three logs treated as a single bulk mass at Waiakea corresponding to the data shown in Table 5.3.

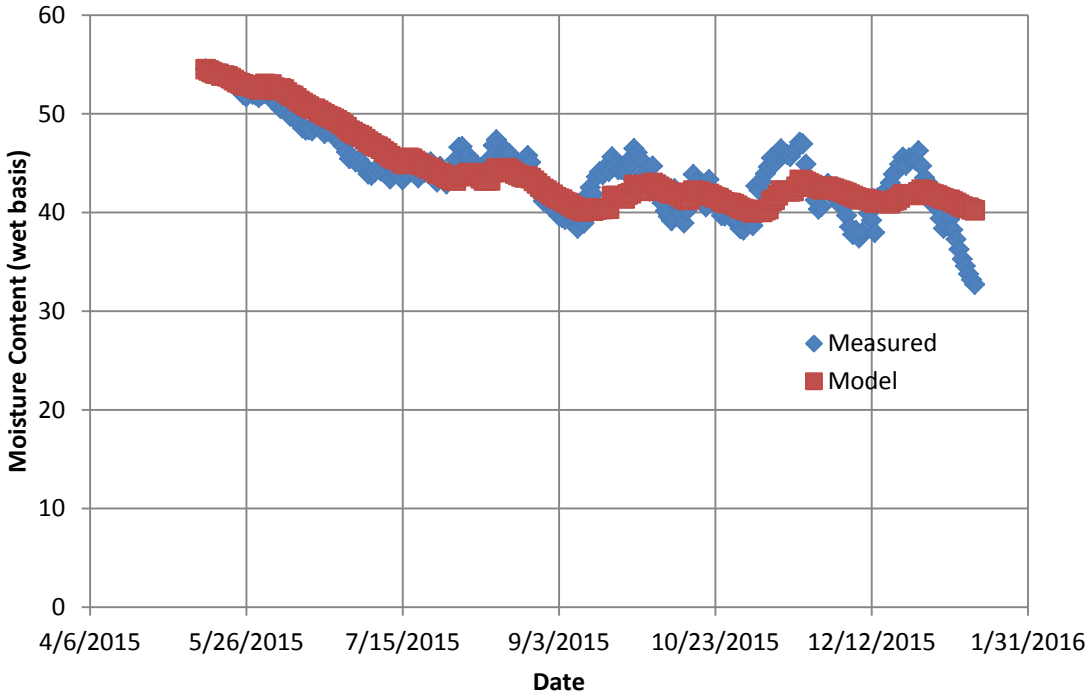

Figure 5.15- Predicted moisture content (Liang model) and experimentally-determined moisture content for three logs combined at Waiakea. Note: Liang model coefficients were derived from this experimental data set.

Figures 5.16 to 5.18 compares moisture content values determined experimentally and predicted by the Liang model (coefficients derived from the experimental values) for each log at Lalamilo corresponding to the data shown in Table 5.3. Lalamilo data has a two week gap caused by the power outage in the data logger that occurred between May 27- June 17, 2016. In Figures 5.16 to 5.18, this gap was filled by linearly interpolating between the experimental log

mass values on May 26 and June 17. Figure 5.19 displays the gap in the mass of the three logs combined.

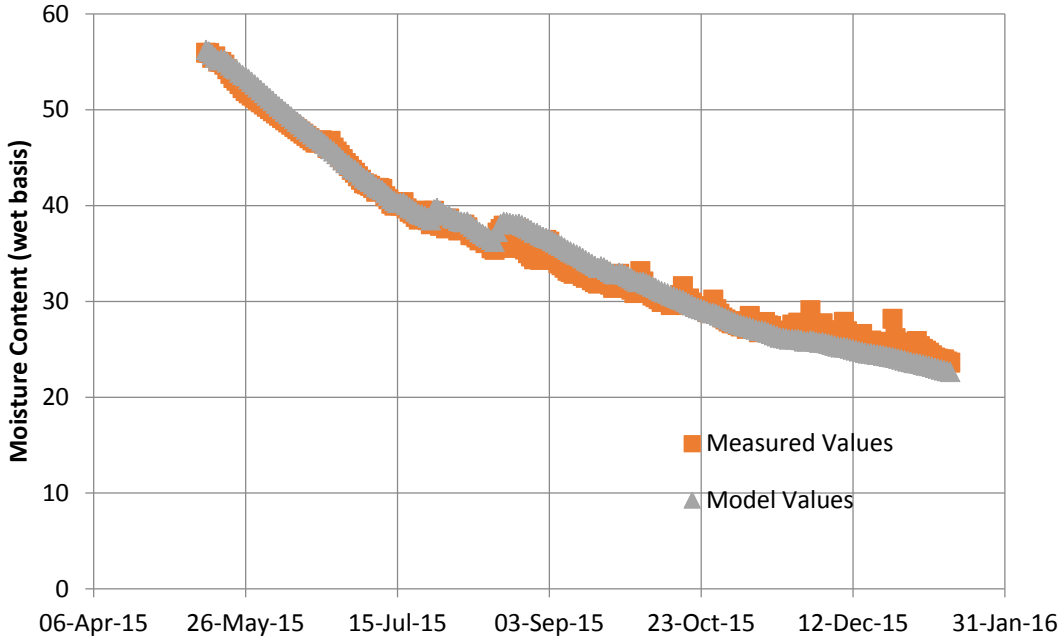

Figure 5.16- Predicted moisture content (Liang model) and experimentally-determined moisture content for Lalamilo Log B. Note: Liang model coefficients were derived from this experimental data set.

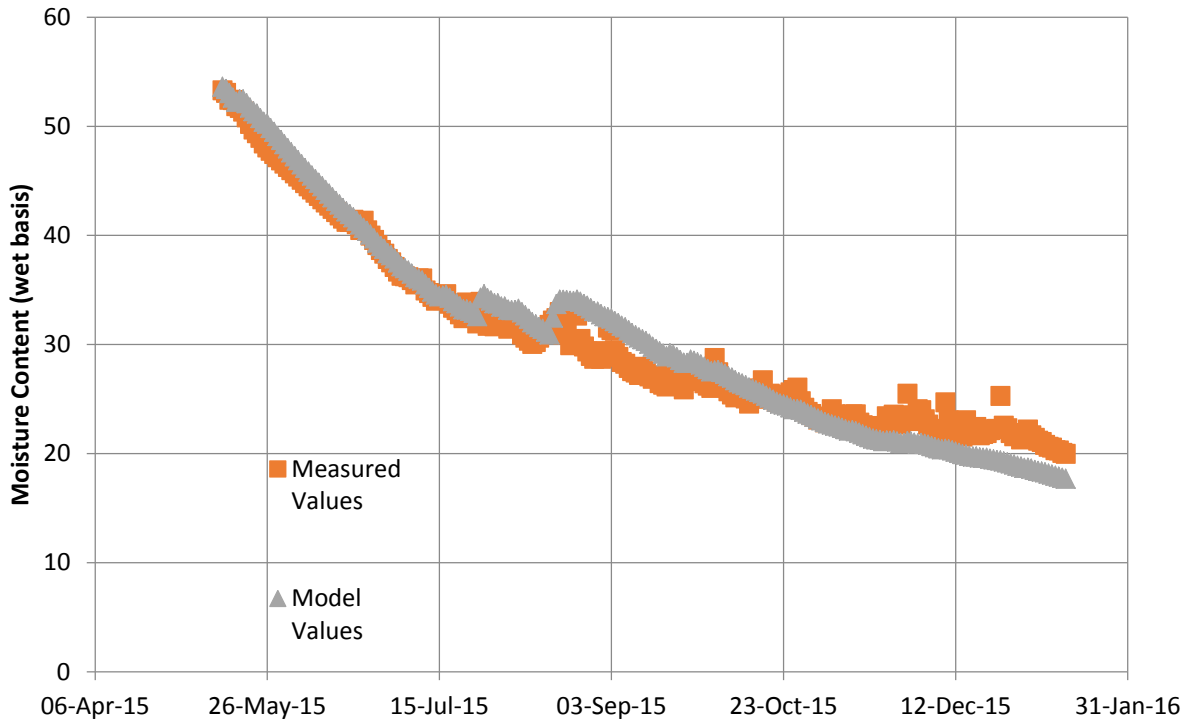

Figure 5.17- Predicted moisture content (Liang model) and experimentally-determined moisture content for Lalamilo Log D. Note: Liang model coefficients were derived from this experimental data set.

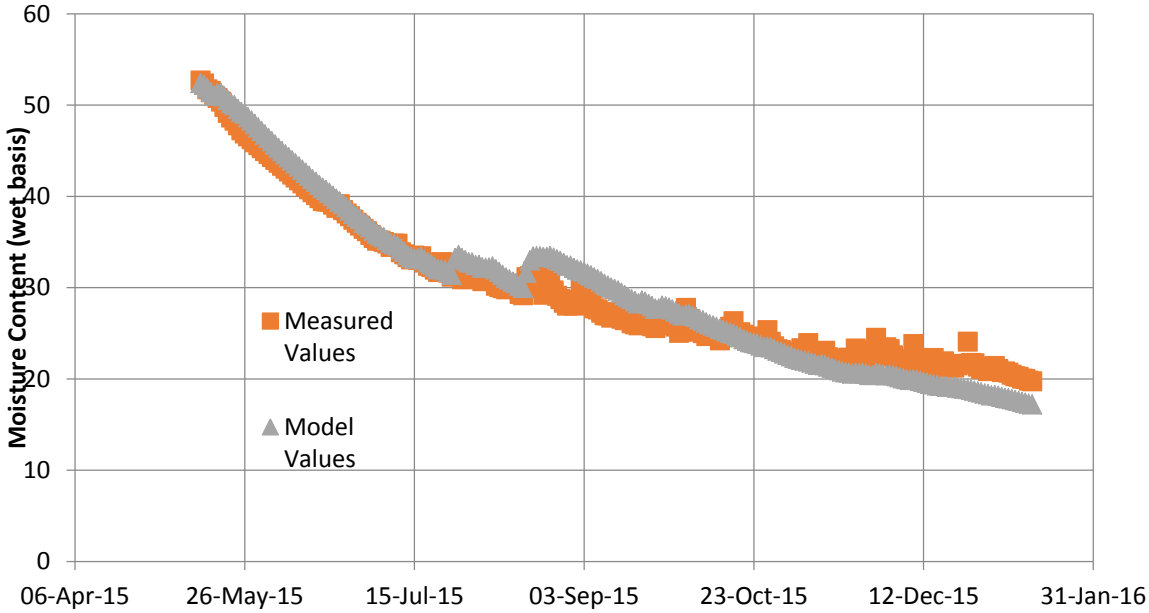

Figure 5.18- Predicted moisture content (Liang model) and experimentally-determined moisture content for Lalamilo Log F. Note: Liang model coefficients were derived from this experimental data set.

Figure 5.19 compares moisture content values determined experimentally and predicted by the Liang model (coefficients derived from the experimental values) for the three logs treated as a single bulk mass at Waiakea corresponding to the data shown in Table 5.3.

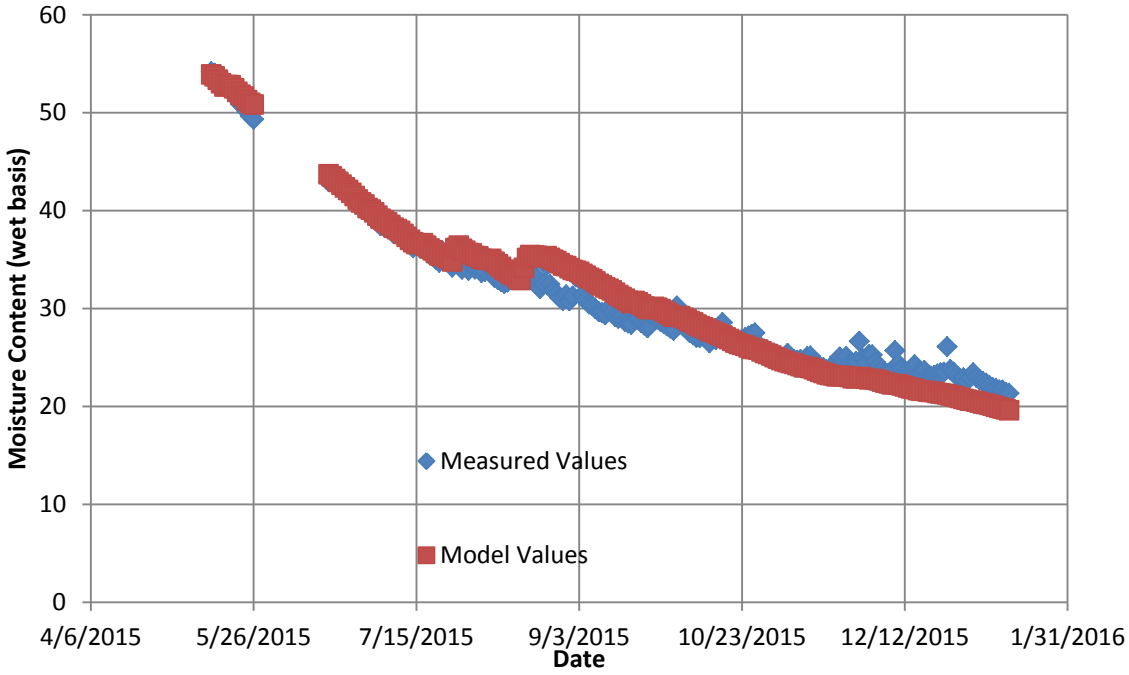

Figure 5.19- Predicted moisture content (Liang model) and experimentally-determined moisture content for three logs combined at Lalamilo. Note: Liang model coefficients were derived from this experimental data set.

The *a*, *b* and *c* values for each log were used to predict the moisture contents for the other logs dried in the same location to assess their interchangeability. Table 5.4 summarized the results of this analysis predicting log moisture contents after 246 days of drying.

Table 5.4-Predicted values of log moisture content after t= 246 days using *a*, *b*, and *c* values from logs at each site to predict the moisture content of the other logs at the same site.

Lalamilo			
Sum of evapotranspiration = 918 mm		Sum of Precipitation = 248 mm	
	----------Predicted MC, wb ----------		
a , b, c values from	**Log B**	**Log D**	**Log F**
Log B	0.226	0.216	0.211
Log D	0.175	0.168	0.164
Log F	0.174	0.166	0.163
Experimental	0.236	0.200	0.197
Waiakea			
Sum of evapotranspiration = 771 mm		Sum of Precipitation = 4,020 mm	
	----------Predicted MC, wb ----------		
a,b,c values from	**Log B**	**Log D**	**Log F**
Log B	0.439	0.401	0.393
Log D	0.419	0.383	0.376
Log F	0.410	0.375	0.367
Experimental	0.363	0.316	0.286

Table 5.5 compares the predicted final moisture content values summarized in Table 5.4 with the experimentally determined moisture content values for each log. Comparison of the final moisture values after 246 days reveals differences ranging from 1 to 6% (absolute) at Lalamilo and 3 to 12% (absolute) at Waiakea. The use of final moisture content as a comparator is more suited to Lalamilo's smoother moisture content curve than Waiakea's drying curve which is characterized by greater variability. While Waiakea model predictions capture some of this variability (Figures 5.12 to 5.15), the final moisture values used for comparison were in a period of rapid drying not captured by the model.

Table 5.5- Differences between the predicted values of log moisture content after 246 days using *a*, *b*, and *c* values from logs at each site to predict the moisture content of the other logs at the same site (values from Table 5.4) and the experimentally determined moisture content after 246 days.

Lalamilo	**Differences between Predicted and Experimental MC values**		
a , b, c values from	**Log B**	**Log D**	**Log F**
Log B	-0.010	0.016	0.014
Log D	-0.061	-0.032	-0.034
Log F	-0.062	-0.034	-0.035
Waiakea	**Differences between Predicted and Experimental MC values**		
a , b, c values from	**Log B**	**Log D**	**Log F**
Log B	0.077	0.104	0.124
Log D	0.039	0.067	0.088
Log F	0.031	0.060	0.081

Since there were apparent differences between the *a*, *b*, and *c* values determined for the two sites, the applicability of using Lalamilo's values to predict Waiakea's logs drying behavior, and vice versa, was investigated, i.e. the *a*, *b*, and *c* values from one site were used with the initial moisture content and weather data sets from the other site to see if the results were similar. The results of these exercises are summarized in

Table 5.6. For each log, the first two data columns contain the final moisture content values (*t*=246 days) determined experimentally and using the Liang model parameters derived for the log at the location it was dried. The last data column contains the final moisture content for each log predicted using the Liang model parameters from the same log section at the other drying location, e.g. Lalamilo Log B Liang model parameters used to predict final moisture content of Log B at Waiakea.

The Waiakea model parameters predicted the final moisture content of individual Lalamilo logs with absolute values of the differences from the experimental results in a range from 6 to 10% (absolute). Model parameters derived from the three Waiakea logs combined as a single mass improved the agreement with the experimental value, differing by <4% (absolute).

The Lalamilo model parameters derived at the drier site were not able to predict the drying behavior at the wetter Waiakea location as shown in

Table **5.6**. Unrealistic moisture contents of greater than 100% were predicted. This difference in the apparent applicability of the two models results largely from the difference in the value of the b coefficient for precipitation (e.g. 0.0018 and 0.00016 for the combined log drying models at Waiakea and Lalamilo, respectively). The b value from the drier location, Lalamilo, was larger and when applied at the wetter location resulted in overestimated values of moisture content. Conversely, the smaller b value derived at the wetter location, Waiakea, predicted more representative values. Further work is warranted to understand the full range of model applicability across a range of climatic zones. Graphs for each log using the a, b, and c values from logs at the other drying site are presented in Appendix C.

Table 5.6-Predicted final moisture contents (decimal) using the Waiakea model values to predict the Lalamilo drying behavior and vice versa.

Lalamilo	Experimental MC, t=246 day (wet basis)	Liang model final moisture predicted using *a*,*b*,*c* from Lalamilo	Liang model final moisture predicted using *a*,*b*,*c* from Waiakea
Log B	0.236	0.226	0.302
Log D	0.200	0.215	0.142
Log F	0.197	0.209	0.093
Logs Combined	0.218	0.190	0.184
Waiakea		Liang model final moisture predicted using *a*,*b*,*c* from Waiakea	Liang model final moisture predicted using *a*,*b*,*c* from Lalamilo
Log B	0.363	0.439	54.366
Log D	0.316	0.383	1579.273
Log F	0.286	0.367	3755.592
Logs Combined	0.327	0.402	235.704

Waiakea a,b, c parameters were used in the scenario analysis because they produced reasonable values for both Waiakea and Lalamilo. Drying eucalyptus at the seven plantation locations shown in Figure 4.10 was investigated using the Liang model and Waiakea-derived values of *a*, *b*, and *c* for the bulk log mass. Assuming an initial moisture content of 56% wet basis and a six month drying period, the final moisture content was predicted assuming the harvest date was the first of every month. Figure 5.20 summarizes the results. Predicted final moisture content values range from 20% to nearly 70% wet basis. Trees harvested and dried at the Hauola site were generally predicted to have the lowest moisture content with the Weloka and Waipao sites exhibiting similar values. Trees harvested at the Hilo site were predicted to have very small moisture loss or, more frequently, moisture gain. Hamakua, Pahala, and Waipunalei were characterized by intermediate drying behavior with final values ranging from 30 to 50% over the year. April and May harvest dates at any of the locations were predicted to achieve the lowest moisture contents after six months of drying. These are preliminary predictions and should be validated experimentally.

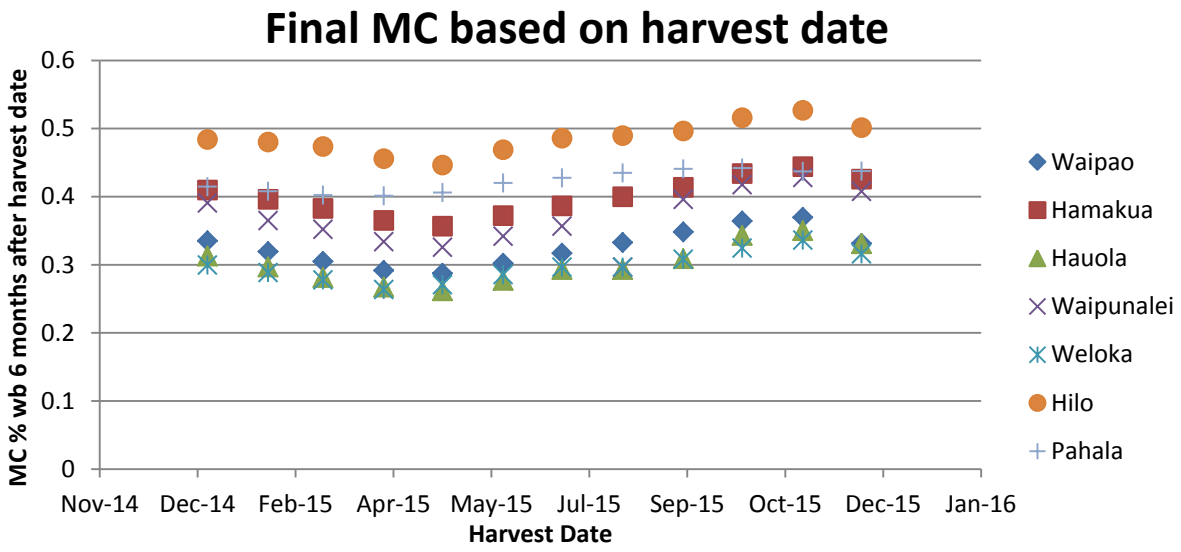

Figure 5.20- Predicted moisture contents after six months, using the *a,b, and c* values from Waiakea and assuming an intitial moisture content of 0.56 (starting the first of every month).

Hauola exhibited the lowest, six month moisture content for all harvest dates and was chosen as the example site to determine the time necessary to dry logs. The final moisture content was predicted for drying periods of seven through fourteen months. For every length of time, starting the harvest in April or May yielded the lowest moisture contents as shown in Figure 5.21.

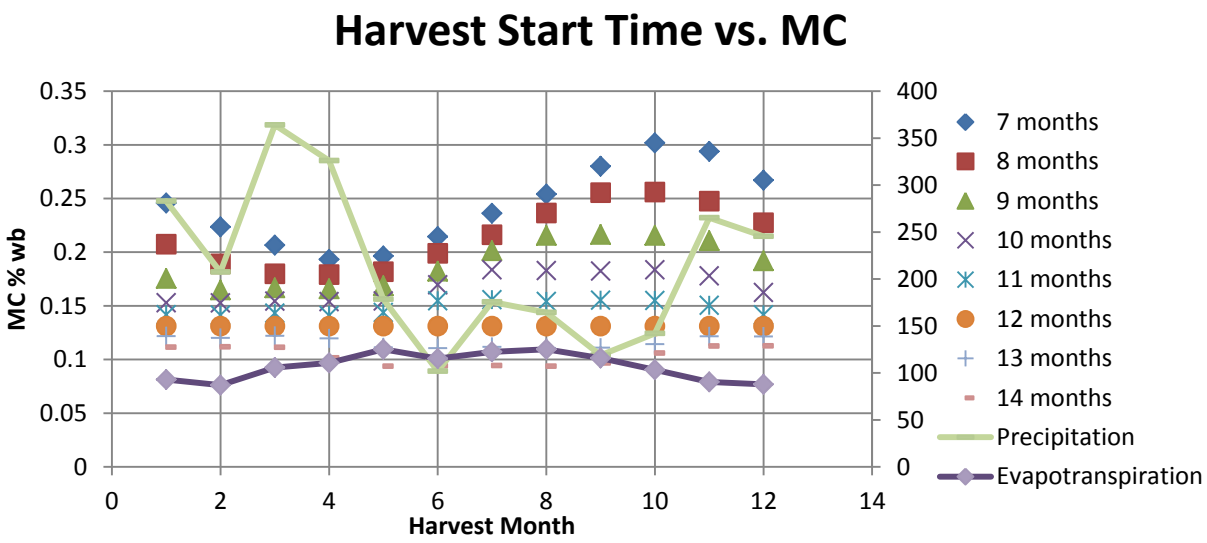

Figure 5.21-Predicted final moisture contents for monthly harvest dates and drying durations of 7 to 14 months. Monthly evaporation and precipitation values are read off of the right hand axis.

The Liang Model relied on daily weather data for the test period and the *Interactive Climate Atlas* provides average monthly data (Giambelluca et al., 2014). To determine if it was possible to make accurate predictions using monthly values, the daily temperature data was used to produce monthly averages and the total monthly solar insolation were used to calculate a monthly evapotranspiration value. The monthly precipitation total and evapotranspiration value were used with the *a*, *b*, and *c* coefficients derived from the daily experimental data to predict log moisture content at monthly intervals. This analysis is summarized in Figure 5.22 at Waiakea and Figure 5.23 at Lalamilo and generally supports the application of the model coefficients derived from daily data with monthly averages. This should be validated further with additional experimental work, but appears to support the use of climate axis data for predicting log moisture and drying times.

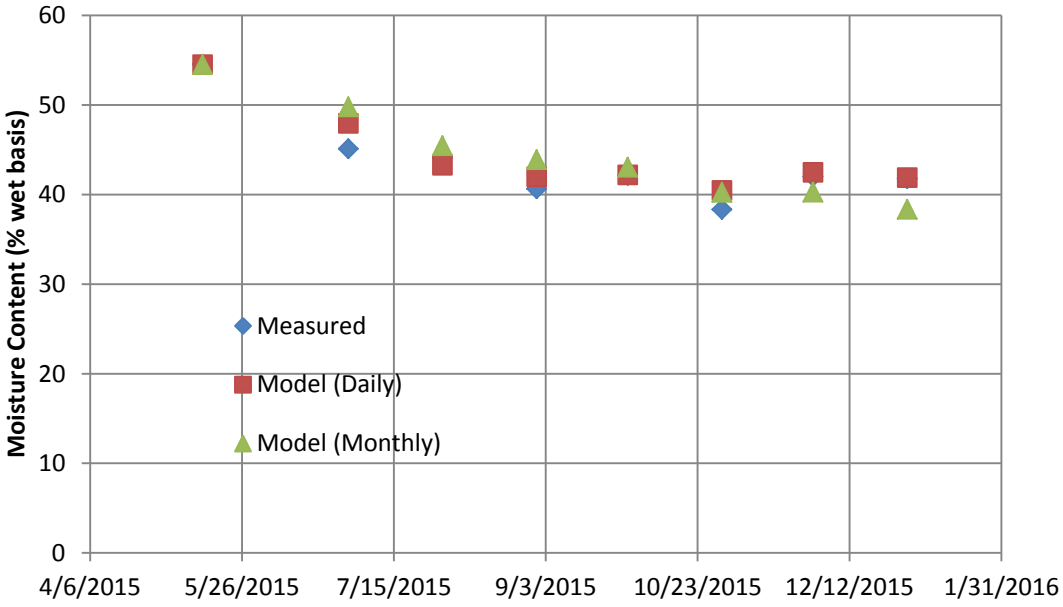

Figure 5.22- Waiakea moisture content measured values and modeled values with monthly and daily averages.

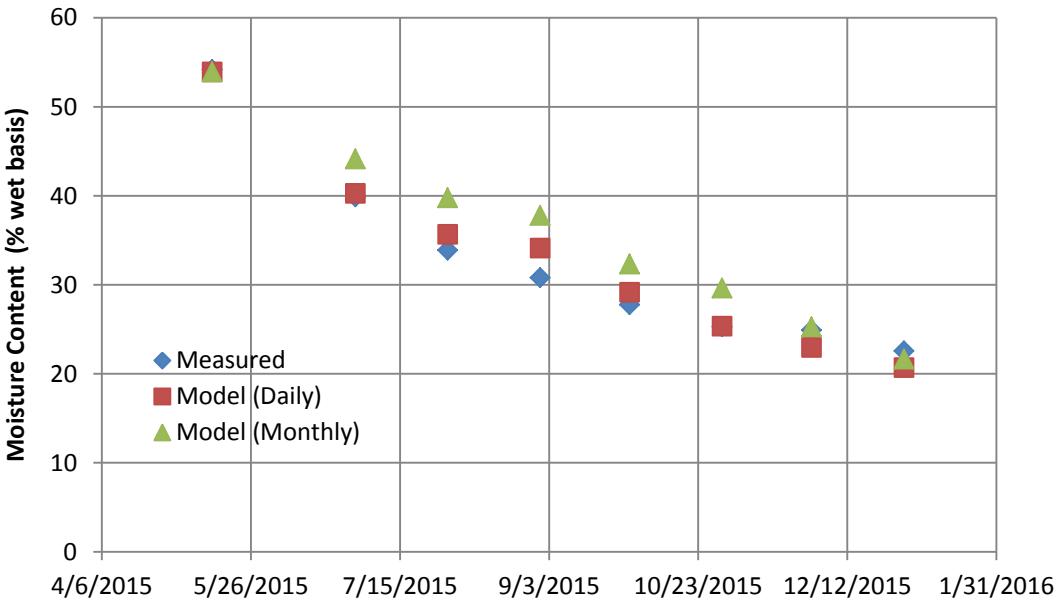

Figure 5.23- Lalamilo moisture content measured values and modeled values with monthly and daily averages.

5.3 Phenomenological Model Results

The phenomenological model of log drying was formulated using the COMSOL equation library. Although initial consideration was given to simplifying assumptions, the final formulation Table 5.7 summarizes different model formulations that included (1) hourly wind speed as determined from the weather station data, (2) average wind speed, (3) radial diffusion of moisture in the log, and (4) and impermeable boundary layer on the outer surface of the

cylindrical log. The impermeable boundary layer represents bark. In COMSOL an impermeable boundary layer, means that no mass will move through the boundary. If present, the impermeable boundary condition was imposed for the top and bottom of the log.

Table 5.7-File names for results from models formulations that included different physical phenomena.

File names for model formulations	Figure No.	Hourly Wind Data	Wind Speed Average	Radial Diffusion	Impermeable Boundary
20150916 Waiakea Log B with wind	5.24	yes	no	yes	no
20150917 Waiakea Log B no wind pl	5.25	no	no	yes	no
20150923 Waiakea Log B wind no rad diff	5.26	yes	no	no	no
20150930 Waiakea Log B no rad diff	5.27	no	no	no	no
20151009 Waiakea Log B Thin wind Impermeable boundary diffrad	5.28	yes	no	yes	yes
20151002 Waiakea Log B thin impermeable boundary with average wind speed	5.29	no	yes	yes	yes
20151002 Waiakea Log B thin impermeable boundary	5.30	no	no	yes	yes

The results of the seven different model formulations are presented in Figures 5.24 through 5.30 as scatter plots comparing the results from the different models with the measured data for Waiakea Log B from May 13 to Sep 3, 2015.

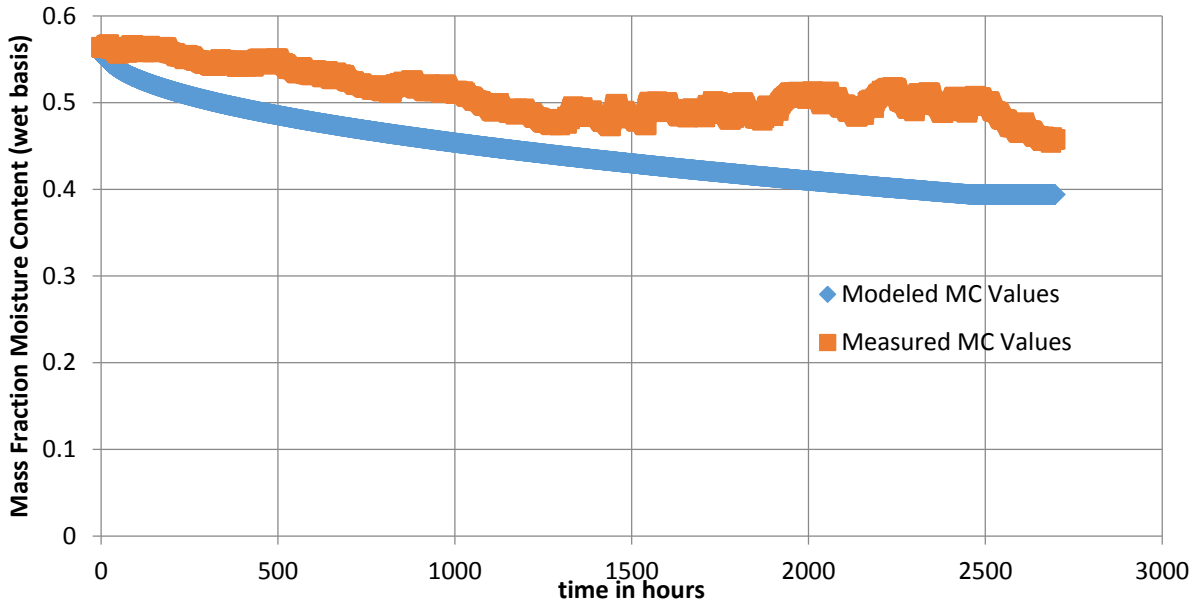

Figure 5.24-Waiakea Log B experimentally determined moisture content compared to prediction by COMSOL model formulated with hourly wind data and with radial diffusion.

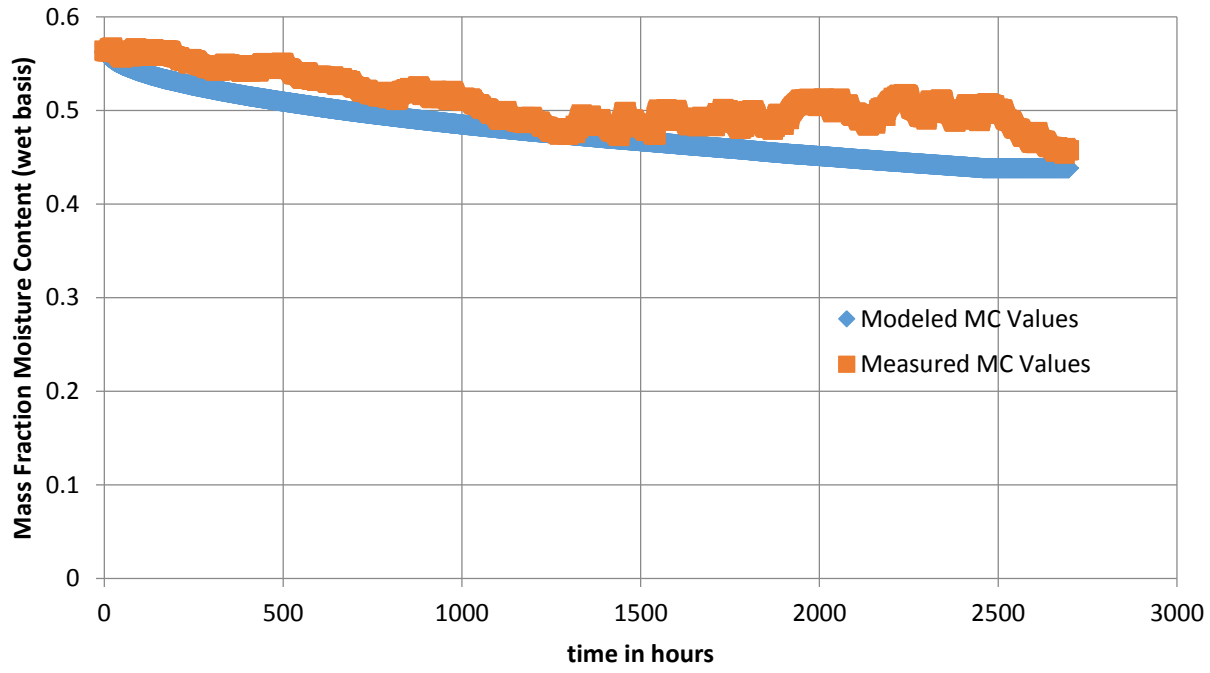

Figure 5.25-Waiakea Log B experimentally determined moisture content compared to prediction by COMSOL model formulated without wind and with radial diffusion model

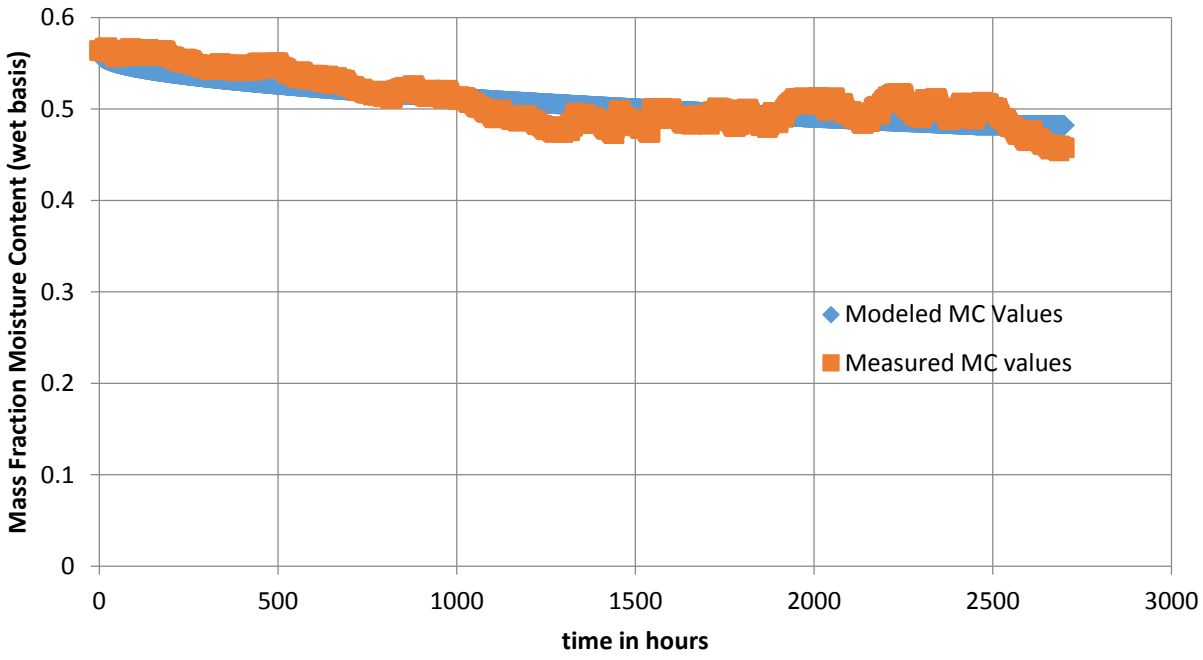

Figure 5.26-Waiakea Log B experimentally determined moisture content compared to prediction by COMSOL model formulated with hourly wind data and without radial diffusion

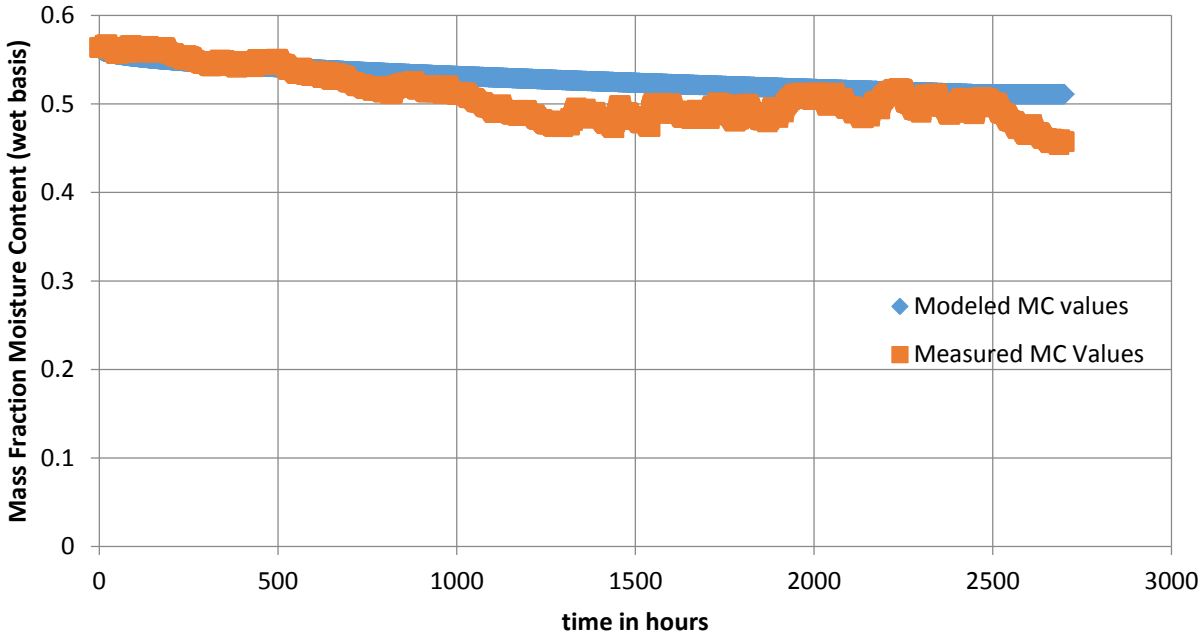

Figure 5.27-Waiakea Log B experimentally determined moisture content compared to prediction by COMSOL model formulated with no wind and without radial diffusion

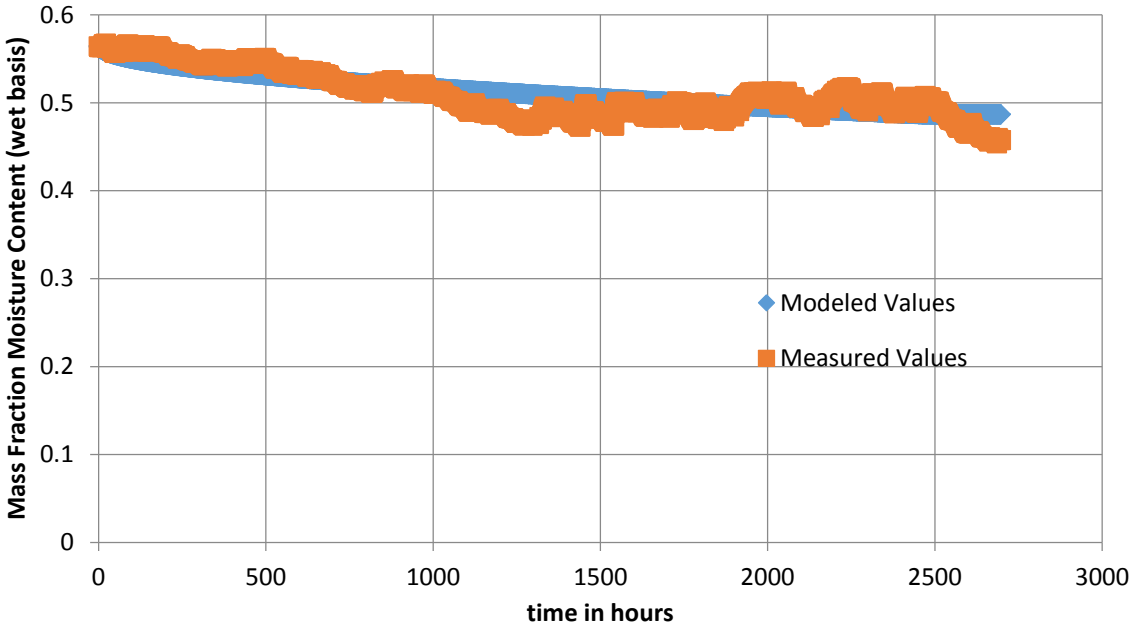

Figure 5.28-Waiakea Log B experimentally determined moisture content compared to prediction by COMSOL model formulated with wind, radial diffusion, and a thin impermeable boundary layer on the sides of the log cylinder.

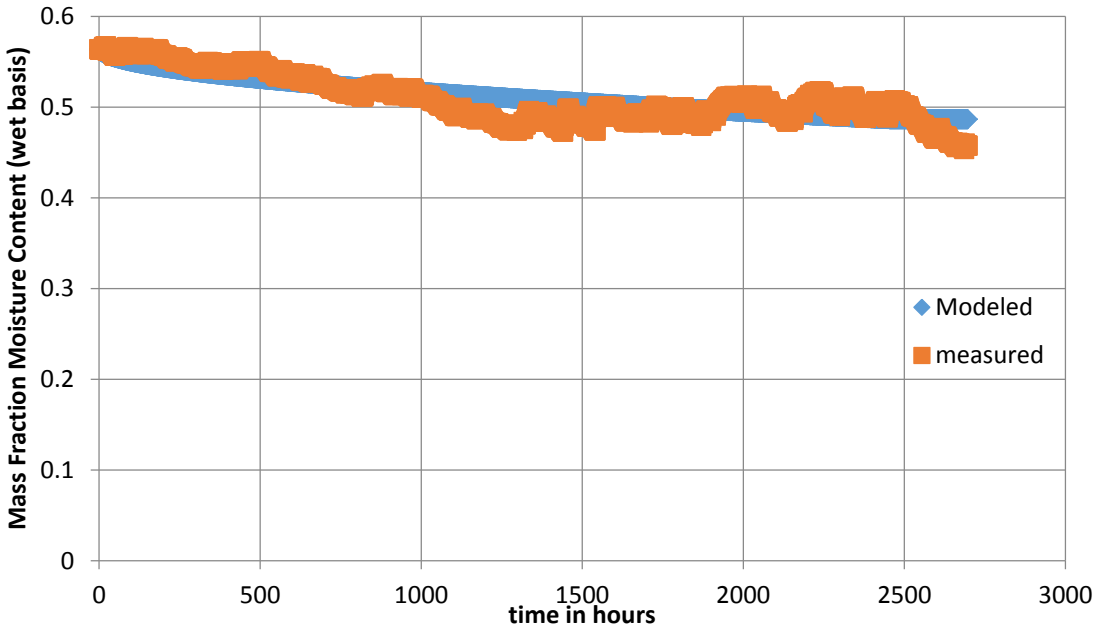

Figure 5.29-Waiakea Log B experimentally determined moisture content compared to prediction by COMSOL model formulated with radial diffusion, thin impermeable boundary layer on the sides of the log cylinder, and an average wind speed.

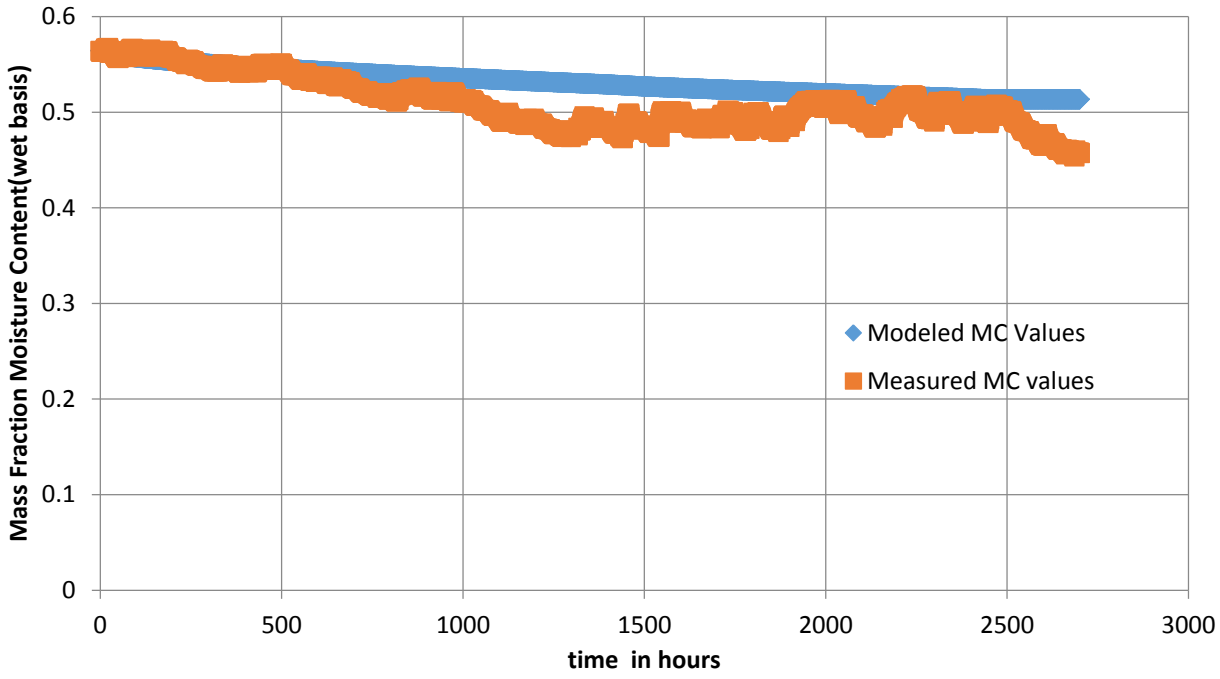

Figure 5.30-Waiakea Log B experimentally determined moisture content compared to prediction by COMSOL model formulated with radial diffusion, thin impermeable boundary layer and no wind speed data.

With wind speed included in the formulation, the COMSOL computation was time consuming. With an interpolated function calculating the wind speed for every hour, the model required 96 hours to complete the simulation. Without wind speed, the same model would complete the simulation in less than ten minutes. Since wind speed affected the outcome of the model, it was necessary to include it. Instead of using hourly wind speed, a constant average wind speed was used for the entire time period. Under this scenario, the model required 6 hours 27 minutes to complete the simulation. The results did not significantly differ from the hourly wind speed.

To determine the reason for the model similarities, the mean average was taken for all weather variables to determine which ones more greatly affected the outcome of the model. The average values for Waiakea and Lalamilo are shown in Table 5.8.

Table 5.8- Average hourly weather variables at Waiakea and Lalamilo experimental sites.

	Ambient air temperature (°C)	Rainfall (mm/ hour)	Solar insolation (MJ/m^2)	Windspeed (m/s)	Relative Humidity (%)
Waiakea	**22.2**	0.66	0.59	0.66	85.9
Lalamilo	**19.5**	0.04	0.72	3.24*	86.1*

*Source: (Giambelluca *et al.*, 2014b)

The simulations were repeated using Lalamilo conditions. By examining plots of the measured values and the model results, it was determined that the following set of assumptions, average wind speed, no impermeable boundary layer, and radial diffusion, produced the best agreement as shown in Figure 5.31. This model is better suited to the low rainfall conditions at Lalamilo because the reabsorption of water present due to rainfall was not included.

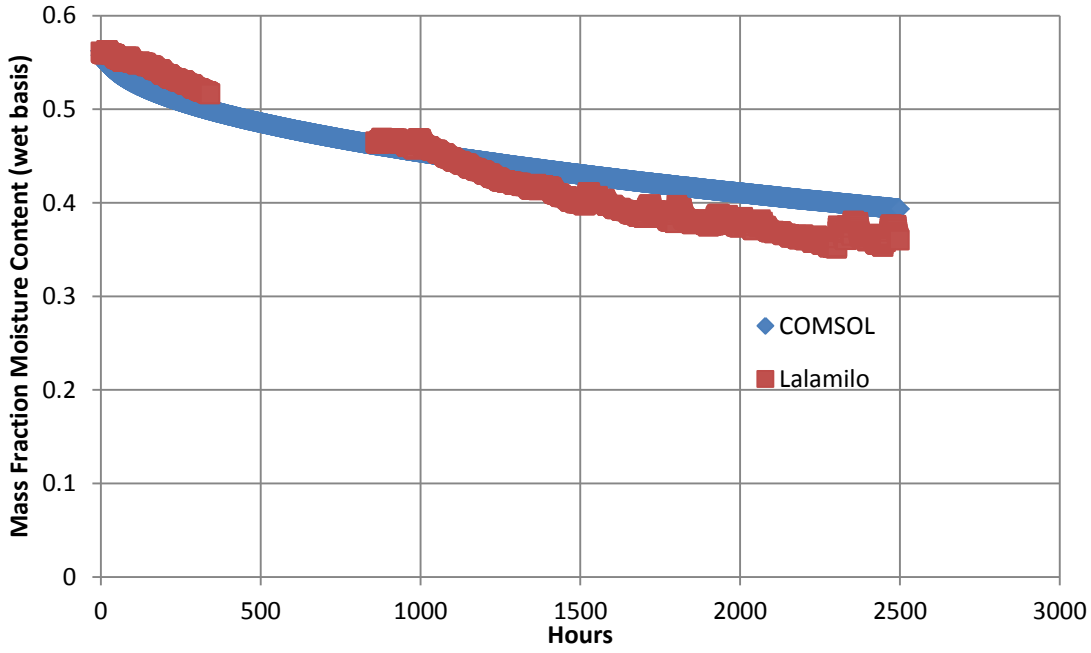

Figure 5.31-Comparison of the model and experimental results with an average windspeed, without an impermeable boundary layer, and with radial diffusion.

The phenomenological model successfully produced a distribution maps for temperature, liquid concentration and vapor concentration in the log interior. Both temperature and vapor distributions changed throughout the day. Figure 5.33 presents the temperature distribution across the domain at four hour intervals over a twenty four hour period. Note that the upper surface of the log and the surrounding air show elevated temperatures by noon. The heat diffuses into the log interior elevating the temperature as the day progresses. While the air temperature returns to an overnight low temperature at midnight, the interior of the log retains heat and a slightly elevated temperature relative to its initial temperature distribution.

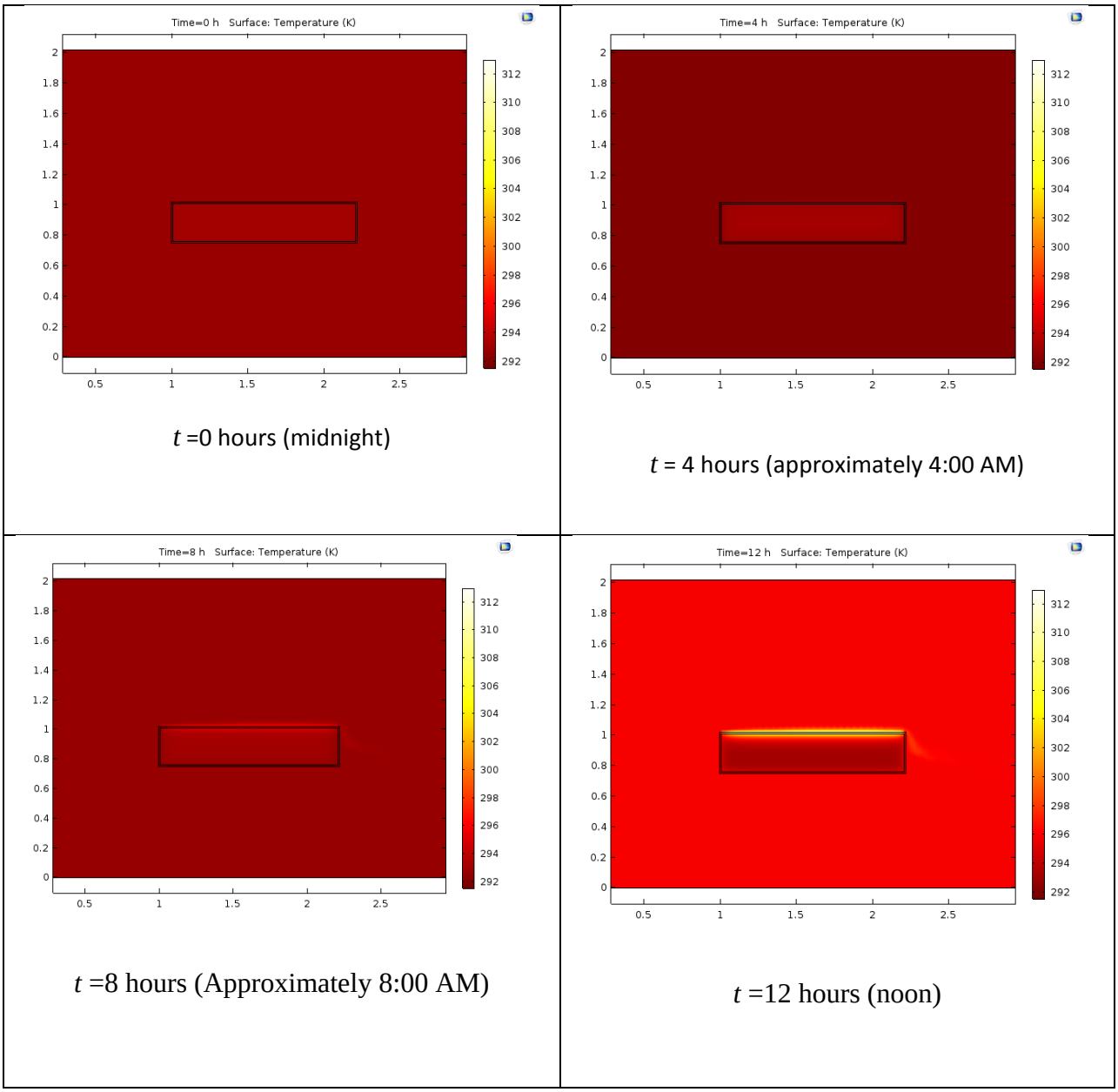

Figure 5.32-Temperature distributions predicted using COMSOL at four hour intervals throughout the first day of the 193 day simulation.

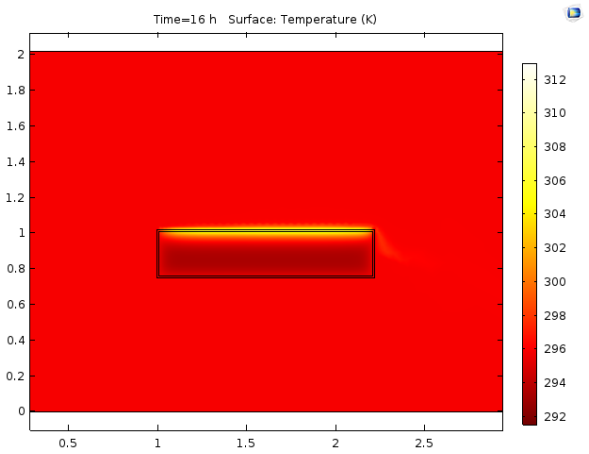

t = 16 hour (4:00 pm)

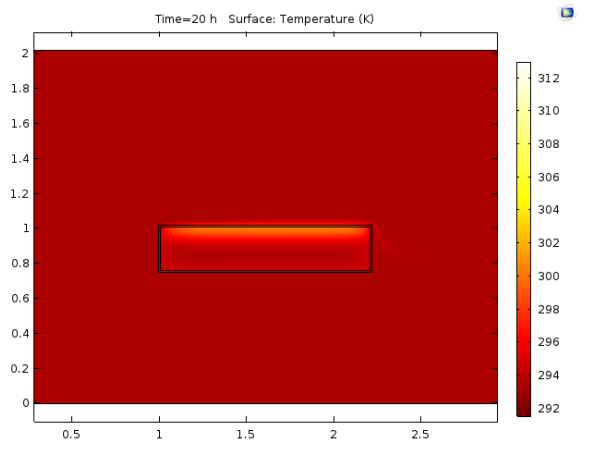

t = 20 hours (8 PM)

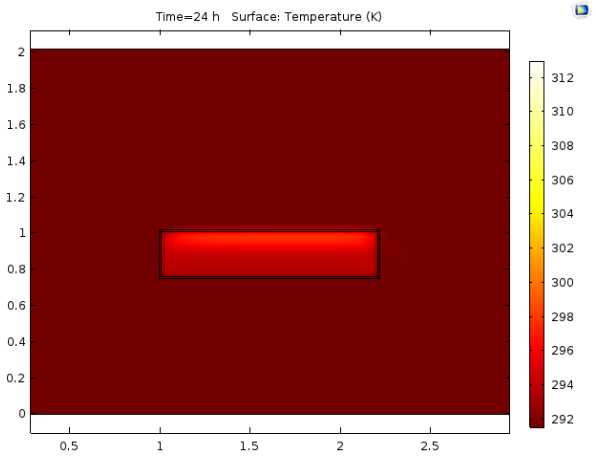

t =24 hours (midnight)

Figure 5.33-Continued. Temperature distributions predicted using COMSOL at four hour intervals throughout the first day of the 193 day simulation.

Figure 5.33 presents the COMSOL simulation results for the water vapor distribution across the domain at five points in time during the 193 day simulation. Initially there is no water vapor in the interior of the log as depicted by its dark blue color. Over time the vapor concentration increases and approaches that of the surrounding air.

Figure 5.34 shows the evolution of the liquid water concentration in the log over the 193 day simulation. Initial liquid moisture content is high as depicted by the solid red color of the log. The surrounding air has no liquid water present, appearing blue. The five points in time shown in Figure 5.35 show the liquid water distribution evolve over time, with the surface concentrations showing lower values while the interior regions remain wet. The liquid concentration gradient moves inward over time and the upper surface of the log that is exposed to solar radiation exhibits a wider drying zone than the lower surface (see t=2230 hours).

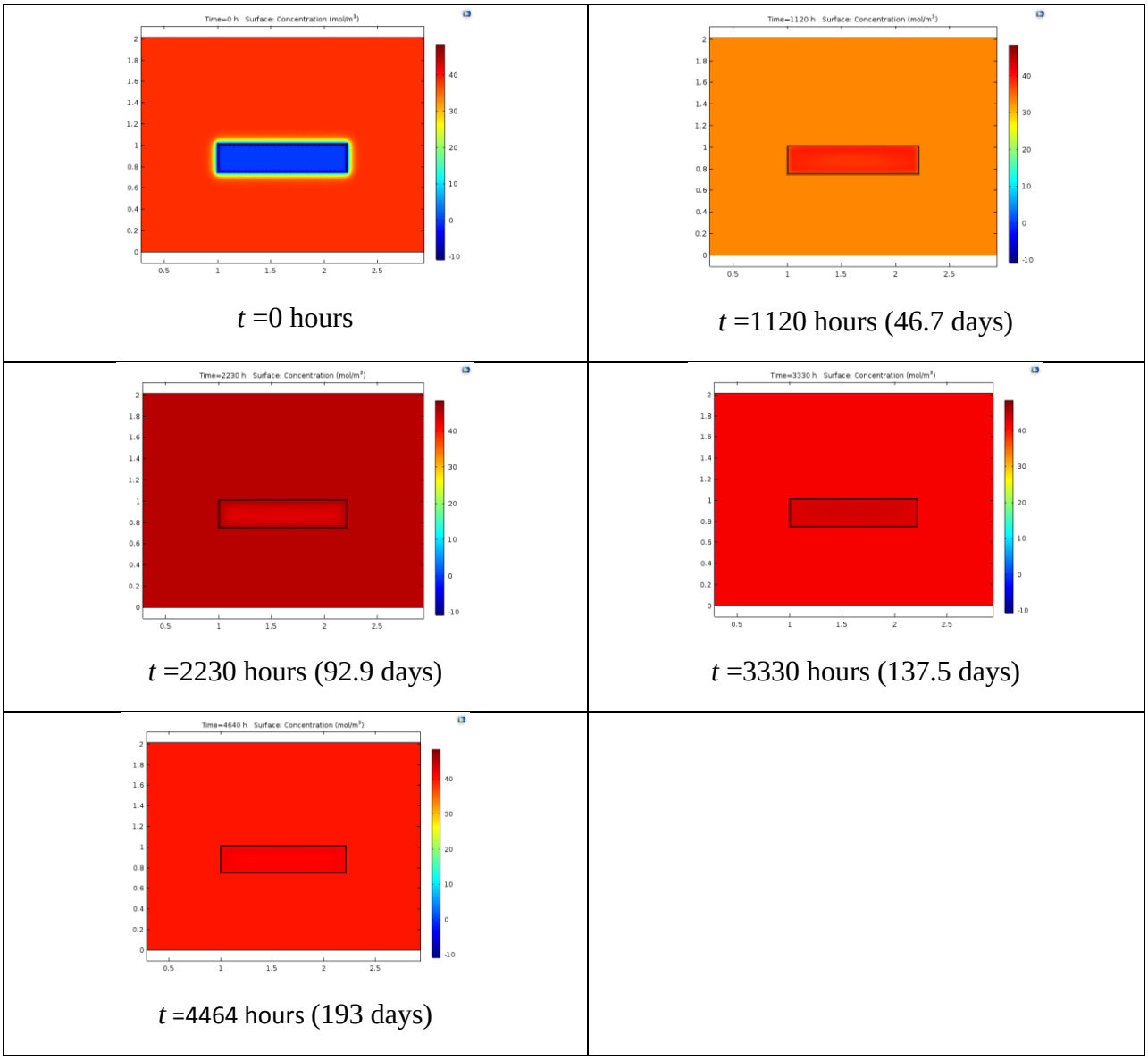

Figure 5.34-Water vapor concentration distributions predicted using COMSOL during the 193 day drying history.

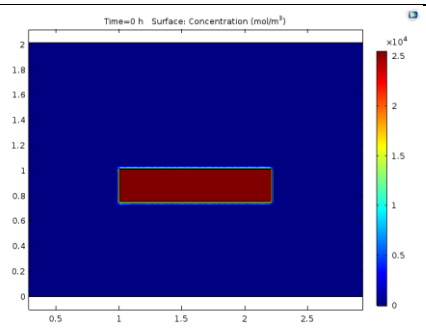

t= 0 hours

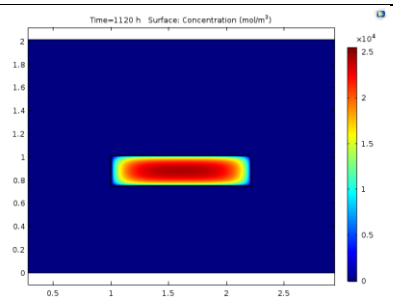

t =1120 hours (46.7 days)

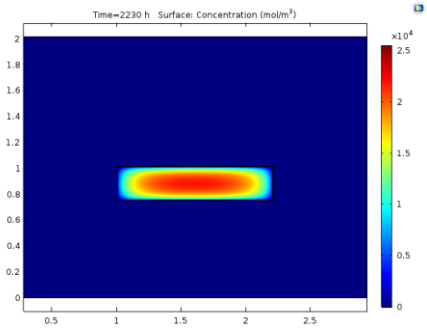

t =2230 hours (92.9 days)

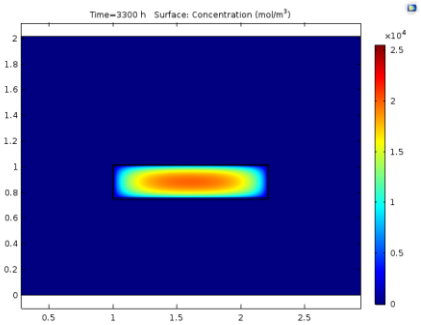

t =3300 hours (137.5 days)

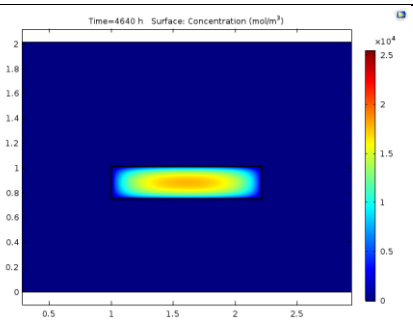

t = 4644 hours (193 days)

Figure 5.35-Liquid water concentration distributions predicted using COMSOL during the 193 day drying history.

Cross sectional line plot profiles for temperature, liquid and vapor concentrations were developed. Figure 5.36 shows the temperature profile from the bottom of log (x=0) to the top of the log through the cylindrical axis. Note that the top of the log located on the right hand side of the graph has a temperature history that reflects greater heat addition from solar radiation. Temperature variation on the bottom of the log is less pronounced. The profile also shows the retention of heat by the interior of the log during periods of cooling as shown in the 24 hour line.

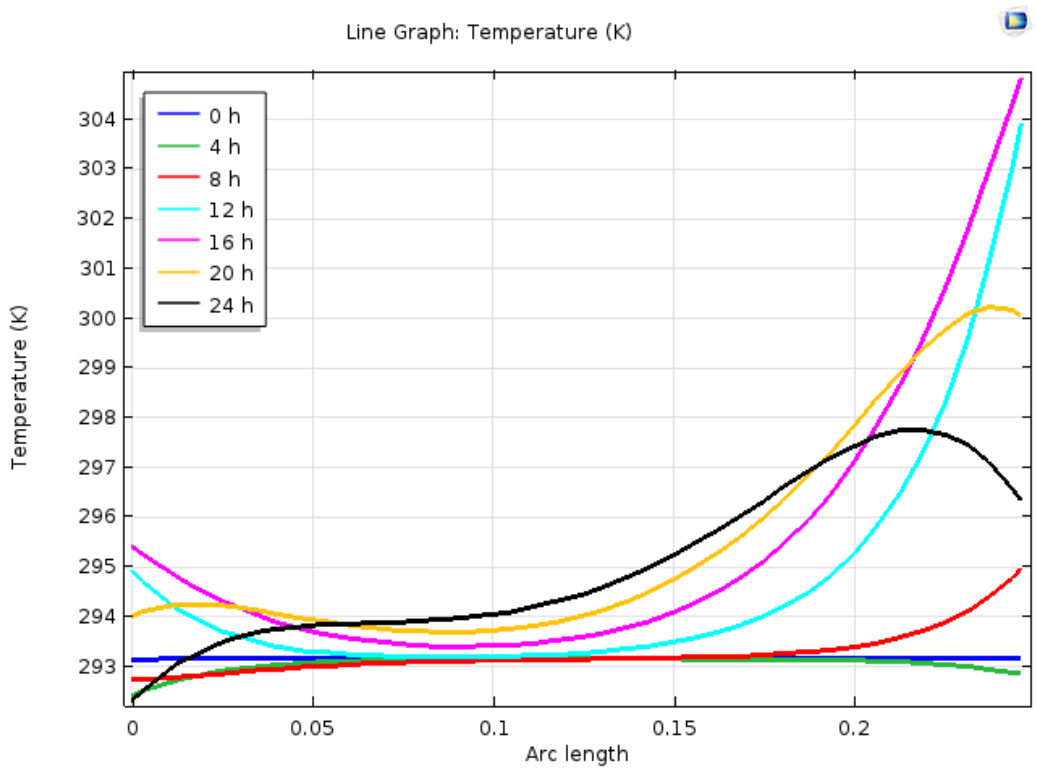

Figure 5.36-Cross sectional profile across the diameter for temperature for every hour for a typical day (x=0 m is the bottom of the log and x=0.25 m is the top of the log)

Figures 5.36 and 5.37 present vapor concentration cross sectional line profiles across the diameter and the longitudinal direction (from one end of log to the other), respectively. From the initial conditions of no water vapor present in the interior, the vapor concentration first increases

during the simulation and then approaches a reduced value reflecting the vapor concentration of the surrounding air.

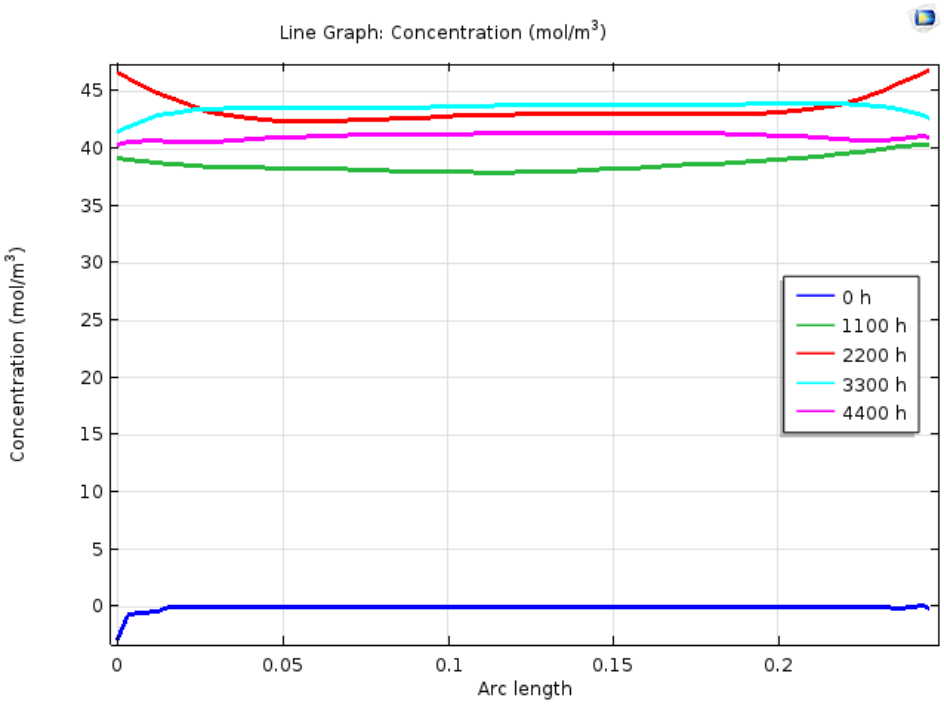

Figure 5.37- Vapor concentration plots across the log diameter passing through the longitudinal axis over 4644 hours.

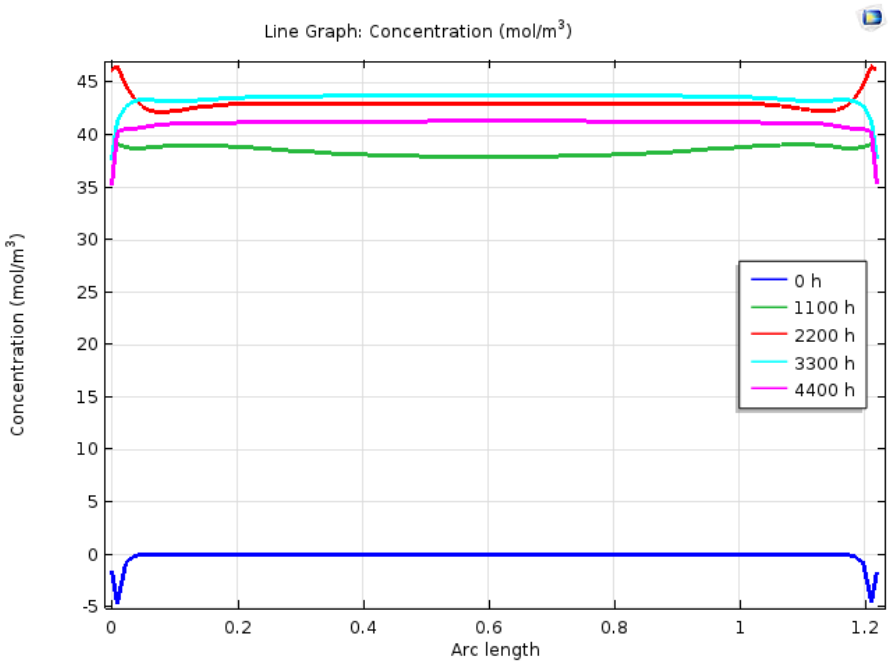

Figure 5.38— Vapor concentration plots along the log longitudinal axis over 4644 hours.

Figures 5.38 and 5.39 present liquid water concentration cross sectional line profiles in the radial direction and the longitudinal direction (from one end of log to the other), respectively. The liquid concentration decreases steadily in both figures over the course of the simulation period. In both cases, the interior concentrations remained higher that the concentrations near the log surfaces.

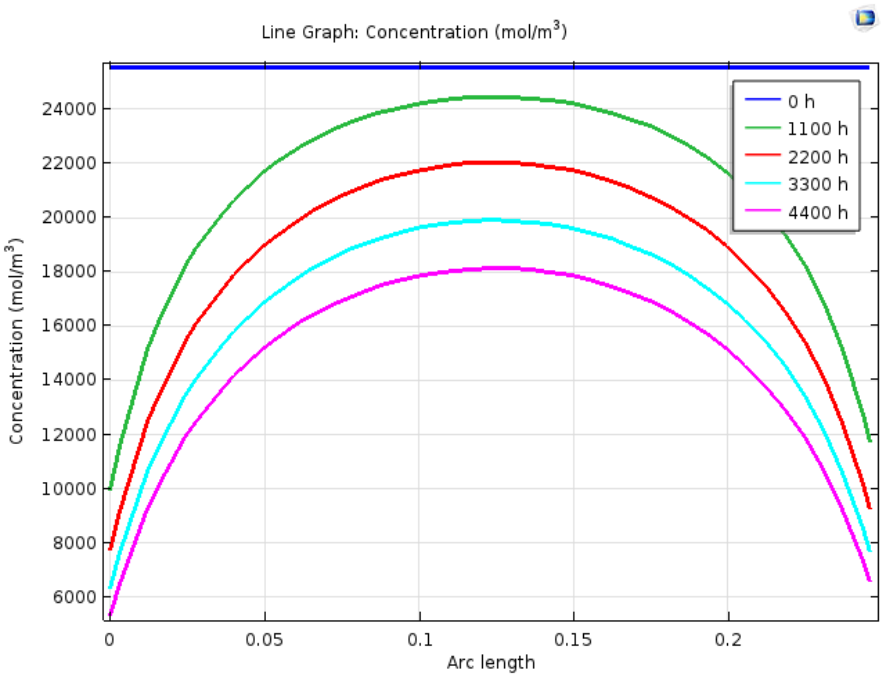

Figure 5.39- Liquid concentration plots across the log diameter passing through the longitudinal axis over 4644 hours.

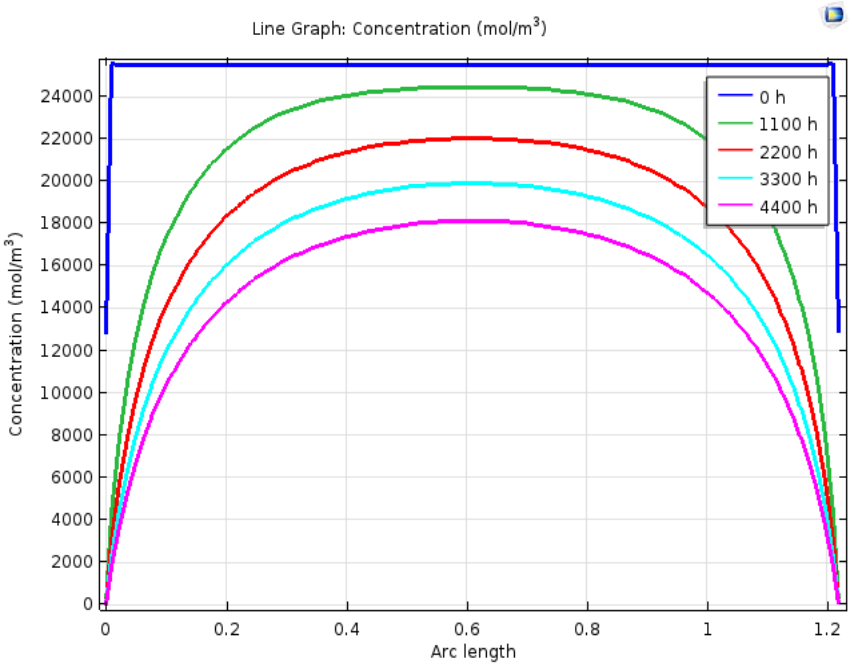

Figure 5.40-Liquid concentration plots along the log longitudinal axis over 4644 hours

Figure 5.41 presents a comparison of the total moisture content for Log B predicted by COMSOL and the experimentally determined moisture content values for Log B at Waiakea and Log B at Lalamilo. The weather data from Lalamilo were used in the COMSOL simulation. The modeled moisture content after six months was 39 %, and the actual moisture contents for Waiakea and Lalamilo were 49.9 % and 36.0 % respectively. In general, agreement between the model and experiment is good for this initial formulation. Agreement between the two could be improved by incorporating the effects of rainfall and log cracking, both of which are neglected by the model. During the experiment, there was a significant difference in rainfall between the two locations, with Waiakea having the greater amount (See figure 4.14). At the beginning of the experiment, cracks appeared in all logs, thereby increasing the surface area. Increased surface area presents greater opportunity for mass transfer, e.g. more vapor can diffuse outward during periods of drying and more liquid water can be absorbed during rainfall events.

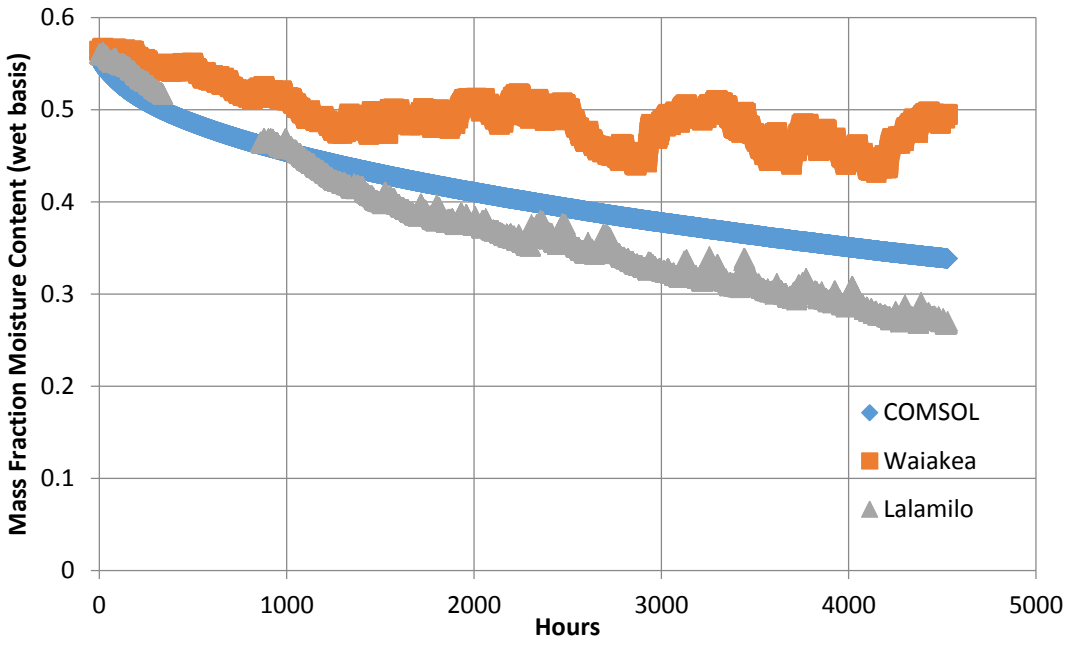

Figure 5.41 -COMSOL model data compared with experimental data for Lalamilo and Waiakea for six months of simlation.

5.4 Model Application/ Scenario Analysis

Using monthly averages for precipitation and evapotranspiration (Giambelluca *et al.*, 2014a), the time required for logs to dry below 30% wb moisture content was estimated for locations at Kawaihae, Lalamilo, and the seven plantation sites identified in Figure 4.10. The analysis assumed a harvest date in May and an initial moisture content of 54% wb. Results are presented in Table 5.9 and the time evolution of log moisture is shown in in Figure 5.42. Drying times vary from five months at Weloka and Hauola to infinite in the wet locations. The predicted moisture content trends in the figure are considerably smoother than the model results determined using daily averages. Models developed from data at one location and applied to predict drying behavior at a second location merits further experimental verification.

Table 5.9- The estimated time (in months) needed for eucalyptus logs to reach a moisture content of 30% wb at nine locations on Hawaii Island.

Site	Estimated time to reach below 30% Mc wb
Lalamilo	11 months
Kawaihae	never
Hamakua	12 months
Waipao	6 months
Hauola	5 months
Waipunalei	8 months
Weloka	5 months
Hilo	never
Pahala	14 months

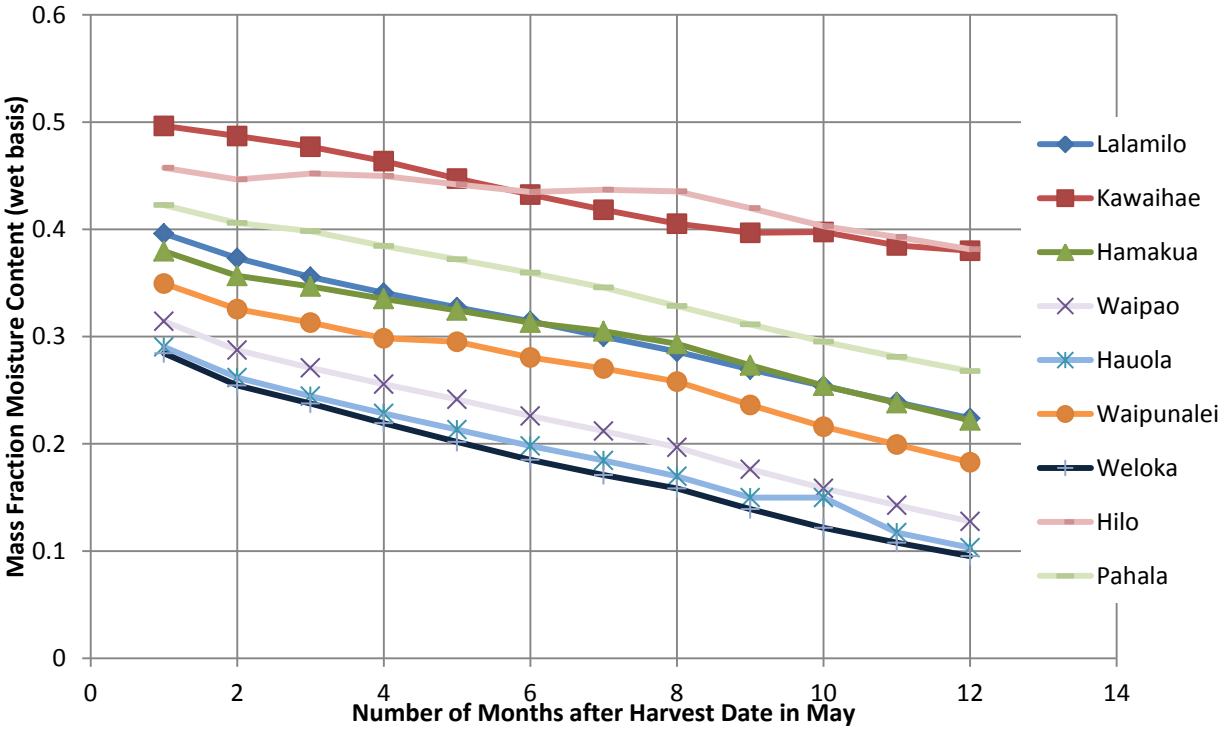

Figure 5.42-The estimated time rquired to reach 30% wb moisture content for nine locations on Hawai'I Island.

Table 5.10. summarizes the analysis comparing direct transport of logs from Hilo to Kawaihae vs transport of logs from Hilo to Lalamilo, offloading in Lalamilo and allowing them to dry, reload dry logs in Lalamilo and transport to Kawaihae. These are the two scenarios outlined in Figure 4.11. The analysis is based on delivering fully loaded truck (24.5 Mg) at a final moisture in Kawaihae for both scenarios. The direct transport of logs from Hilo to Kawaihae results in the delivery of a truck load containing 24.5 Mg of eucalyptus at a moisture content of 54% wb and a delivered cost of $671 per truck or $1.68 per GJ. The alternative scenario of drying logs at Lalamilo prior to delivery to Kawaihae results in the delivery of truck load containing 24.5 Mg of eucalyptus at a moisture content of 30% wb and a delivered cost of $850 per truck or $2.54 per GJ. The scenario that includes drying delivers more total energy, 334 GJ, than the wet wood delivery, 220 GJ, but the handling costs of loading and unloading at Lalamilo increase the delivered price. This preliminary analysis provides a framework for analyzing drying and log handling costs that can be improved upon.

Table 5.10-Summary of analysis comparing direct transport of logs from Hilo to Kawaihae vs transport of logs from Hilo to Lalamilo, offloading in Lalamilo and allowing them to dry, reload dry logs in Lalamilo and transport to Kawaihae. Analysis based on delivering fully loaded truck (24.5 Mg) at final moisture in Kawaihae for both scenarios.

	Hilo to Kawaihae Direct	Hilo to Lalamilo, dry in Lalamilo, Lalamilo to Kawaihae
Harvest Site	Hilo	Hilo
Harvest moisture content (-)	0.54	0.54
Log mass on truck in Hilo (Mg/truck)	24.5	24.5
Harvest log density in Hilo (Mg/m^3)	0.770	0.770
Log volume in Hilo to deliver full truck to Kawaihae (m^3)	31.8	48.4
Number of truckloads required to deliver log volume from Hilo	1	1.52
Loading cost in Hilo ($/$m^3$)	3.39	3.39
Distance from Hilo to Lalamilo (km)		88.5
Travel time from Hilo to Lalamilo (h)		1.23
Distance from Hilo to Kawaihae (km)	106.2	
Travel time from Hilo to Kawaihae (h)	1.5	
Trucking cost ($/h)	120	120
Unloading cost in Kawaihae & Lalamilo ($/$m^3$)	2.71	2.71
Loading cost in Lalamilo ($/$m^3$)		3.39
Dry log moisture content at Lalamilo (% wet basis)		30
Dry log density in Lalamilo (Mg/m^3)		0.506
Log mass on truck in Lalamilo (Mg/truck)		24.5
Log volume in Lalamilo to deliver full truck to Kawaihae (m^3)		48.4
Distance from Lalamilo to Kawaihae (km)		17.7
Travel time from Lalamilo to Kawaihae (h)		0.28
Unloading cost in Kawaihae ($/$m^3$)		2.71
Loading cost in Hilo ($)	107.88	164.16
Transport cost Hilo to Kawaihae ($)	174.00	
Transport cost Hilo to Lalamilo ($)		225.22
Unloading cost for wet logs in Lalamilo ($)		131.33
Loading cost for dry logs in Lalamilo ($)		164.16
Transport cost Lalamilo to Kawaihae ($)		34.00
Unloading cost in Kawaihae ($)	86.30	131.33
Total Cost ($)	671.67	850.20
Total wood energy delivered (GJ, truck load)	220	334
Net wood energy delivered (MJ/kg)	8.97	13.65
Total cost ($/GJ delivered)	1.68	2.54

6 Conclusions

The objectives of constructing empirical and phenomenological models for ambient drying of wood, validating the models with experimental data, and conducting scenario analyses using the model results were satisfied.

Experimental test stands to monitor log weight and thereby log moisture content were developed and installed at two locations representing wet and dry climate conditions. Drying data for three logs at each location were recorded over a period of nine months to provide the basis for the empirical model development and validation for both the empirical and phenomenological models.

6.1 Empirical Model Conclusions

Empirical models were developed to predict log drying behavior at both locations using weather data, i.e. temperature, solar insolation, and precipitation. The model parameters developed for a single log were capable of predicting drying trends for the other two logs at the same location although agreement was better for logs of similar diameters (D and F). Combining the log data into a bulk drying mass provided a more robust model. Future experiments should compare results of single logs and log stacks.

Use of model parameters developed at one location to predict the drying behavior at the other location met with limited success. Model values from the wet Waiakea location predicted the drying trends at the Lalamilo location but the dryer Lalamilo location model did not predict

drying behavior at the wet Waiakea location. The *b* coefficient for the cumulative rainfall data in the Liang model was the reason for these inconsistencies. Additional work should assess the applicability of the location-dependent models across a range of climates by developing experimental data sets for different wood species and locations.

6.2 Phenomenological Model Conclusions

A phenomenological model based on the conservation of mass and energy and heat and mass transport was developed in COMSOL Multiphysics to predict temperature and vapor and liquid concentration fields in a log undergoing ambient drying. These results were used to predict moisture content of the log and drying behavior. The model deviated significantly from the log drying data collected at Waiakea. The modeled moisture content after six months was 33.7% whereas the actual final moisture content after six months was 49.46 %. This is largely due to the fact that the model in COMSOL did not adequately include rainfall events.

The phenomenological model results were more comparable to experimental data at the dryer Lalamilo location. After six months, the modeled moisture content was 39.3 % and the actual measured moisture content was 36 %. The first two weeks of the simulation were in closer agreement with experiment but deviated more noticeably afterwards. This may be due to the cracking of the logs that was observed and the associated increased rates of vapor and liquid flux at the exposed surfaces. A structural model of the log could be developed to improve the agreement. COMSOL has a stress strain module that may be used to predict where cracking would occur.

6.3 Model Application/ Scenario Analysis Conclusions

Costs of direct trucking of wet logs from Hilo to Kawaihae were compared with a scenario that transported wood from Hilo to Lalamilo where they were offloaded and dried and then reloaded for shipment to Kawaihae. The direct transport of logs from Hilo to Kawaihae results in the delivery of a truck load containing 24.5 Mg of eucalyptus at a moisture content of 54% wb and a delivery cost of $671 per truck or $1.68 per GJ. The alternative scenario of drying logs at Lalamilo prior to delivery to Kawaihae results in the delivery of truck load containing 24.5 Mg of eucalyptus at a moisture content of 30% wb and a delivery cost of $850 per truck or $2.54 per GJ. The scenario that includes drying delivers more total energy, 334 GJ, than the wet wood delivery, 220 GJ, but the handling costs of loading and unloading at Lalamilo increase the delivered price. It is not clear whether the higher cost of the drier wood would be offset by higher value.

One reason that extra cost could be justified is if time was saved by drying at a given location. Time required to reach 30% moisture (wb) (11 months) predicted using monthly averaged weather data was not in agreement with the ~4 months determined experimentally at Lalamilo. This suggests that the use of historical weather records should be pursued to provide a broader perspective on predicted drying times.

7 Suggestions for Future Work

This project provides a framework for future work. Since Liang's model parameters were site specific, other empirical drying models should be considered and verified for various locations in Hawai'i.

The phenomenological model can be improved by implementing a three dimensional model that include a stress strain analysis to predict log cracking. This project did not account for rain which proved to be a very important variable. A future phenomenological model for ambient air drying should include rainfall. Effects of implementing turbulent wind flow should also be investigated.

Average monthly values used in this project came from Giambelluca et al.'s Climate Atlas (2014). Many weather stations have data that have been recorded over several decades. A distribution of expected drying times should be derived using these historical data.

8 Bibliography

Uncategorized References

Alvear, M., Broche, W., Salinas, C., & Ananias, R. A. (2003). Alvear Drying Kinetic of Chilean Coigue: Study of the Global Drying Coefficient. *International IUFRO Wood Drying Conference, 8*, 383-387.

Alves, S. S., & Figueiredo, J. L. (1989). A Model for Pyrolysis of Wet Wood. *Chemical Engineering Science, 44*(12), 2861-2869.

ASTM. (2015). ASTM D4442-15, Standard Test Methods for Direct Moisture Content Measurments of wood and Wood-Based Materials (pp. 6). West Conshocken, PA.

Awadalla, H. S. F., El-Dib, A. F., Mohamad, M. A., Reuss, M., & Hussein, H. M. S. (2004). Mathematical modelling and experimental verification of wood drying process. *Energy Conversion and Management, 45*(2), 197-207. doi:10.1016/s0196-8904(03)00146-8

Baronas, R., Ivanauskas, F., Juodeikiene, I., & Kajalavicius, V. (2001). Modelling of Moisture Movement in Wood during Outdoor Storage. *Nonlinear Analysis: Modelling and Control, 2001, 6*(2), 3-14.

Baronas, R., Ivanauskas, F., & Sapagovas, M. (1999). Modelling of Wood Drying and an Influence of Lumber Geometry on Drying Dynamics. *Nonlinear Analysis: Modelling and Control, 4*, 11-22.

Bedane, A. H., Afzal, M. T., & Sokhansanj, S. (2011). Simulation of temperature and moisture changes during storage of woody biomass owing to weather variability. *Biomass and Bioenergy, 35*(7), 3147-3151. doi:10.1016/j.biombioe.2011.04.008

Bekkioui, N., Hakam, A., Zoulalian, A., Sesbou, A., & El kortbi, M. (2011). Solar drying of pine lumber: Verification of a mathematical model. *Maderas. Ciencia y tecnología*, *13*(1), 29-40. doi:10.4067/s0718-221x2011000100003

Berberović, A. (2007). *Numerical Simulation of Wood Drying.* (Master of Science), Oregon State University, Corvallis, Oregon.

Binkley, D. (2012). Brazil Eucalyptus Potential Productivity. *Brazil Eucalyptus Potential Productivity.* Retrieved from http://www.nrel.colostate.edu/binkley-brazil-eucalyptus-potential-production.html

Bixler, N. E. (1985). *NORIA-A Finite Element Computer Program for Analyzing Water, Vapo, Air, and Energy Transport in Porous Media*. Retrieved from

Bousquet, D. (2000). Lumber Drying: An Overview of Current Processes. *University of Vermont School of Natural Resources*.

Bramhall, G. (1979). A Mathematical Description of Lumber Drying. *George Bramhall and Associates*, 11-16.

Britt, J. (2011). Eucalyptus May provide Hawaii with Alternative Energy. *Conservation Hawaii.* Retrieved from http://www.conservationhawaii.org/eucalyptus-may-provide-hawaii-with-alternative-energy/

Brown, G. (2005). Darcy's Law Basics and More. *Henry Darcy and His Law.* Retrieved from https://bae.okstate.edu/faculty-sites/Darcy/LaLoi/Basics.htm

Chen, C. S., & Johnson, W. H. (1967). *Kinetics of Moisture Movement in Hygroscopic Materials (I. Theoretical Considerations of Drying Phenomena*. Paper presented at the Winter Meeting of the American Society of Agricultural Engineers, Detroit, Michigan.

Chieh, C. (2008). The Clausius-Clapeyron Equation. *Computer Assisted Chemistry Tutorial.* Retrieved from http://www.science.uwaterloo.ca/~cchieh/cact/c123/clausius.html

Chui, T. F. M., & Freyburg, D. L. (2007). *The Use of COMSOL for Integrated Hydrological Modeling*. Retrieved from

COMSOL Multiphysics™. (2016). COMSOL Multiphysics™. Palo Alto, CA.

COMSOL Multiphysics™. (2013). *Heat Transfer Module User Guide*

da Silva, M. R., Machado, G. O., Deiner, J., & Calil, C. J. (2010). Permeability Measurements of Brazilian Eucalyptus. *Materials Research, 13*(3), 281-286.

Datta, A. K. (2014). Popular Mathematical Approach used by A. Datta group (Version 5.2) [2-D Finite Element model]: COMSOL Multiphysics, TM.

Diamond, H. J., Karl, T. R., Palecki, M. A., Baker, C. B., Bell, J. E., Leeper, R. D., Easterling, D. R., Lawrimore, J. H., Helfert, M. R., Goodge, G., Thorne, P. W. (2013). U.S. Climate Reference Network after one decade of operations: status and assessment. *Bull. Amer. Meteor. Soc, 94*, 489-498. doi: 10.1175/BAMS-D-12-00170.1

Dudley, N. S., & Osgood, R. V. (1996). *Evaluating Eucalyptus Urophylla Provenances*. Retrieved from Hawaii:

Elustondo, D. M., & Avramidis, S. (2005). Comparative Analysis of Three Methods for Stochastic Lumber Drying Simulation. *Drying Technology, 23*, 131-142.

Forest Solutions Inc., F. (Cartographer). (2012). Forest Solutions Hawaii Projects. Retrieved from http://www.forestsolutionshawaii.com/fsi_index.php/pages/projects

Geankoplis, C. J. (1993). *Transport Processes and Unit Operations- third edition*. Upper Saddle River, NJ: Prentice Hall PTR.

Ghaffariyan, M. R., Naghdi, R., Ghajar, I., & Nikooy, M. (2012). Time Prediction Models and Cost Evaluation of Cut-To-Length (CTL) Harvesting Method in a Mountainous Forest. *Small-scale Forestry, 12*, 181-192.

Giambelluca, T. W., Shuai, M. L., Barnes, R. J., Aliss, R. J., Longman, T., Miura, Q., Chen, A. G., Fraizier, R.G., Mudd, L., Cuo, Businger, A. D. (2014a). Evapotranspiration of Hawaii. Honolulu, Hawaii: U.S. Army Corps of Engineeris-Honolulu District, and the Commission on Water Resource Management, State of Hawaii.

Giambelluca, T. W., Shuai, M. L., Barnes, R. J., Aliss, R. J., Longman, T., Miura, Q., Chen, A. G., Fraizier, R.G., Mudd, L., Cuo, Businger, A. D. (2014b). *Evaportranspiration of Hawaii*. Retrieved from Honolulu, Hawaii: http://climate.geography.hawaii.edu/

Gieck, K., & Gieck, R. (1990). *Engineering Formulas* (6 ed.). New York: McGraw-Hill.

Goff, J. A., & Gratch, S. (1946). Low-pressure properties of water from -160 to 212 F. *Transactions of the American Society of Heating and Ventilating Engineers*(52), 95-122.

Google Earth, LDEO-Columbia, NSF, NOAA, Landsat, Data SIO, U GEBCO (Cartographer). (2016). Hawai'i Island. 19.67 N, 155.48 W

Halder, A., Dhall, A., & Datta*, A. K. (2015). Evaporation in Porous Media with Small Evaporation Rates (Version 5.1): COMSOL Multiphsics.

Hargreaves, G. H., & Samani, Z. A. (1982). Estimating Potential Evapotransiration. *Journal of Irrigation and Drainage Division, 108*(3), 225-230.

Hawaii Agricultural Research Center (HARC). (2012). Forestry Research. *Hawaii Agricultural Research Center*. Retrieved from http://www.harc-hspa.com/forestry.html

Hayhoe, H. N., & Jackson, L. P. (1974). Weather Effects on Hay Drying Rates. *Canada Journal of Plant Science, 54*, 479-484.

Hunter, A. J. (1995). Equilibrium Moisture Content and the Movement Water Through Wood Above Fibre Saturation. *Wood Science and Technology, 29*, 129-135.

Jankowsky, I. P., & dos Santos, R. V. (2004, 22-25 August 2004). *Drying Behavior and Permeability of Eucalyptus grandis Lumber.* Paper presented at the Proceedings of the 14th International Drying Symposium, Sao Paulo, Brazil.

Juvik, J. O., Singleton, D. C., & Clarke, G. G. (1978). *Climate and Water Balance on the Island of Hawaii*. Mauna Loa Observatory: a 20th Anniversary report. Retrieved from Hilo, Hawaii

Kamke, F. (2014, January 2014). [Personal Email Correspondance].

Kanevce, G. H., Kanevce, L. P., Dulikravich, G. S., & Orlande, H. R. B. (2005). Estimation of thermophysical properties of moist materials under different drying conditions. *Inverse Problems in Science and Engineering, 13*(4), 341-353. doi:10.1080/17415970500098485

Kang, W., Woo, Y. C., Eom, C. D., & Yeo, H. (2008). Some Considerations in Heterogeneous Nonisothermal Transport Models for Wood: a Numerical Study. *Journal of Wood Science, 54*, 267-277.

Khattabi, A., & Steinhagen, P. (1993). Analysis of Transient Nonlinear Heat Conduction in Wood Using Finite-Differnce Solutions. *Holz als Roh- und Werkstoff, 51*, 272-278.

Krabbenhøft, K. (2003). *Moisture Transport in Wood- A Study of Physical-Mathematical Models and their Numerical Implementation.* (Ph.D), Technical University of Denmark, Copenhagen, Denmark.

Lamb, F. M., & Wengert, E. M. (1991). *SOUTHERN PINE TDAL: A Computer Program to Simulate Lumber Drying in a kiln*. Paper presented at the Western Dry Kiln Association Meeting, Blacksburg, VA.

Lewis, W. L., Nithiarasu, R., & Seetharamu, K. N. (2004). *Fundamentals of the Finite Element Method for Heat and Fluid Flow*. West Sussex, England: John Wiley & Sons Ltd.

Li, D. (2015). VCSM-Eucalyptus. Hawaii: Microsoft Excel.

Liang, T., Khan, M. A., & Meng, Q. (1996). Spatial and Temporal Effects in Drying Biomass for Energy. *Biomass and Bioenergy, 10*(5/6), 330-360.

Murphy, G., Kent, T., & Kofman, P. D. (2012). Modeling Air Drying of Sitka Spruce (Picea sitchensis) Biomass in Off-Forest Storage Yards in Ireland. *Forest Products Journal, 62*(6), 443-449.

NOAA. (2016). University of Hawaii Waiakea Experiment Station Period of Record Sep 26 2005-Apr 25 2016. Retrieved from http://www.ncdc.noaa.gov/crn/station.htm?stationId=1186

Noorolahi, S., Khazaei, J., & Jafari, S. (2008). *Modeling Cyclic Water Absorption and Desorption Characteristics of Three Varieties of Wood*. Paper presented at the WORLD CONFERENCE ON AGRICULTURAL INFORMATION AND IT, Tokyo University of Agriculture.

Pang, S. (1996). Moisture Content Gradient in a Softwood Drying: Simulation From a 2-D Model and Measurement. *Wood Science and Technology, 30*, 165-178.

Pang, S. (2007). Mathematical Modeling of Kiln Drying of Softwood Timber: Model Development, Validation, and Practical Application. *Drying Technology, 25*(3), 421-431. doi:10.1080/07373930601183751

Perre, P., & Turner, I. W. (1999). A 3-D Version of TransPore: a Comprehensive Heat and Mass Transfer Computational Model for Simulating the Drying of Porous Media. *International Journal of Heat and Mass Transfer, 42*, 4501-4521.

Perré, P., & Turner, I. W. (2002). A heterogeneous wood drying computational modek that accounts for material property variation across growth rings. *Chemical Engineering Journal, 86*, 117-131.

Pinheiro, P. C. C., Raad, T. J., & Yoshida, M. I. (1998). MODEL OF A PROCESS FOR DRYING Eucalyptus spp AT HIGH TEMPERATURES. *Brazilian Journal of Chemical Engineering, 15*(4). doi:10.1590/s0104-66321998000400007

Redman, A. L., Bailleres, H., & Perré, P. (2012). Mass Transfer Properties (Permeability and Mass Diffusivity) of Four Australian Hardwood Species. *Bioresources, 7*(3), 3410-3424.

Reeb, J. E. (1997). *Drying Wood*. Retrieved from

Reeb, J. E. (2011). Fuel Cost Calculator & Estimator of Lumber Drying Costs. Portland Oregon: Microsoft Excel

Salvucci, G. D. (1996). Series Solution for Richards Equation Under Concentration Boundary Conditions and Uniform Initial Conditions. *Water Resources Research, 32*(8), 2401-2407. doi:10.1029/96wr01106

Sandoval-Torres, S., Wahbi, J., & Puiggali, J. R. (2012). *Solving a Two-Scale Model for Vacuum Drying by Using COMSOL Multiphysics.* Paper presented at the Proceedings of the 2012 COMSOL Conference in Milan, Milan, Italy.

Sensirion. (2015). Application Note Dew Point Calculation. Retrieved from http://irtfweb.ifa.hawaii.edu/~tcs3/tcs3/Misc/Dewpoint_Calculation_Humidity_Sensor_E.pdf

Siau, J. F. (1995). *WOOD: Influence of Moisture on physical properties*. Blacksburg, VA: Department of Wood Science and Forest Products-Virginia Polytechnic Institute and State University Press.

Simpson, W. T., & Hart, C. A. (2000). Estimates of Air Drying Times for Several Hardwoods and Softwoods. *Forest Products Laboratory USDA, 121*, 1-70.

Skolmen, R. G. (1964). *Air-Drying of Robusta Eucalyptus Lumber*. Retrieved from Berkely California:

Snyder, R., & Snow, R. (1984). Converting Humidity Expressions with Computers and Calculators. *Cooperative Extension Leaflet 21372. University of California Davis*.

Sokhansanj, S. (2011). The Effect of Moisture on Heating Values *Biomass and Energy Data Book*: Oak Ridge National Laboratory.

Spolek, G. A., & Plumb, O. A. (1981). Capillary Pressure in Softwoods. *Wood Science and Technology, 15*, 189-199.

Stape, L. J., Binkley, D., & Ryan, M. G. (2004). Eucalyptus production and the supply, use and the efficiency of use of water, light and nitrogen across a geographic gradient in Brazil. *Forest Ecology and Management, in Review*, 1-17.

Time, B. (1998). *Hygroscopic Moisture Transport in Wood.* (Doctorate of Engineering), Norwegiean University of Science and Technology.

Truscott, S. (2004). *A Heterogeneous Three-Dimensional Computational Model for Wood Drying.* (Doctor of Philosophy-Engineering), Queensland University of Technology, Queensland, Australia.

Tschernitz, J. L. (2001). Energy in Kiln Drying *Forest Products Laboratory Publications* (pp. 239-256): USDA.

Turn, S. Q., Vheissu, K., & Beers, K. (2005). *Physicochemical Analysis of Selected Biomass Materials in Hawaii*. Retrieved from Honolulu, Hawaii:

Turner, I. W. (1996). A Two-Dimensional Orthotropic Model for Simulationg Wood Drying Processes. *Applied Mathematical Modeling, 20*, 60-81.

University of Arizona Meteorological Network (UAMN). (2015). Dewpoint Formulas. Retrieved from https://ag.arizona.edu/azmet/dewpoint.html

University of Hawaii College of Tropical Agriculture and Human Resources (L-CTAHR). (2016). Lalamilo Experiment Station, Hawaii County. *Extension Offices and Research Stations.* Retrieved from http://www.ctahr.hawaii.edu/site/locationdetails.aspx?id=ER-HLALA

University of Hawaii College of Tropical Agriculture and Human Resources (W-CTAHR). (2016, 2016). Waiakea Experiment Station, Hawaii County. *Extension Offices and Research Stations.* Retrieved from http://www.ctahr.hawaii.edu/site/locationdetails.aspx?id=ER-HWAIA

Uslu, A., Faaij, A. P. C., & Bergman, P. C. A. (2008). Pre-treatment technologies, and their effect on international bioenergy supply chain logistics. Techno-economic evaluation of torrefaction, fast pyrolysis and pelletisation. *Energy*, *33*(8), 1206-1223. doi:10.1016/j.energy.2008.03.007

Van den Brande, T., Blocken, B., & Roels, S. (2013). Rain water runoff from porous building facades: Implementation and application of a first-order runoff model coupled to a HAM model. *Building and Environment, 64*, 177-186. doi:10.1016/j.buildenv.2013.03.014

Voigt, H., Krischer, O., & Shaussm, H. (1940). Movement of moisture in the evaporation of drying of wood. *Holz Roh-Werkstoff, 3*(1), 305-321.

Vömel, H. (2015). Saturation Vapor Pressure Formulas. *Dr. Holger Vomel Website.* Retrieved from http://cires1.colorado.edu/~voemel/vp.html

Whitesell, C. D., DeBell, D. S., Schubert, T. H., Strand, R. F., & Crabb, T. B. (1992). *Short-Rotation Management of Eucalyptus: Guidelines for Plantations in Hawaii*. Retrieved from Albany, California:

Wullschleger, S. D., Childs, K. W., King, A. W., & Hanson, P. J. (2011). A model of heat transfer in sapwood and implications for sap flux density measurements using thermal dissipation probes. *Tree Physiol, 31*(6), 669-679. doi:10.1093/treephys/tpr051

Zhang, D. Y., Zhu, L. K., Yin, W. F., & Gui, H. J. (2010, 11-14 July 2010). *A Novel Modeling Method of Wood Moisture Content for Drying Process.* Paper presented at the Ninth International Conference on Machine Learning and Cybernetics, Qinqdao, China.

Zhang, J., & Datta, A. K. (2004). Some Considerations in Modeling of Moisture Transport in Heating of Hygroscopic Materials. *Drying Technology, 22*(8), 1983-2008. doi:10.1081/LDRT-200032740

9 Appendix A-Equations and Parameters

Table A.1- Constant Parameters used in the model

Nomenclare	Parameter(Code)	Description
$A_{sur,length}$	A_Surcyl	Surface area of cylinder lengthwise
$A_{sur,Tot}$	A_surf	Surface area of stump
$c_{atm,vap0}$	c_atmv0	initial atmopsheric Concentration
c_{H2O0}	c_H2O0	initial concentration of water
$c_{m,H20}$	c_mass0	water mass concentration
Cp_{H2O}	Cp_H2O	Heat Capacity of water
Cp_{wood}	Cp_Wood	Heat Capacity of Bone Dry E. grandis wood
d	Diam	Outer diameter of log including bark
D_{lon}	difflong	longitudinal diffusivity of a species similar to e. grandis
D_{rad}	diffrad	radial diffusivity of species similar to wood
D_{tan}	difftan	tangential diffusivity for similar species
m_{dry}	drymass	mass of dry wood

$D_{Vap,air}$	Dw_air	Diffusivity of water in air
E_a	Ea0	Acitvation energy
ϵ	emmis	Emmsivity of surface of E. Grandis
H_{vap}	H_Vap	Heat of Vaporization for water
K_{Evap}	K_evap	Evaporation rate
$K_{Gas,x,0}$	k_gas_lon0	Longitudinal Wood Permeability for gas in Eucalyptus wood according to Pinheiro

$K_{Gasy,0}$	**k_gas_rad0**	**Radial Wood Permeability ofgas through Eucalyptus wood (Pinheiro)**
$K_{Liq,x0}$	k_Liq_lon0	liquid permeability of similar species
$K_{Liq,y0}$	k_Liq_rad0	liquid perm in radial direction of similar species
$K_{Liq,tan0}$	k_Liq_tan0	liquid Perm in tangential direction
k_{wood}	K_wood	Thermal Conductivity of bone dry Eucalyptus wood
H_{lat}	LatHeat	Latent heat of evaporation of water at standard conditions
L	Length	Length of Log
$m_{H2O,0}$	Mass_H2O0	Initial mass of water
$m_{tot,0}$	MassTot0	mass of system at beggining
M_{C0}	MC0	Initial Moisture content (wet basis) measured from sample after felling tree
$n_{H2O,0}$	mol_H2O	moles of water
μ_{Gas}	mu_gas	Dynamic viscosity of Gas
μ_{Liq}	mu_liq	Dynamic viscosicty of liquid warer at standard conditions
Mw_{air}	Mw_air	molecular wieght of air
Mw_{H2O}	Mw_H2O	Molecular Mass of Water
$P_{Gas,0}$	p_g0	Initial internal Gas Pressure
P_0	p0	ambient pressure
$p_{c,0}$	pc0	Inital value for capilary pressure according to Sandoval's paper
$P_{Liq,0}$	pl0	Initial Liquid Pressure according to Sandoval Pinheiro etc.
ε	Por	Porosity of E. Grandis
$E_{Liq,0}$	Por_Liq0	Liquid Volume to total Volume ratio
$P_{atm,Vap,0}$	pv_atm0	Initial Partial Vapor Pressure of atmosphere
$P_{Sat,Vap0}$	Pvs0	Initial Saturation Vapor Pressure of Wood

R	R	Universal Gas Constant
R_a	Ra	Air equivalent constant
r	Rad	Radius of Log with Bark
ρ_{Air0}	rho_air	Air Density from Engineering Toolbox
$\rho_{H20,0}$	rho_H2O	Density of liquid water
ρ_{wood}	rho_wood	Density of E. grandis published in pinheiro model
R_v	Rv	Vapor equivalent constant
$S_{Gas,0}$	S_g0	Initial Gas Saturation
$S_{Liq,0}$	S_w0	Initial Liquid Saturation
Θ	SG	Specific Gravity of E. grandis
T_0	T0	Initial temperature of Log
V_{sol}	Vol_s	solid volume
V_{void}	Vol_Void	Void Volume of E. Grandis
V_{tot}	Volume	Volume of System
X_{m0}	X_m0	Moisture content on a dry basis

Table A.2- Equations used in the COMSOL Model

Nomenclature	**Code Name**	**Coded Equation**	**Equation Using Nomenclature**	**Source**
α	A	3.776e5[1/s]	3.776e5[1/s]	(Pinheiro *et al.*, 1998)
$\alpha 1$	alpha	1-(Por_Liq/Por)	$1-\frac{\varepsilon_{Liq}}{\varepsilon}$	(Pinheiro *et al.*, 1998)
$\dot{m}_{atm}$	atm_massrate	K*(c_atmvsat-c_atmv)	$K*\left(C_{\mathrm{sat,Vap,atm}}-C_{\mathrm{vap,atm}}\right)$	(Halder *et al.*, 2015)
$C_{vap,atm}$	c_atmv	pv_atm/(R*Temp)	$\frac{\mathrm{P}_{Vap,atm}}{\mathrm{R}*\mathrm{T}}$	
$C_{vap,atm0}$	c_atmv0	pv_atm0/(R*Tamb0)	$\frac{\mathrm{P}_{Vap,atm0}}{\mathrm{R}*\mathrm{T}_{amb0}}$	
$C_{sat,Vap,atm}$	c_atmvsat	Pvs_atm/(R*Temp)	$\frac{\mathrm{P}_{Sat,Vap,atm}}{\mathrm{R}*\mathrm{T}}$	
$C_{eq,H2O}$	c_H2Oeq	molH2Oeq/Volume	$\frac{\mathrm{n}_{\mathrm{eq,H2O}}}{\mathrm{V}_{Tot}}$	
$C_{Sat,Vap}$	c_H2OVapSat	mol_H2OVapSat/V_gas	$\frac{\mathrm{n}_{\mathrm{Sat,Vap}}}{\mathrm{V}_{Gas}}$	
$C_{Sat,Liq}$	c_LiqSat	X_LiqSat*(cLiq+cVap)	$\frac{X_{\mathrm{sat,Liq}}}{c_{Liq}+c_{Vap}}$	
$C_{m,H2O}$	c_mH2O	(c_mLiq+c_mVap)	$(c_{Liq}+c_{Vap})*Mw_{H2O}$	
$C_{m,H2O,Eq}$	c_mH2Oeq	c_H2Oeq*Mw_H2O	$c_{eq,H2O}*Mw_{H2O}$	

$C_{Mass,L}$	c_mLiq	cLiq*Mw_H2O	$c_{Liq} * Mw_{H2O}$	
C_{mVap}	c_mVap	cVap*Mw_H2O	$c_{Vap} * Mw_{H2O}$	
$C_{Sat,Vap}$	c_VapSat	Pvs/(R*Temp)	$\frac{p_{\text{sat,Vap}}}{R * T}$	
C_{Tot}	conc	cLiq+cVap	$c_{Liq} + c_{Vap}$	
D_{av}	D_av	2.2e-5*(p0/pg)*(Temp/T0)^1.75	$2.2 * 10^{-5} \frac{P_0}{P_g} * \frac{T}{T_0}^{1.75}$	
D_m	D_m	2.41e-7[m^2/s]*exp(-0.762e-1/X_m)*exp(-1.49e3[K]/Temp)	$2.41 * 10^{-7} * e^{-\frac{-0.762*10^{-1}}{X_m}} * e^{-\frac{-1.49*10^3}{\text{T}}} [\frac{m^2}{s}]$	(Datta, 2014)
D_0	D0	alpha*D_av[m^2/s]	$\alpha\ 1 * D_{av}[\frac{m^2}{s}]$	(Pinheiro *et al.*, 1998)
D_{eff}	Deff	D0*exp(-E/(R*Tdew2))	$D_0 * e^{\frac{-E_a}{R*T_{Dew}}} [\frac{m^2}{s}]$	(Chen & Johnson, 1967)
D_{eff}	Diff_eff	relk_g*D_av*(1*10^-3)[m^2/s]	$\kappa_{\text{rel,gas}} * D_{av} * 1 * 10^{-3} [\frac{m^2}{s}]$	(Kang *et al.*, 2008)
D_{wc}	Dw_c	1e-8[m^2/s]*exp(-2.8+2*X_m)	$1 * 10^{-8} * e^{-2.8+2*X_m}$	(Datta, 2014)
E_a	E	53.78[kJ/mol]	53.78[kJ/mol]	(Pinheiro *et al.*, 1998)
λ	gamma	(log((RH_Wood>0)/100)+((tmb*Temp)/(tmc+Temp)))/tmb	$\frac{\log(\frac{\varphi_{wood}}{100} + \frac{\beta * T}{(\psi + \text{T})})}{\beta}$	(UAMN, 2015)
λ_{sur}	gammaSur	(log((RH)/100)+((tmb*Temp)/(tmc+Temp)))/tmb	$\frac{\log(\frac{RH_{atm}}{100} + \frac{\beta * T}{(\psi + \text{T})})}{\beta}$	(UAMN, 2015)
J_{Liqx}	J_liqx	cLiqx*(Por_Liq)*Dw_c*X_Liq	$C_{Liq,x} * \varepsilon_L * D_{wc} * X_{Liq}$	
J_{liqy}	J_liqy	cLiqy*(Por_Liq)*Dw_c*X_Liq	$C_{Liq,y} * \varepsilon_L * D_{wc} * X_{Liq}$	

J_{vapx}	J_vapx	cVapx*(Por-Por_Liq)*Diff_eff*X_Vap	$C_{Vap,x} * (\varepsilon - \varepsilon_{L)} * D_{eff} * X_{Vap}$	(Pinheiro *et al.*, 1998)
J_{vapy}	J_vapy	cVapy*(Por-Por_Liq)*Diff_eff*X_Vap	$C_{Vap,y} * (\varepsilon - \varepsilon_{L)} * D_{eff} * X_{Vap}$	(Pinheiro *et al.*, 1998)
K	K	A*exp(-E/(R*Tdew))	$\alpha * e^{\frac{-E_a}{R*T_{Dew}}}$	(Pinheiro *et al.*, 1998)
K_{Sur}	KSur	A*exp(-E/(R*TdewSur))	$\alpha * e^{\frac{-E_a}{R*T_{Dew,atm}}}$	(Pinheiro *et al.*, 1998)
$\kappa_{gas,x}$	k_Gas_Lon	k_gas_lon0*relk_g	$\kappa_{\mathrm{Gas,x,0}} * \kappa_{\mathrm{rel,Gas}}$	(Datta, 2014)
$\kappa_{gas,y}$	k_Gas_Rad	k_gas_rad0*relk_g	$\kappa_{\mathrm{Gas,y,0}} * \kappa_{\mathrm{rel,Gas}}$	(Datta, 2014)
$\kappa_{liq,x}$	k_Liq_Lon	k_Liq_lon0*relk_l	$\kappa_{\mathrm{Liq,x,0}} * \kappa_{\mathrm{rel,Liq}}$	(Datta, 2014)
$\kappa_{liq,y}$	k_Liq_Rad	k_Liq_rad0*relk_l	$\kappa_{\mathrm{Liq,y,0}} * \kappa_{\mathrm{rel,Liq}}$	(Datta, 2014)
$\kappa_{rel,G}$	relk_g	1+(2*S_w-3)*S_w^2	$1 + \left(2 * S_{Liq} - 3\right) * {S_L}^2$	(Perre & Turner, 1999)
$\kappa_{rel,L}$	relk_l	S_w^3	${S_{Liq}}^3$	(Perre & Turner, 1999)
m_{eq}	Mass_H2Oeq	X_m_eq*drymass	$X_{m,eq} * m_{dry}$	
$\dot{m}$	massrate4	K*(c_VapSat-cVap)	$K * (c_{Vap,Sat} - c_{Vap})$	(Halder *et al.*, 2015)
$\dot{m}_{sur}$	massrateSur	KSur*(c_atmvsat-c_atmv)	$K_{Sur} * (c_{Vap,Sat,atm} - c_{Vap,atm})$	(Halder *et al.*, 2015)
Mc_{eq}	MC_eq	0.0799*(RH^2)+0.0638*RH+0.0003	$0.0799 * RH^2 + 0.0638 * RH + .0003$	(Li, 2015)
$n_{sat,vap}$	mol_H2OVapSat	(Pvs*V_gas)/(R*Temp)	$\frac{P_{Vap,Sat} * V_{void}}{R * T}$	

$n_{eq,H2O}$	molH2Oeq	Mass_H2Oeq/Mw_H2O	$\frac{m_{eq}}{Mw_{H2O}}$	
p_{vap}	p_Vap	cVap*R*Temp	$C_{Vap} * R * T$	
P_c	rpc	56.75e3*(1-S_w)*exp(1.062/S_w)[Pa]	$56.75 * 10^3 * e^{\frac{1.062}{S_{Liq}}} [Pa]$	(Sandoval-Torres *et al.*, 2012)
P_{Gas}	pg	p	p_{Gas}	
$P_{Gas,x}$	pgx	px	$p_{Gas,x}$	
$P_{Gas,y}$	pgy	py	$p_{Gas,y}$	
P_L	pl	pg-pc	$p_{Gas} - p_c$	(Pinheiro *et al.*, 1998)
$P_{L,x}$	plx	pgx-pc[1/m]	$p_{Gas,x} - p_c$	
$P_{L,y}$	ply	pgy-pc[1/m]	$p_{Gas,y} - p_c$	
ε_L	Por_Liq	(rho_wood*X_m)/rho_H2O	$\frac{\rho_{Wood} * X_m}{\rho_{H2O}}$	(Pinheiro *et al.*, 1998)
$\varepsilon_{L,eq}$	Por_Liq_eq	(rho_wood*X_m_eq)/rho_H2O	$\frac{\rho_{Wood} * X_{m,eq}}{\rho_{H2O}}$	
$P_{Vap,atm}$	pv_atm	(RH*Pvs_atm)/100	$\frac{RH_{atm} * p_{Sat,Vap,atm}}{100}$	
$P_{Vap,atm0}$	pv_atm0	(RH0*Pvs0)/100	$\frac{RH_{atm0} * p_{sat,vap,atmp0}}{100}$	

$P_{Sat,Vap}$	Pvs	101324.6[Pa]*10^(-7.90298*(Tamb/Temp-1)+5.02808*log10(abs(Tamb/Temp))-1.3816e-7*(10^(11.344*(1-Temp/Tamb))-1)+8.1328e-3*(10^(3.49149*(1-Tamb/Temp))-1))	$101324.6[Pa] * 10^{-7.90298*\left(\frac{T_{amb}}{(T-1)}\right)} + 5.02808 * \log_{10}(\frac{T_{amb}}{T}) - 1.3816 * 10^{-7} * (10^{\left(11.344*\left(1-\frac{T}{T_{amb}}\right)\right)} - 1) + 8.1328 * 10^{-3} * (10^{\left(3.49149*\left(1-\frac{T}{T_{amb}}\right)\right)} - 1)$	(Goff & Gratch, 1946)
$p_{atm,Sat,Vap}$	Pvs_atm	101324.6[Pa]*10^(-7.90298*(T0/Tamb-1)+5.02808*log10(abs(T0/Tamb))-1.3816e-7*(10^(11.344*(1-Tamb/T0))-1)+8.1328e-3*(10^(3.49149*(1-T0/Tamb))-1))	$101324.6[Pa] * 10^{-7.90298*\left(\frac{T_0}{(T_{amb}-1)}\right)} + 5.02808 * \log_{10}(\frac{T_0}{T_{amb}}) - 1.3816 * 10^{-7} * (10^{\left(11.344*\left(1-\frac{T_0}{T_{amb}}\right)\right)} - 1) + 8.1328 * 10^{-3} * (10^{\left(3.49149*\left(1-\frac{T_0}{T_{amb}}\right)\right)} - 1)$	(Goff & Gratch, 1946)

$p_{atm,sat,vap\ 0}$	Pvs0	101324.6[Pa]*10^(-7.90298*(T0/Tamb0-1)+5.02808*log10(abs(T0/Tamb0))-1.3816e-7*(10^(11.344*(1-Tamb0/T0))-1)+8.1328e-3*(10^(3.49149*(1-T0/Tamb0))-1))	$101324.6[Pa] * 10^{-7.90298*\left(\frac{T_0}{(T_{amb0}-1)}\right)} + 5.02808 * \log_{10}(\frac{T_0}{T_{amb0}}) - 1.3816 * 10^{-7} * (10^{(\left(11.344*\left(1-\frac{T_0}{T_{amb0}}\right)\right)} - 1) + 8.1328 * 10^{-3} * (10^{(\left(3.49149*\left(1-\frac{T_0}{T_{amb0}}\right)\right)} - 1)$	(Goff & Gratch, 1946)
φ_{atm}	RH	RelHum(t)	RH(t)	
φ_{wood}	RH_Wood	abs((p_Vap)/Pvs)*100	$\frac{p_{vap}}{p_{sat,vap}} * 100$	
φ_0	RH0	RelHum(0)	RH(0)	
ρ_G	rho_G	(X_Vap*Mw_H2O+(1-X_Vap)*Mw_air)*p/(R*Temp)	$X_{Vap} * Mw_{H2O} + (1 - X_{Vap}) * Mw_{air} * \frac{p_{Gas}}{R * T}$	(Datta, 2014)
ρ_{Tot}	rho_Tot	(1-Por)*rho_wood+Por*S_g*rho_G+Por*S_w*rho_H2O	$(1 - \varepsilon) * \rho_{wood} + \varepsilon * S_{Gas} * \rho_{Gas} + \varepsilon * S_{Liq} * \rho_{H2O}$	(Datta, 2014)
ρ_{Vap}	rho_Vap	c_mVap/(Por*S_g)	$\frac{C_{m,v}}{(\varepsilon * S_G)}$	(Datta, 2014)
S_G	S_g	1-S_w	$1 - S_L$	(Datta, 2014)
S_L	S_w	c_mLiq/(rho_H2O*Por)	$\frac{C_{m,L}}{(\varepsilon * \rho_{H2O})}$	(Datta, 2014)
c_{SurLiq}	Sur_cLiq	massrateSur[s]+cLiq*Por*S_w	$\dot{m}_{Sur}(t) + C_L * \varepsilon * S_L$	

c_{survap}	Sur_cVap	c_atmv-massrateSur[s]+Por*S_g*cVap	$C_{atm,V} - \dot{m}_{Sur}(t) + c_L * \varepsilon * S_G - c_V$	
T_{amb}	Tamb	AmbTemp(t)	AmbTemp(t)	
T_{amb0}	Tamb0	AmbTemp(0)	AmbTemp(0)	
T_{dew}	Tdew	((tmc*gamma)/(1-gamma))	$\frac{\psi * \lambda}{1 - \lambda}$	(UAMN, 2015)
$T_{dew,sur}$	TdewSur	((tmc*gammaSur)/(1-gammaSur))	$\frac{\psi * \lambda_{Sur}}{1 - \lambda_{Sur}}$	
T	Temp	T	T	
ω	tma	611.2[Pa]	611.2[Pa]	(Sensirion, 2015)
β	tmb	17.62	17.62	(Sensirion, 2015)
ψ	tmc	516[K]	516[K]	(Sensirion, 2015)
V_g	V_gas	Por-V_Liq	$\varepsilon - V_{Liq}$	
V_{liq}	V_Liq	Por_Liq*Volume	$\varepsilon_{Liq} - V_{Tot}$	
$V_{liq,eq}$	V_Liq_eq	Por_Liq_eq*Volume	$\varepsilon_{Liq,eq} - V_{Tot}$	
$u_{g,y}$	Vel_gas_x	u/(Por*S_g)	$\frac{u_x}{\varepsilon * S_{Gas}}$	(Datta, 2014)
$u_{g,x}$	Vel_gas_y	v/(Por*S_g)	$\frac{u_y}{\varepsilon * S_{Gas}}$	(Datta, 2014)
$u_{L,y}$	Vel_liq_x	-(py*k_Liq_Rad)/(Por*S_w*mu_liq)	$\frac{p_y * \kappa_{Liq,y}}{\varepsilon * S_{Liq} * \mu_{Liq}}$	(Datta, 2014)

$u_{L,x}$	Vel_liq_y	-(px*k_Liq_Lon)/(Por*S_w*mu_liq)	$\frac{p_x * \kappa_{liq,x}}{\varepsilon * S_w * \mu_{Liq}}$	(Datta, 2014)
$u_{tot,x}$	Vel_Totx	-px*(Por*S_g*rho_G*k_Gas_Lon/mu_gas+Por*S_w*rho_H2O*k_Liq_Lon/mu_liq)/rho_Tot	$\frac{-p_x * \left(\frac{\varepsilon * S_{Gas} * \rho_{Gas} * \kappa_{Gas,x}}{\mu_{Gas}}\right) +}{\rho_{Tot}}$	(Datta, 2014)
$u_{tot,y}$	Vel_Toty	-py*(Por*S_g*rho_G*k_Gas_Rad/mu_gas+Por*S_w*rho_H2O*k_Liq_Rad/mu_liq)/rho_Tot	$\frac{-p_y * \left(\frac{\varepsilon * S_{Gas} * \rho_{Gas} * \kappa_{Gas,y}}{\mu_{Gas}}\right) +}{\rho_{Tot}}$	(Datta, 2014)
X_L	X_Liq	1-X_Vap	$1 - X_{Vap}$	
$X_{sat,}$	X_LiqSat	1-X_VapSat	$1 - X_{Vap,Sat}$	
X_m	X_m	(c_mLiq+c_mVap)/(1-Por)/(rho_wood)	$\frac{\frac{C_{Mass,Liq} - C_{Mass,Vap}}{1 - \varepsilon}}{\rho_{Wood}}$	(Datta, 2014)
$X_{m,eq}$	X_m_eq	(MC_eq/(100-MC_eq))	$\frac{Mc_{eq}}{100 - Mc_{eq}}$	
X_{vap}	X_Vap	p_Vap/(p+eps)	$\frac{p_{Vap}}{p_{Gas}}$	(Datta, 2014)
$X_{sat,Vap}$	X_VapSat	Pvs/(p+eps)	$\frac{p_{Sat,Vap}}{p_{Gas}}$	(Datta, 2014)

10 Appendix B- Datta Logger Program Code and Wiring Diagram

CR23X

Wiring Diagram

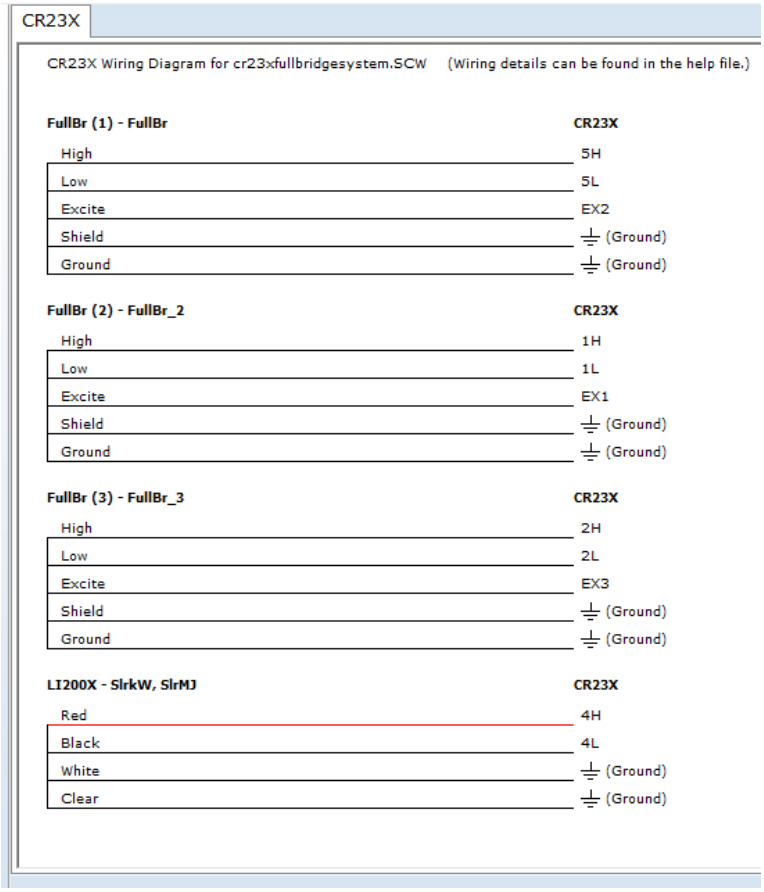

Code-

```
C:\Campbellsci\SCWin\cr23xfullbridgesystem.DEF
 4/2/2016
 14:22:49
 Created by Short Cut (3.1)
 Short Cut Program:  cr23xfullbridgesystem.DEF

 -Wiring for CR23X-

  Full Bridge (1)
    Ground:  Ground
    Ground:  Shield
    5H:  High
    5L:  Low
```

EX2: Excite

Full Bridge (2)
1H: High
1L: Low
Ground: Ground
Ground: Shield
EX1: Excite

Full Bridge (3)
Ground: Ground
Ground: Shield
2H: High
2L: Low
EX3: Excite

LI200X Pyranometer
Ground: White
Ground: Clear
4H: Red
4L: Black

-Measurement Labels-

Default Measurements
1 BattV
2 ProgSig

Full Bridge (1)
11 FullBr

Full Bridge (2)
12 FullBr_2

Full Bridge (3)
13 FullBr_3

LI200X Pyranometer
16 SlrkW
17 SlrMJ

102 Output_Table 60.00 Min
1 102 L
2 Year_RTM L
3 Day_RTM L
4 Hour_Minute_RTM L
5 BattV_MIN L
6 ProgSig L
7 FullBr_AVG L
8 FullBr_2_AVG L
9 FullBr_3_AVG L
10 BattV_AVG L
11 SlrkW_AVG L
12 SlrMJ_TOT H

Estimated final storage locations used per day: 312

CR1000

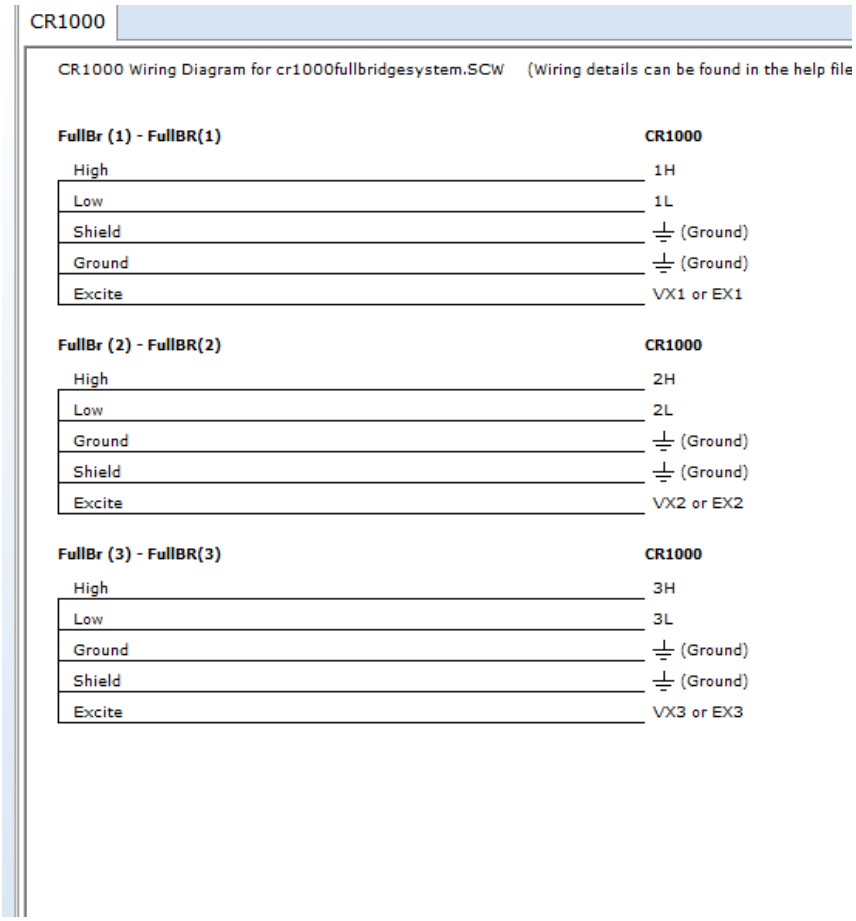

Code-

```
C:\Campbellsci\SCWin\cr1000fullbridgesystem.DEF
  4/2/2016
  14:26:09
  Created by Short Cut (3.1)
  Short Cut Program:  cr1000fullbridgesystem.DEF

  -Wiring for CR1000-

    Full Bridge (1)
      1H:  High
      1L:  Low
      Ground:  Ground
      Ground:  Shield
      VX1 or EX1:  Excite

    Full Bridge (2)
      Ground:  Ground
      Ground:  Shield
      2H:  High
```

```
    2L:  Low
    VX2 or EX2:  Excite

  Full Bridge (3)
    Ground:  Ground
    Ground:  Shield
    3H:  High
    3L:  Low
    VX3 or EX3:  Excite

-Measurement Labels-

  Default Measurements
    BattV
    PTemp_C

  Full Bridge (1)
    FullBR(1)

  Full Bridge (2)
    FullBR(2)

  Full Bridge (3)
    FullBR(3)

---------------------------------------------------
Table: Table1
Interval: 60 MIN
Fields:
 BattV_Avg Units: Volts
 PTemp_C_Avg Units: Deg C
 FullBR_Avg(1) Units: mV/V
 FullBR_Avg(2) Units: mV/V
 FullBR_Avg(3) Units: mV/V

---------------------------------------------------
Table: Table2
Interval: 1440 MIN
Fields:
 BattV_Min Units: Volts

---------------------------------------------------
Table: Public
Fields:
 BattV Units: Volts
 PTemp_C Units: Deg C
 FullBR(1) Units: mV/V
 FullBR(2) Units: mV/V
 FullBR(3) Units: mV/V
 Mult(1)
 Mult(2)
 Mult(3)
 Offs(1)
 Offs(2)
 Offs(3)
```

11 Appendix C- Charts depicting Measured Results, vs. Model results

Graphs using interchangeable a,b, c values for each different log

Liang Model Waiakea, Using Waiakea Log B Values

a=	0.000702
b=	7.2E-05
c=	0

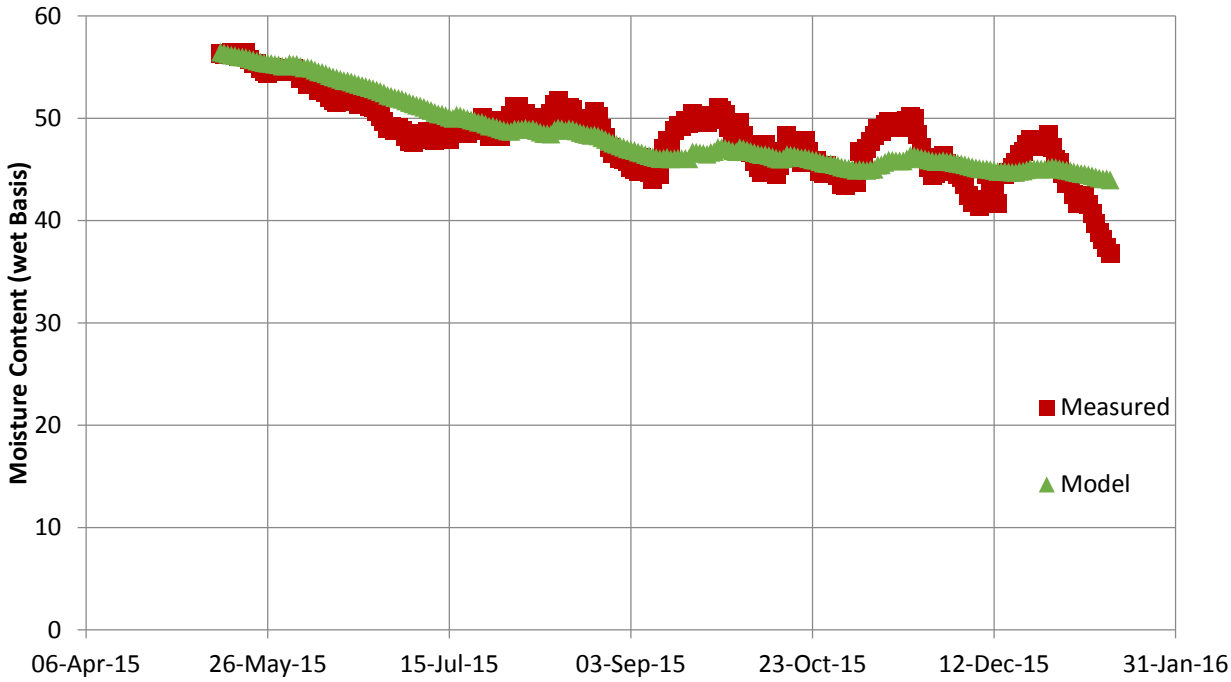

Figure C.1: Waiakea Log B moisture content: measured vs model prediction derived from Waiakea Log B

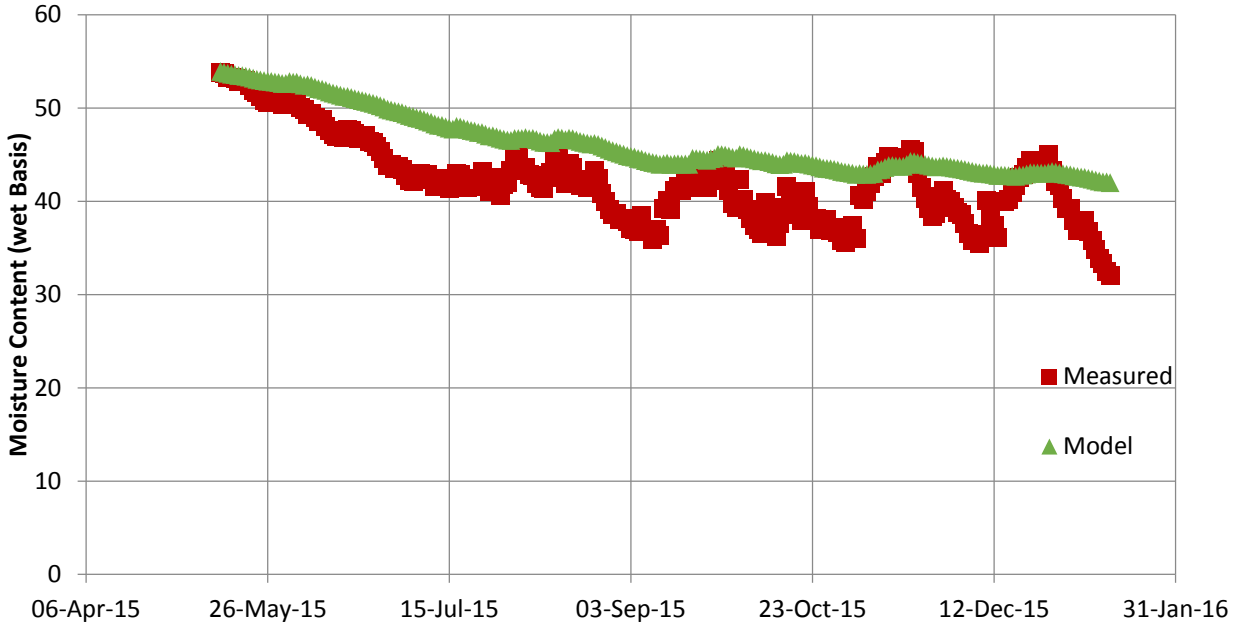

Figure C.2: Waiakea Log D moisture content: measured vs model prediction derived from Waiakea Log B

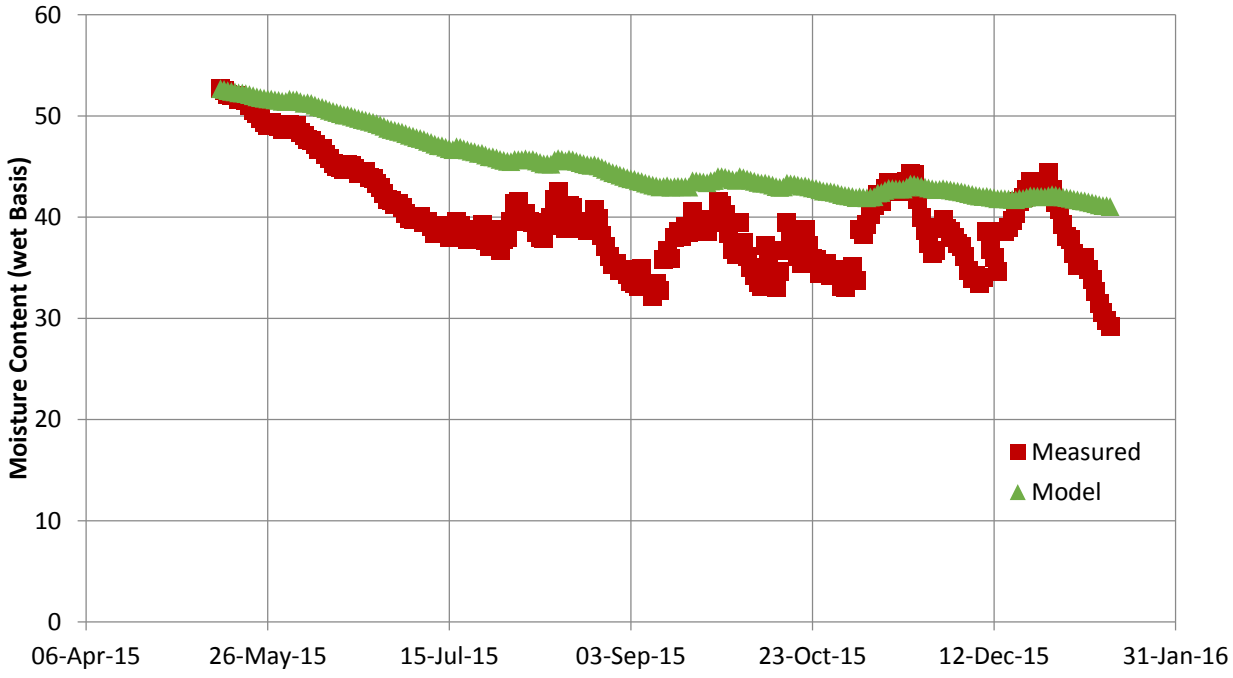

Figure C.3: Waiakea Log F moisture content: measured vs model prediction derived from Waiakea Log B

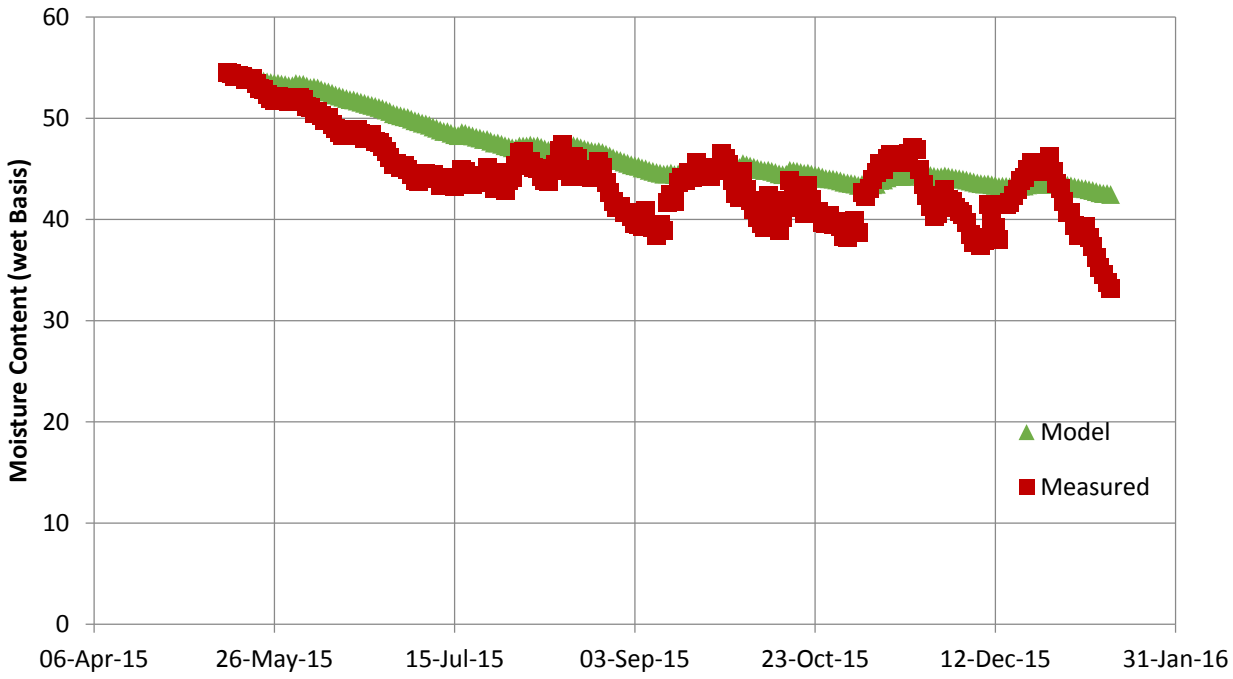

Figure C.3: Waiakea Log bulk moisture content: measured vs model prediction derived from Waiakea Log B

Liang Model Waiakea, Using Waiakea Log D Values

a=	0.001508
b=	0.000204
c=	0

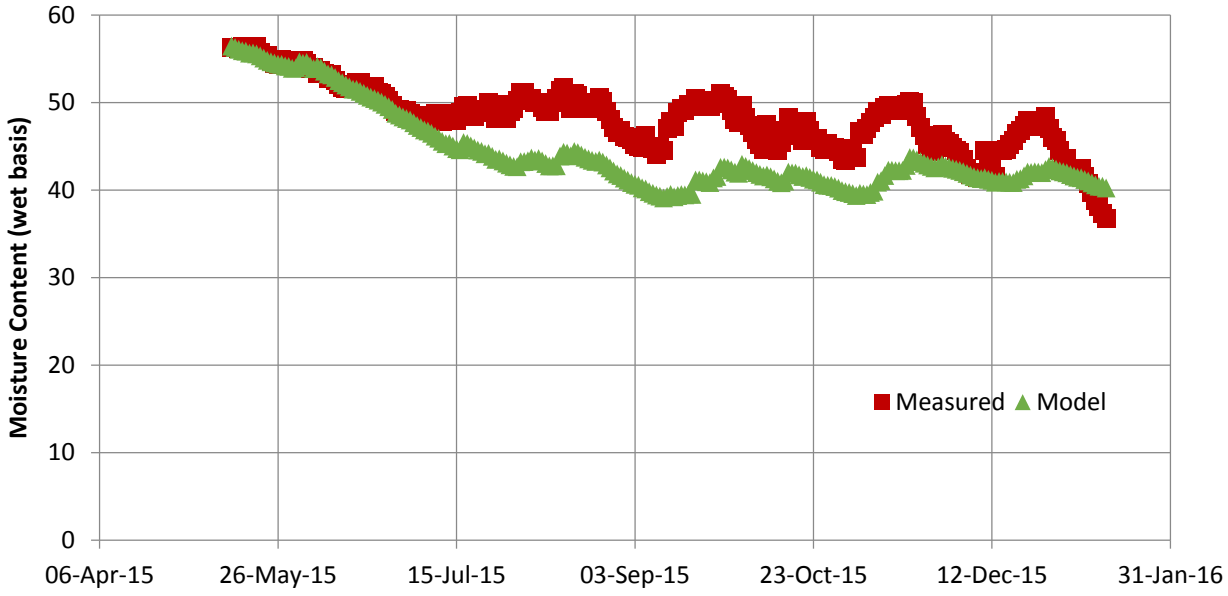

Figure C.5: Waiakea Log B moisture content: measured vs model prediction derived from Waiakea Log D

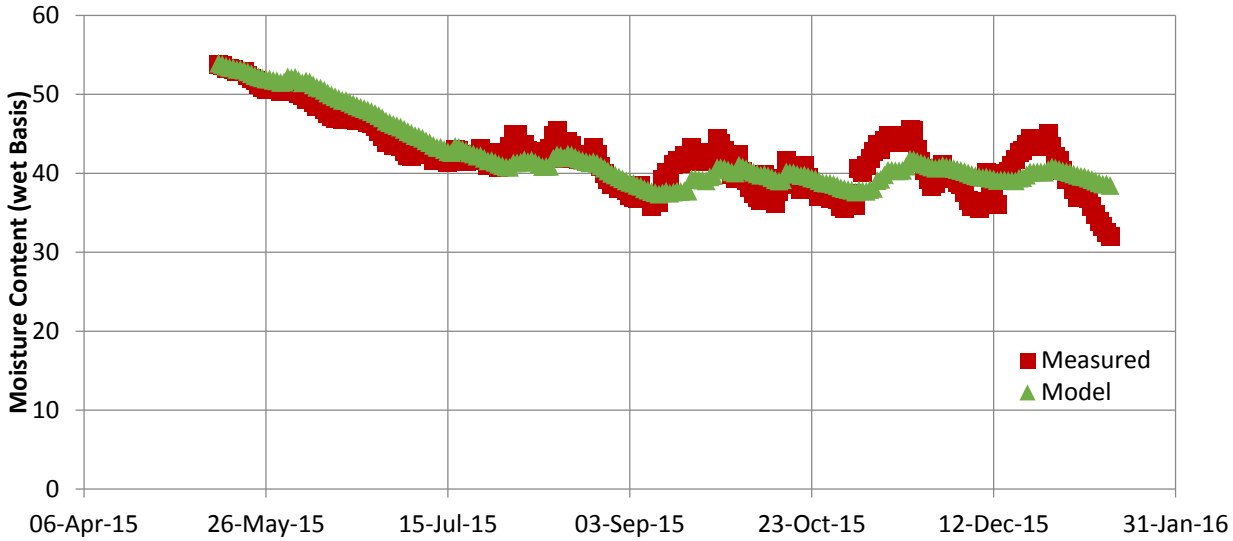

Figure C.6: Waiakea Log D moisture content: measured vs model prediction derived from Waiakea Log D

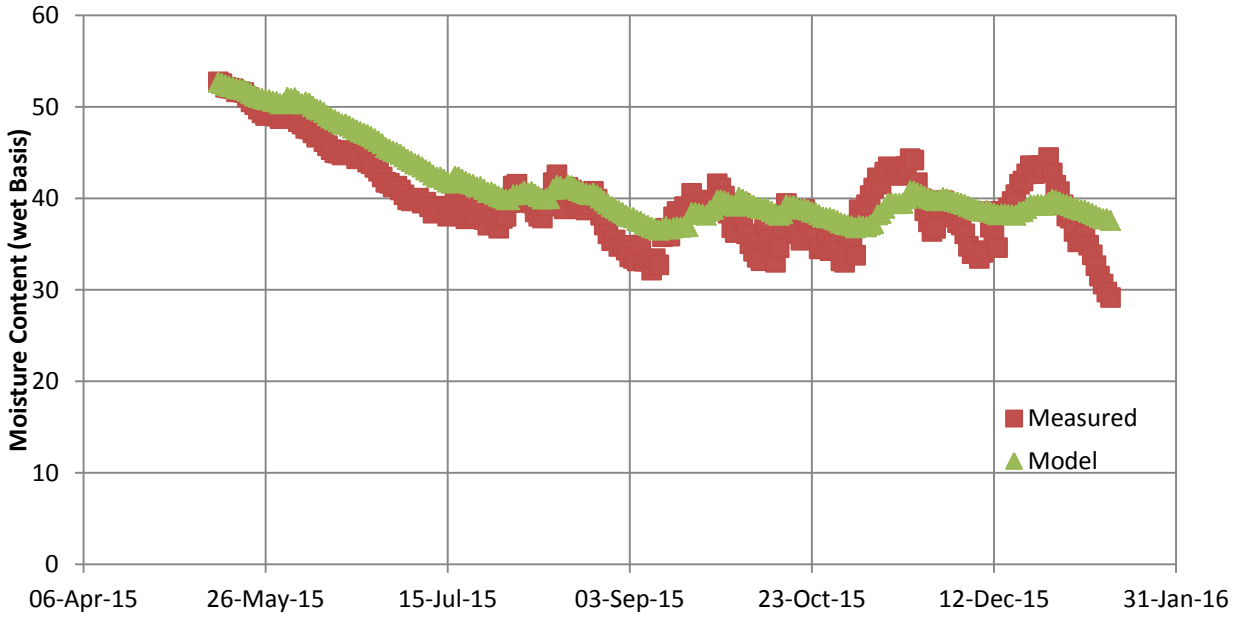

Figure C.7: Waiakea Log F moisture content: measured vs model prediction derived from Waiakea Log D

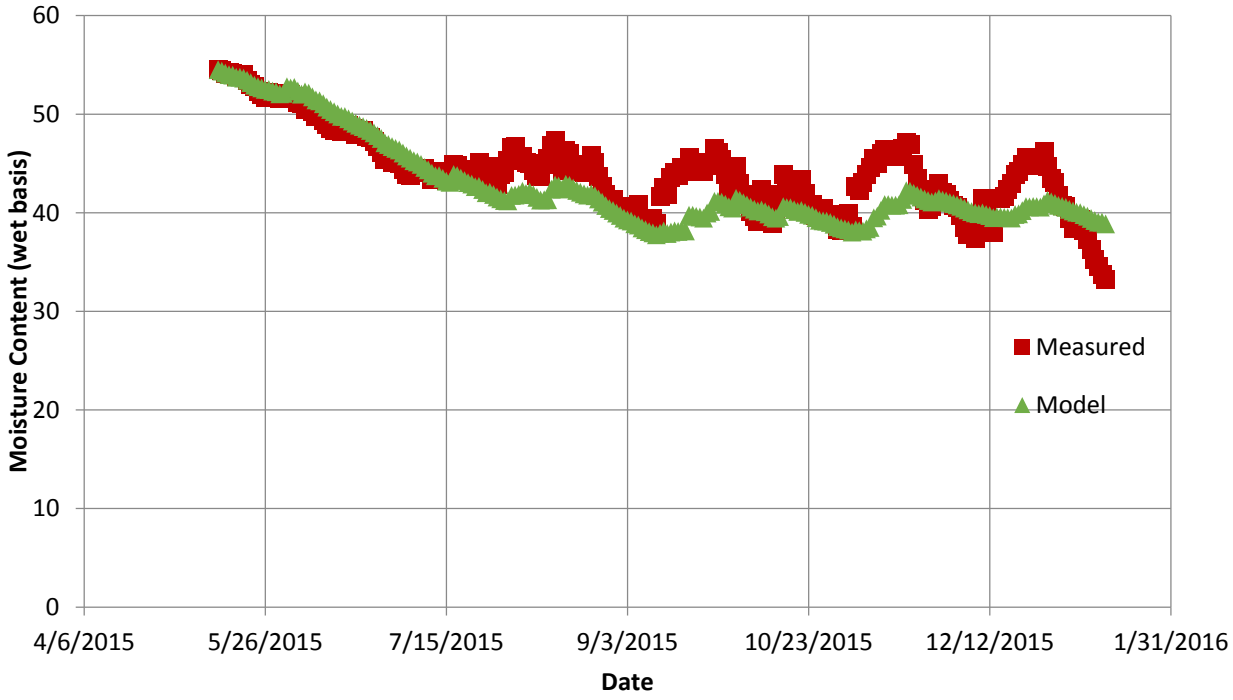

Figure C.8: Waiakea bulk moisture content: measured vs model prediction derived from Waiakea Log D

Liang Model Waiakea, Using Waiakea Log F Values

a=	0.001964
b=	0.000287
c=	0

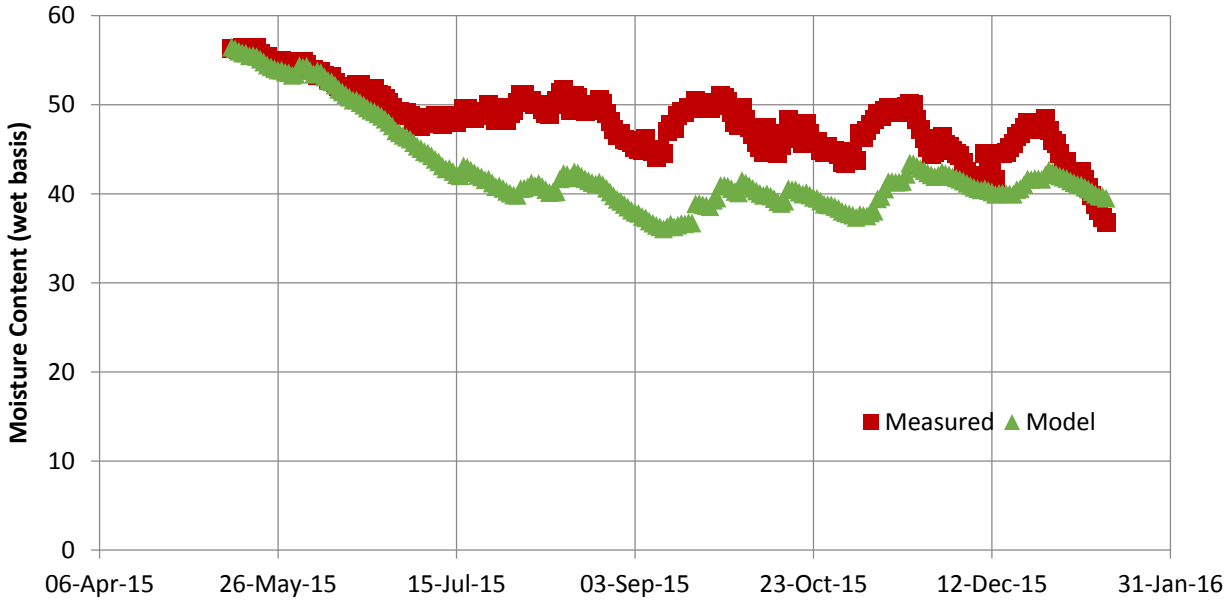

Figure C.9: Waiakea Log B moisture content: measured vs model prediction derived from Waiakea Log F

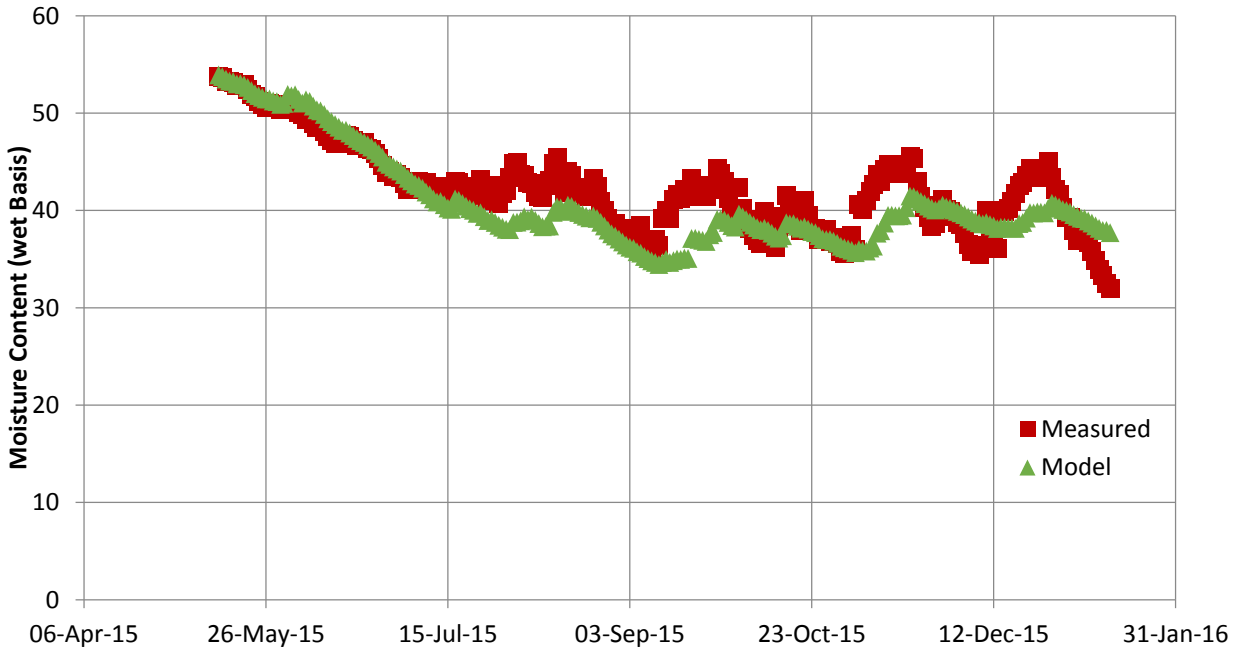

Figure C.10: Waiakea Log D moisture content: measured vs model prediction derived from Waiakea Log F

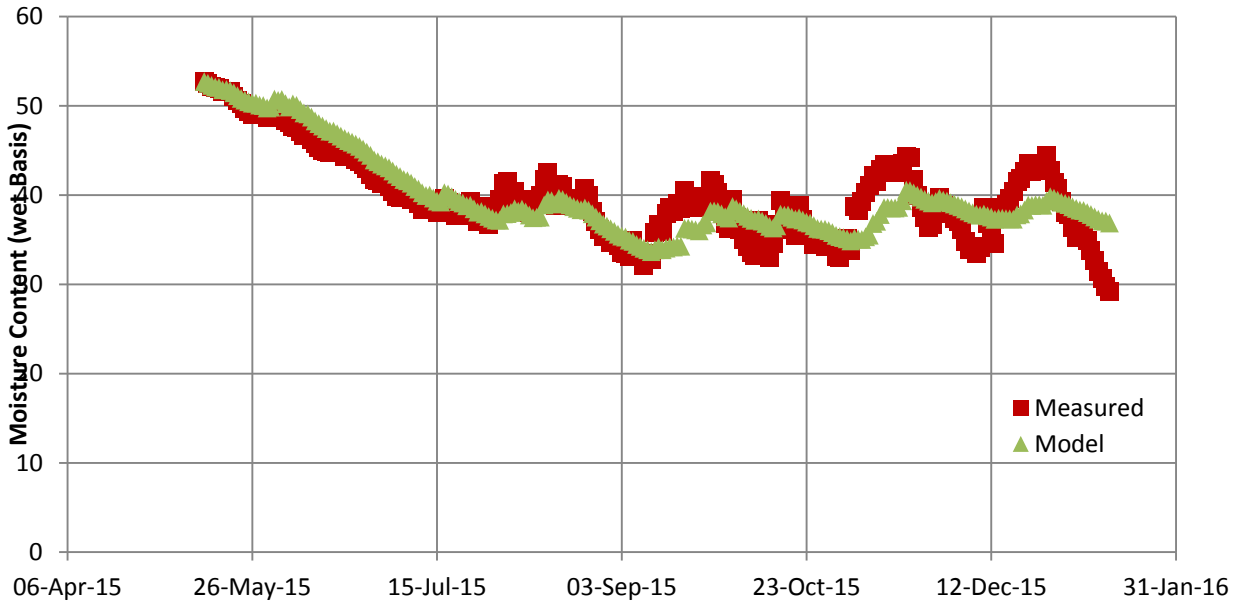

Figure C.11: Waiakea Log F moisture content: measured vs model prediction derived from Waiakea Log F

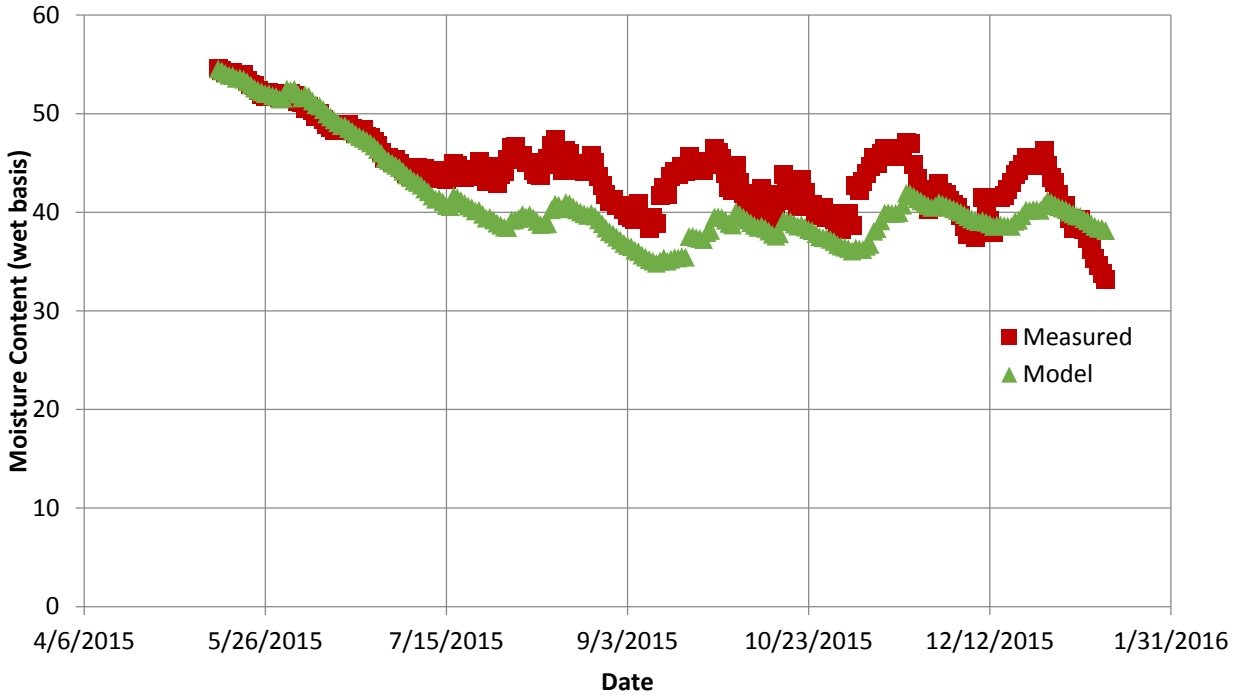

Figure C.12: Waiakea Log Bulk moisture content: measured vs model prediction derived from Waiakea Log F

Waiakea Using Bulk Values

a=	0.001221
b=	0.000158
c=	0

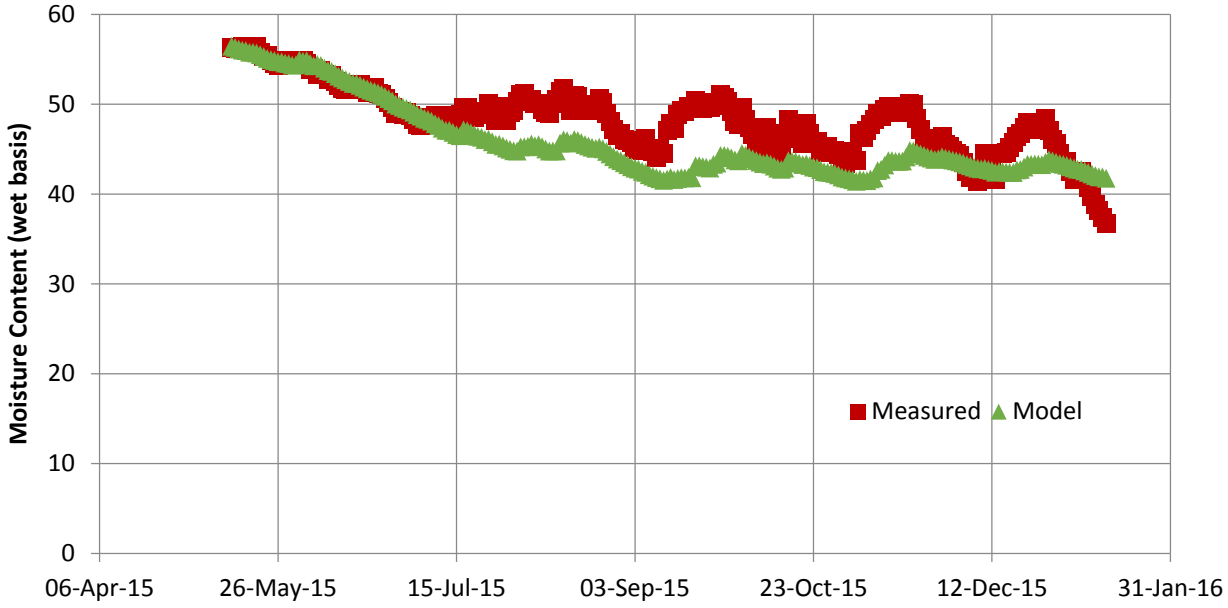

Figure C.13: Waiakea Log B moisture content: measured vs model prediction derived from Waiakea Bulk

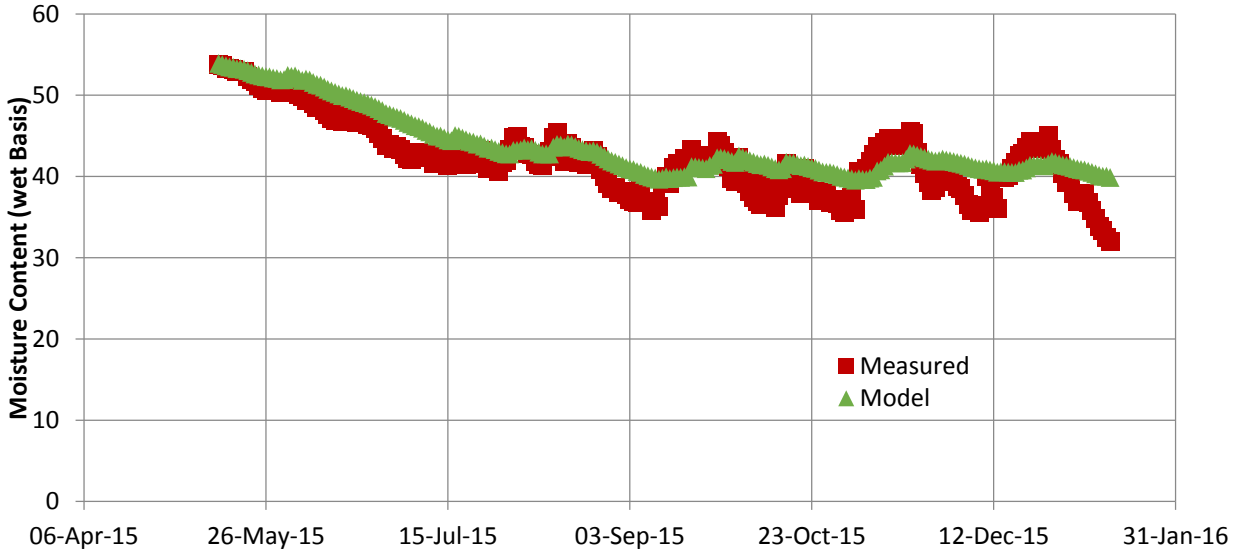

Figure C.14: Waiakea Log D moisture content: measured vs model prediction derived from Waiakea Bulk

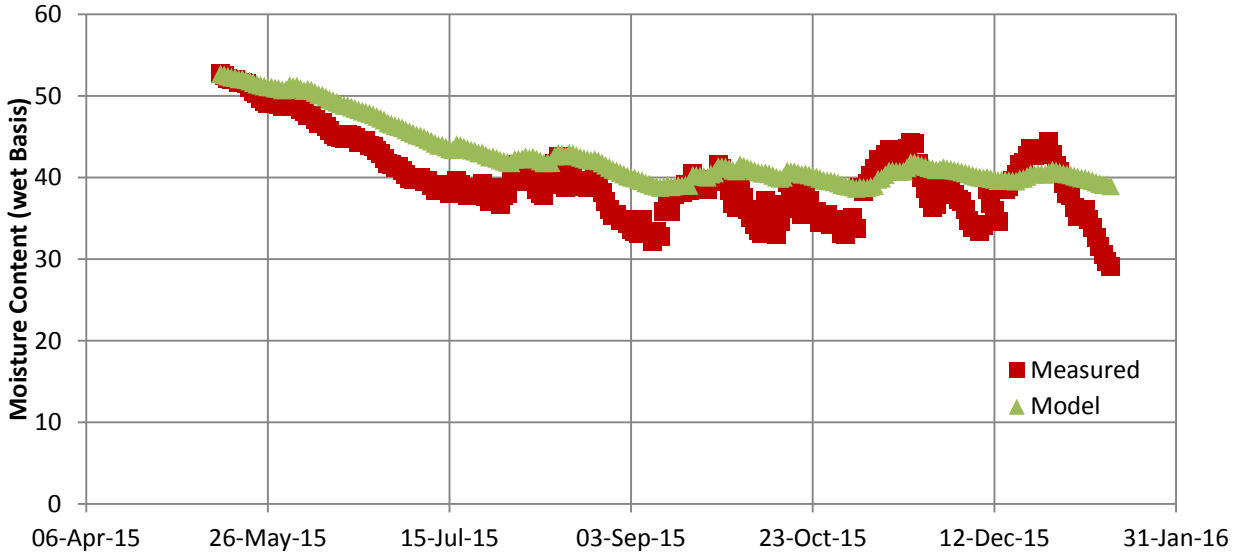

Figure C.15: Waiakea Log F moisture content: measured vs model prediction derived from Waiakea Bulk

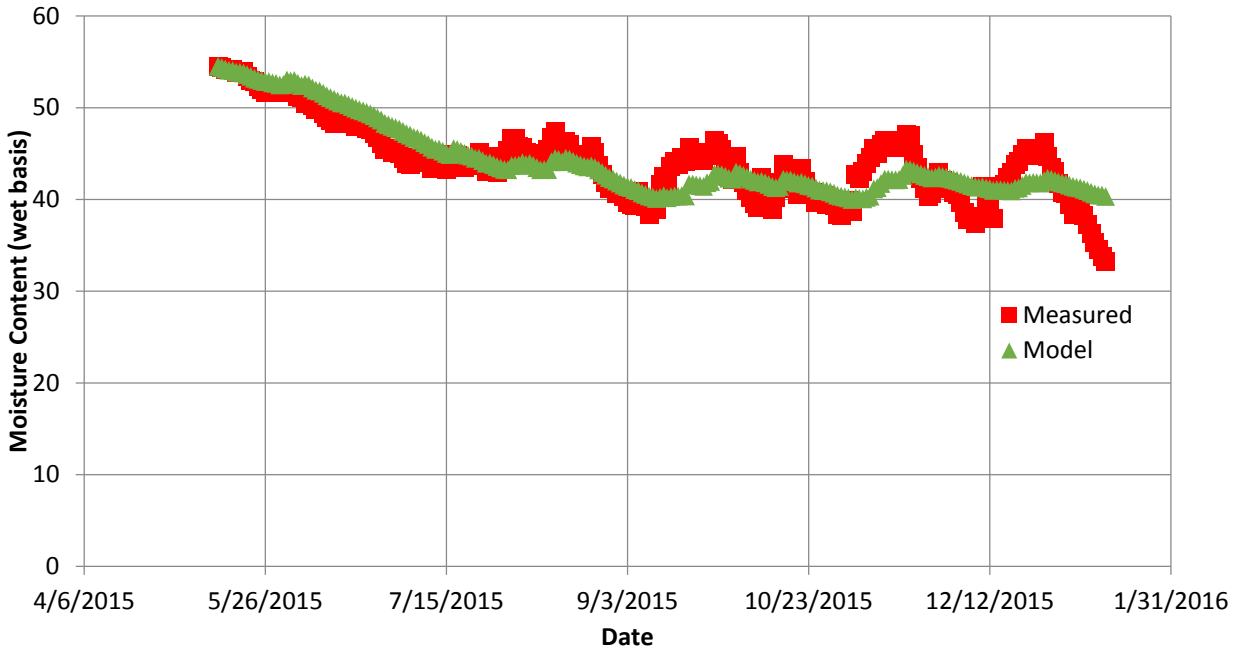

Figure C.16: Waiakea Bulk moisture content: measured vs model prediction derived from Waiakea Bulk

Lalamilo Using Log B Values

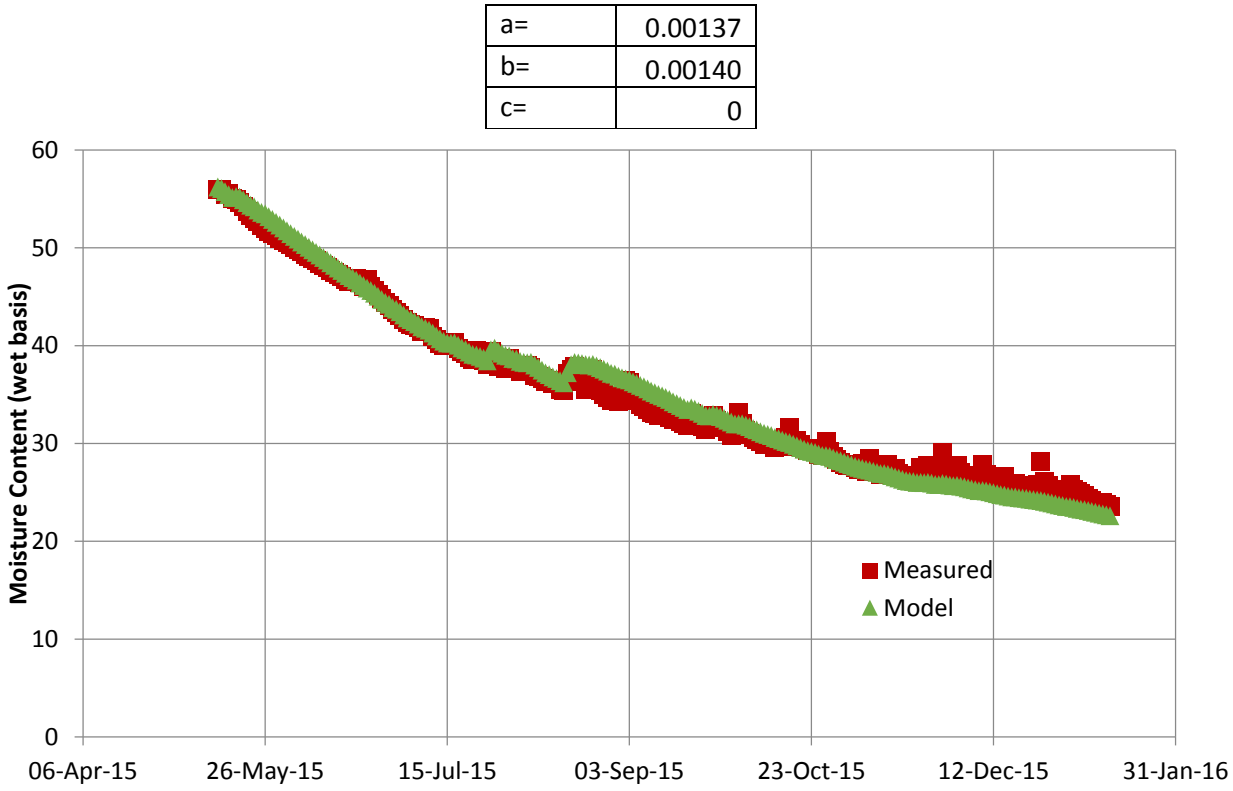

Figure C.17: Lalamilo Log B moisture content: measured vs model prediction derived from Lalamilo Log B

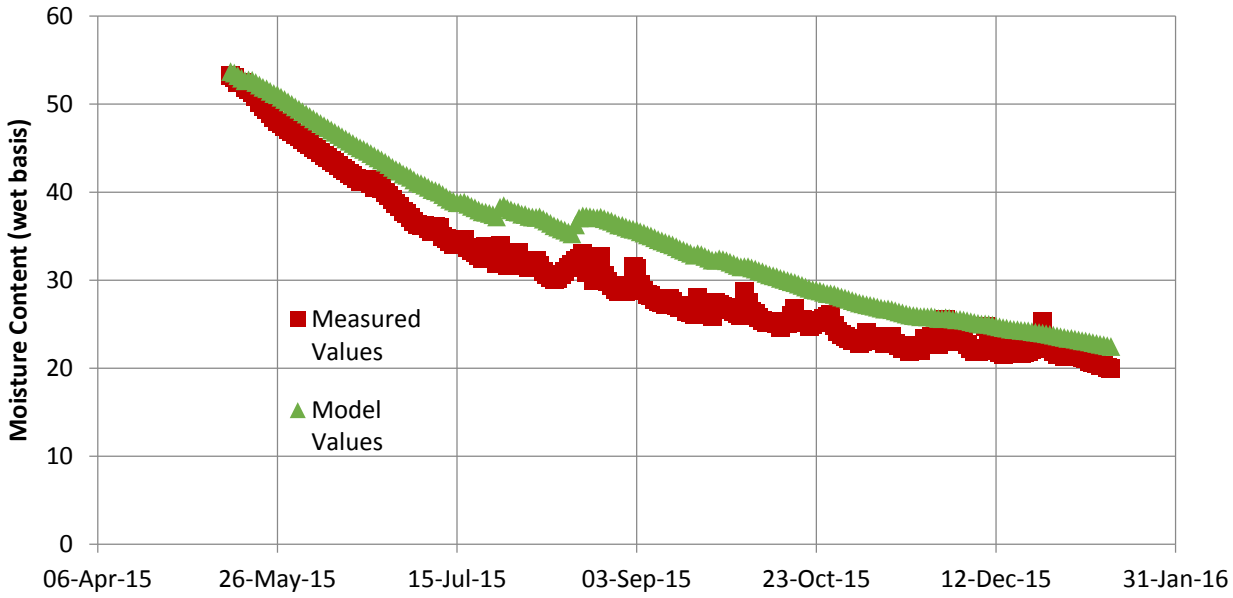

Figure C.18: Lalamilo Log D moisture content: measured vs model prediction derived from Lalamilo Log B

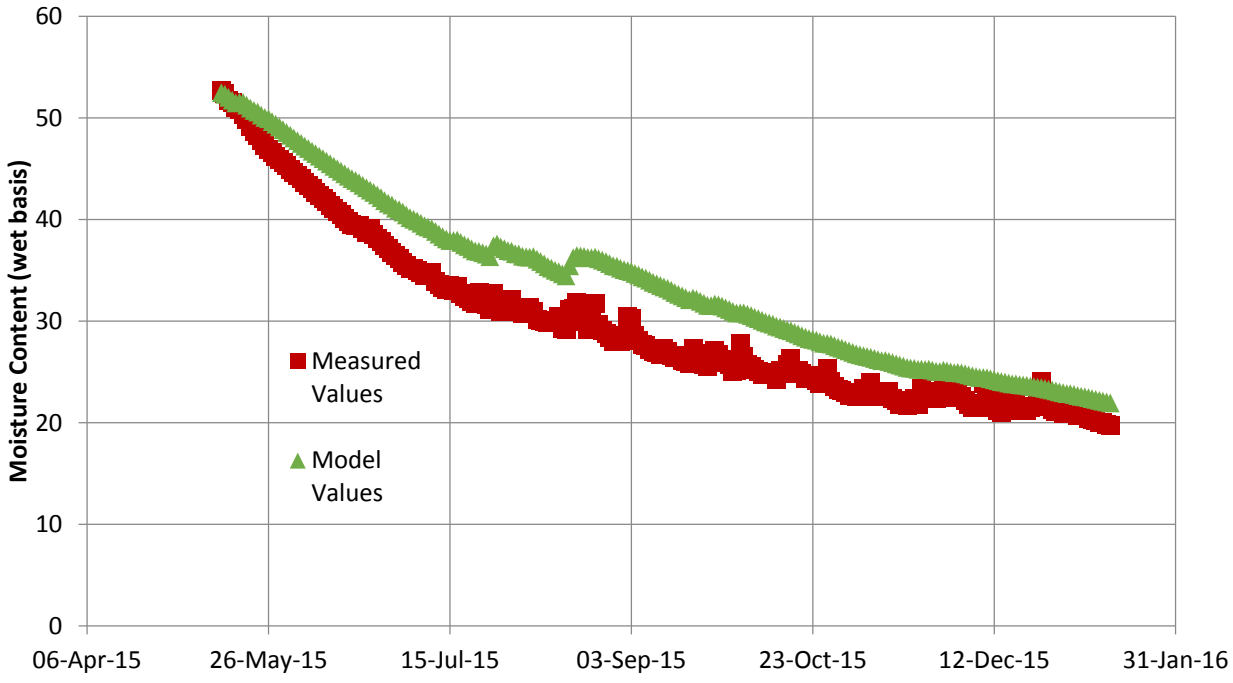

Figure C.19: Lalamilo Log F moisture content: measured vs model prediction derived from Lalamilo Log B

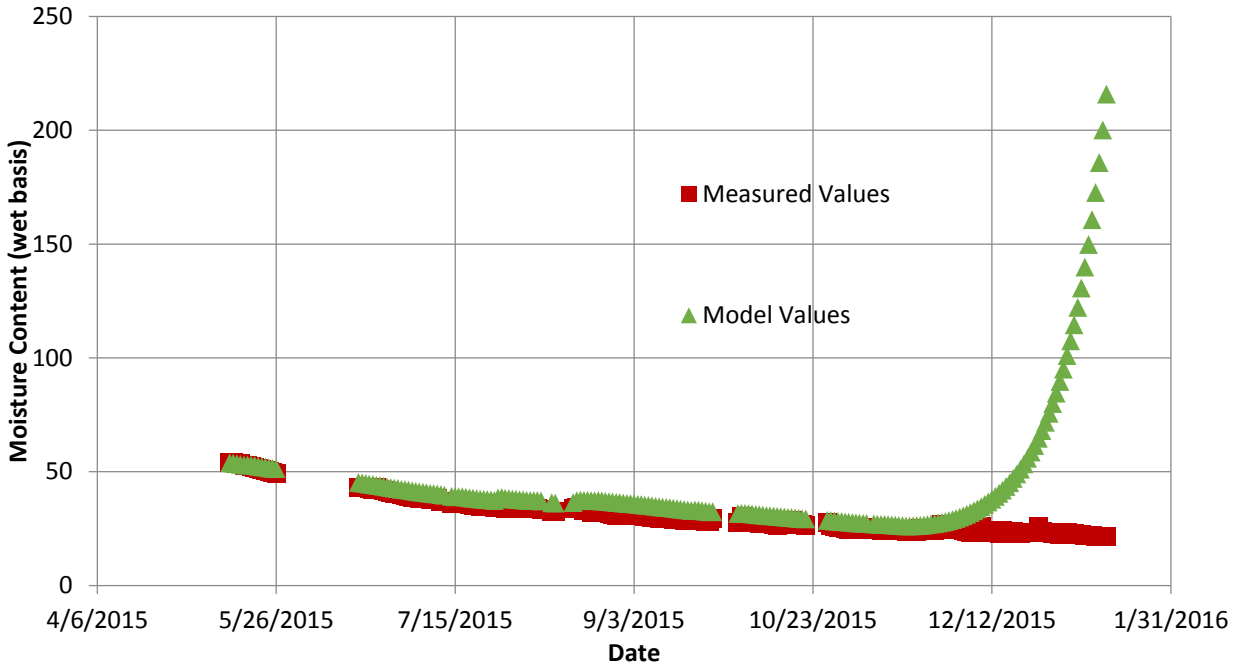

Figure C.20: Lalamilo Bulk moisture content: measured vs model prediction derived from Lalamilo Log B

Lalamilo Using Log D Values

a=	0.00191
b=	0.00235
c=	0

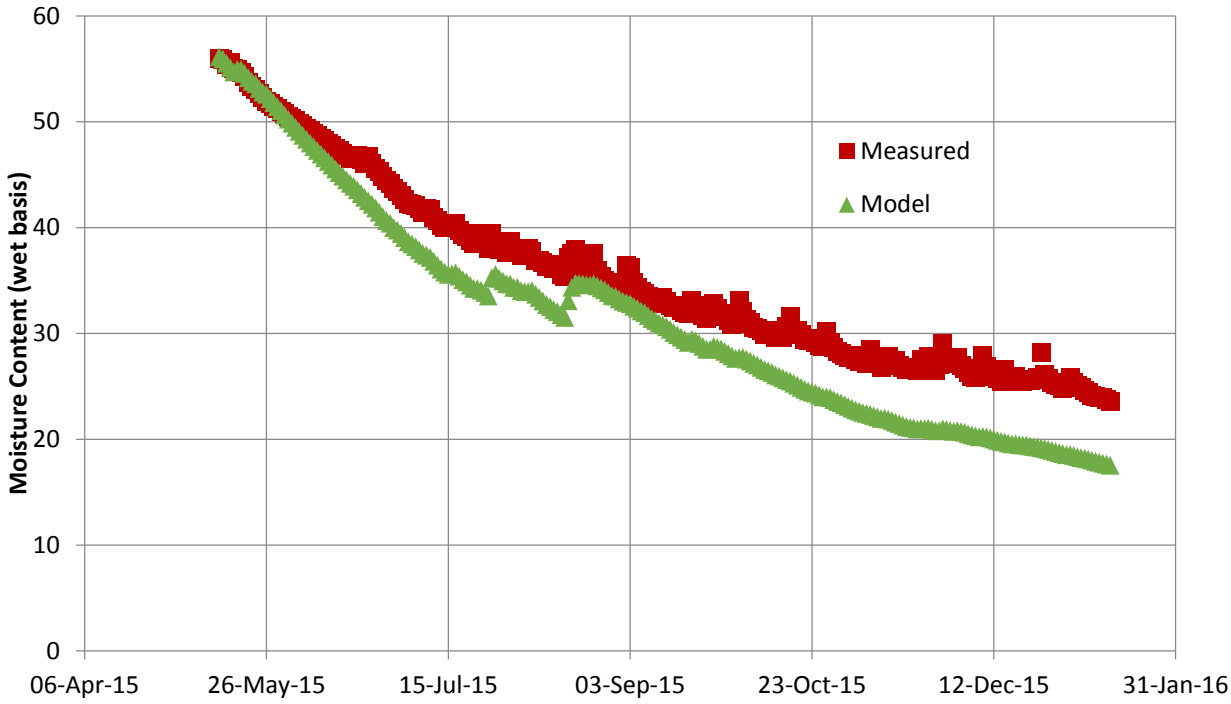

Figure C.21: Lalamilo Log B moisture content: measured vs model prediction derived from Lalamilo Log D

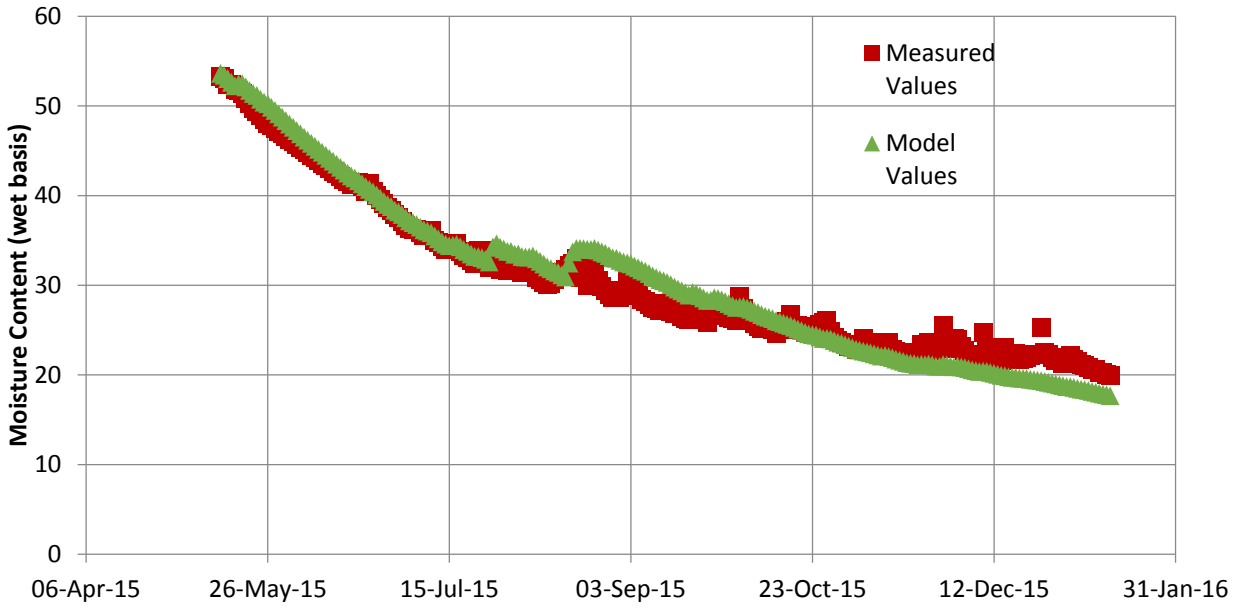

Figure C.22: Lalamilo Log D moisture content: measured vs model prediction derived from Lalamilo Log D

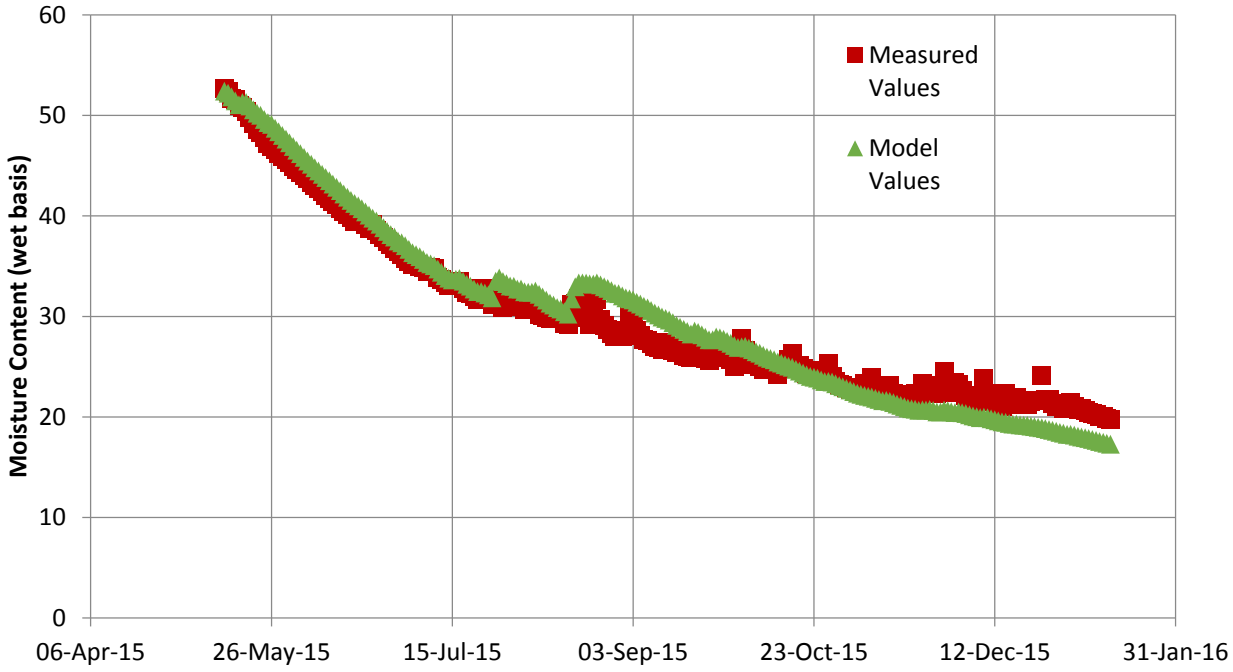

Figure C.24: Lalamilo Log F moisture content: measured vs model prediction derived from Lalamilo Log D

Lalamilo Using Log F Values

a=	0.00198
b=	0.00259
c=	0

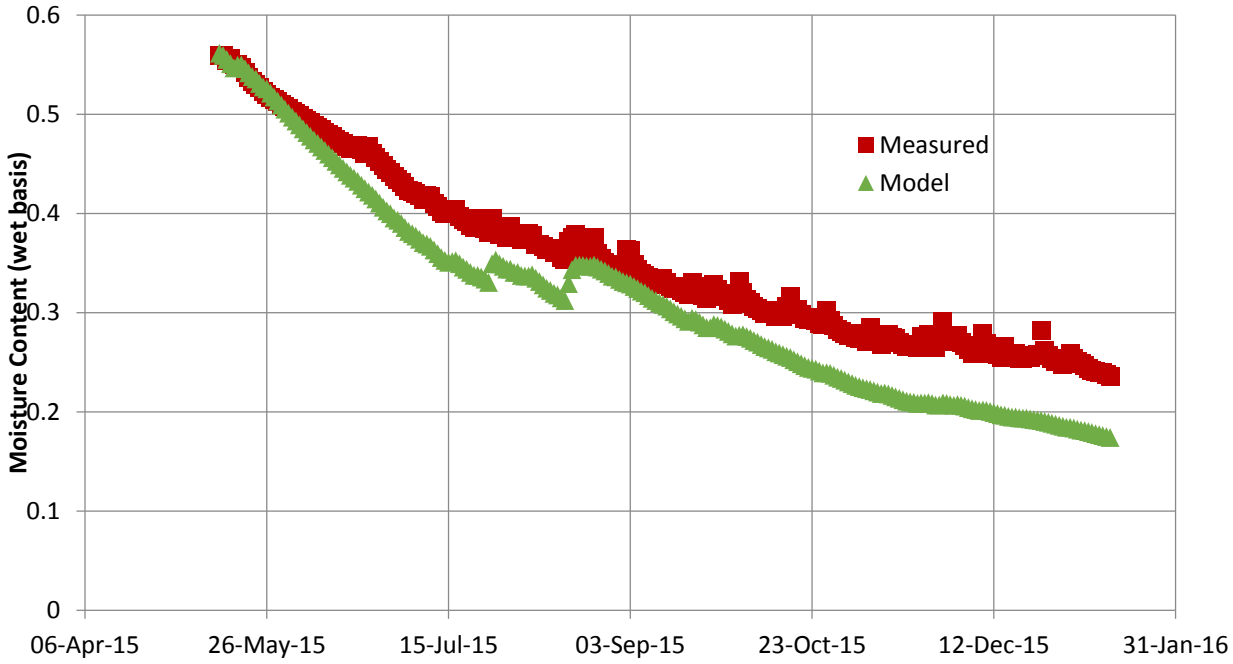

Figure C.25: Lalamilo Log B moisture content: measured vs model prediction derived from Lalamilo Log F

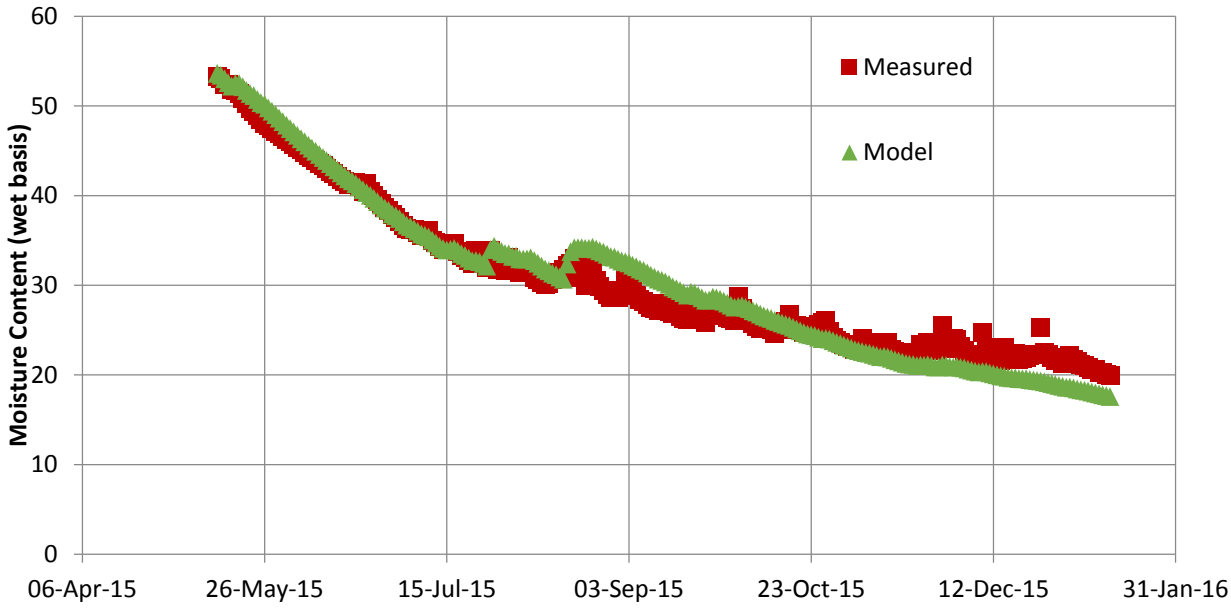

Figure C.26: Lalamilo Log D moisture content: measured vs model prediction derived from Lalamilo Log F

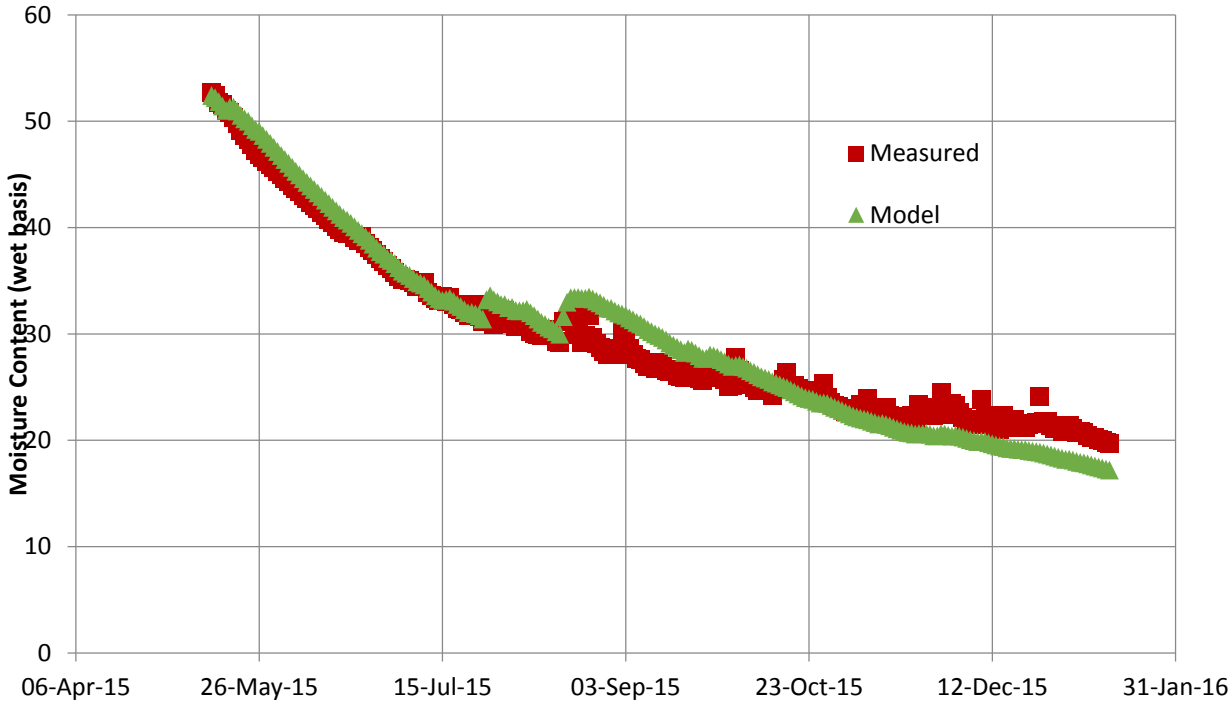

Figure C.27: Lalamilo Log F moisture content: measured vs model prediction derived from Lalamilo Log F

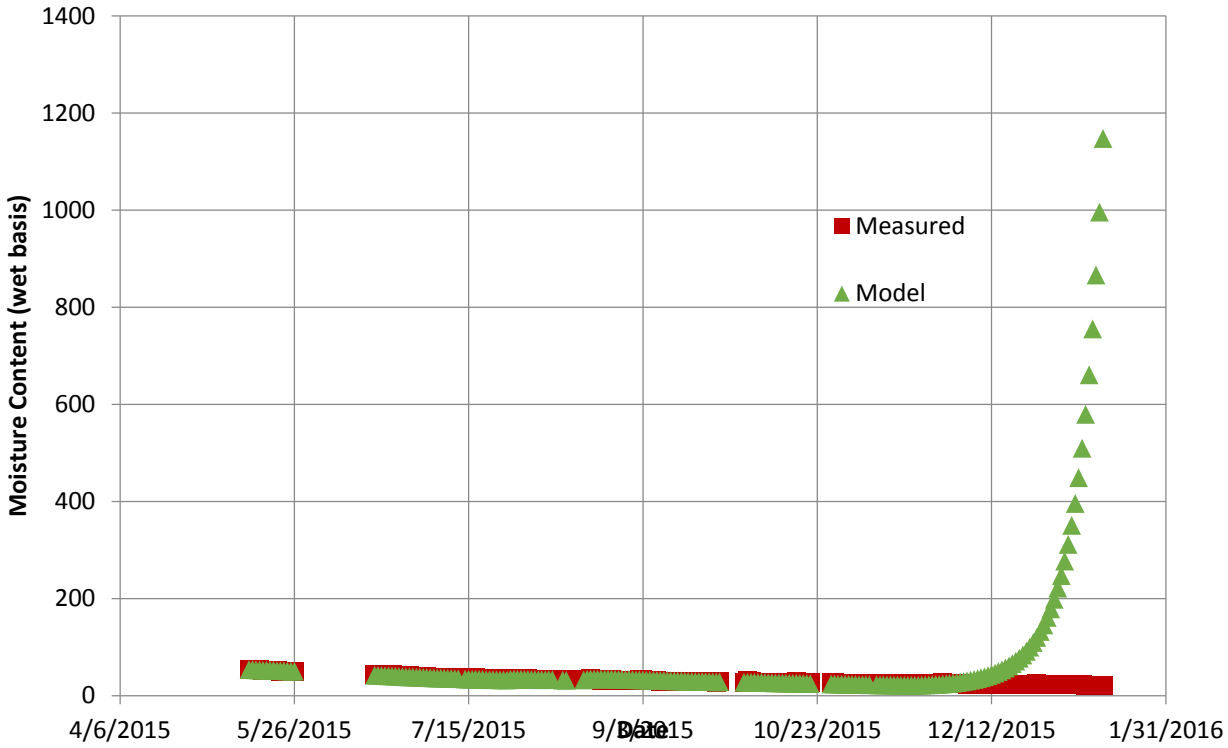

Figure C.28: Lalamilo Bulk moisture content: measured vs model prediction derived from Lalamilo Log F

Lalamilo Using Bulk Values

a=	0.00122
b=	0.0018
c=	0

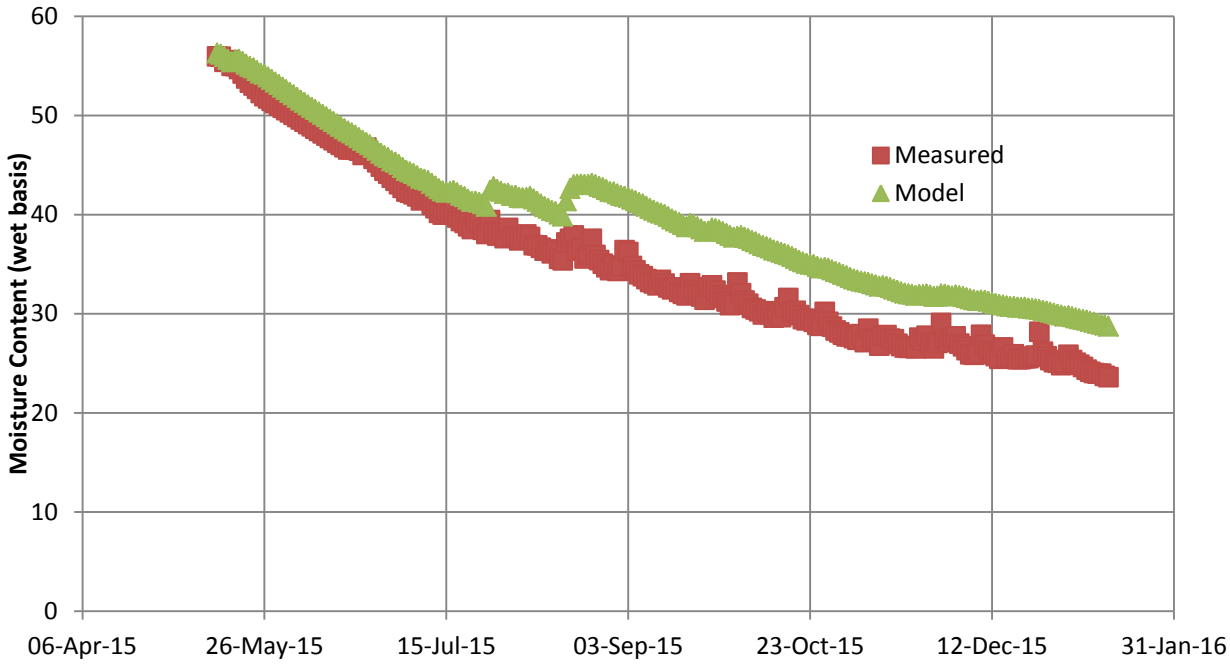

Figure C.29: Lalamilo Log B moisture content: measured vs model prediction derived from Lalamilo Bulk

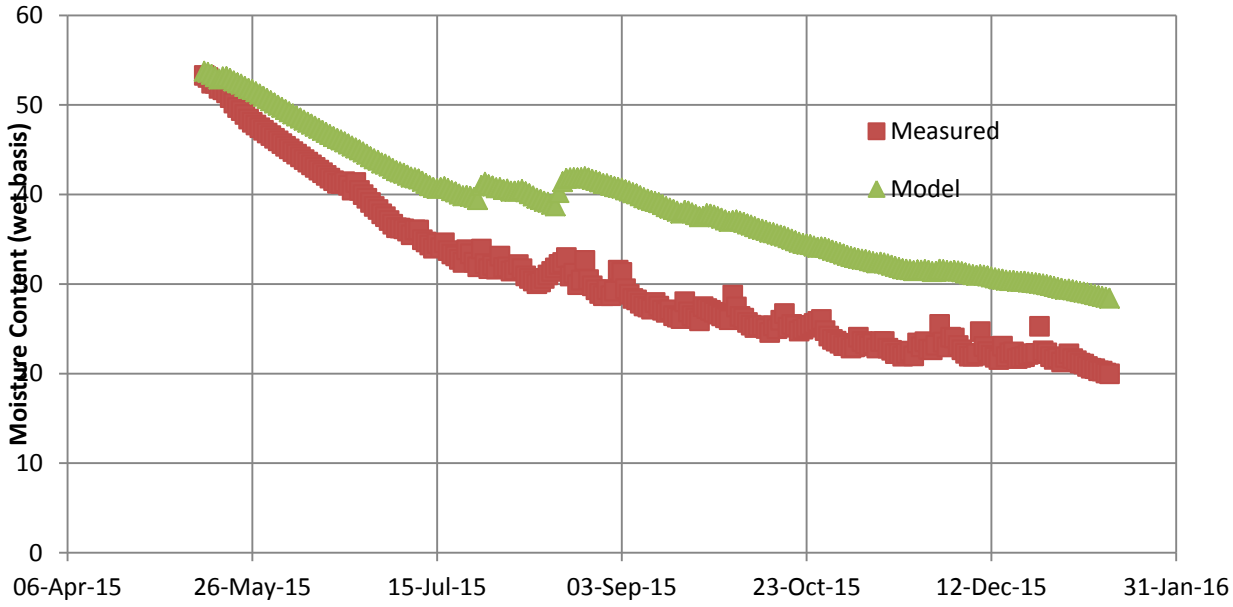

Figure C.30: Lalamilo Log D moisture content: measured vs model prediction derived from Lalamilo Bulk

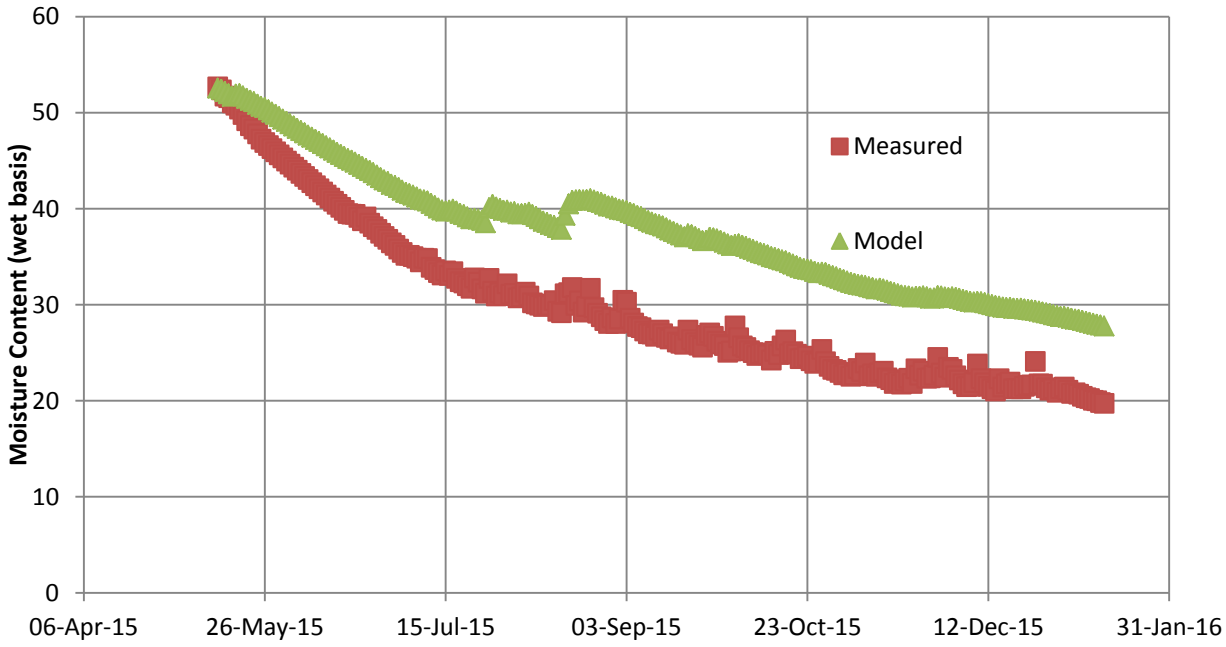

Figure C.31: Lalamilo Log F moisture content: measured vs model prediction derived from Lalamilo Bulk

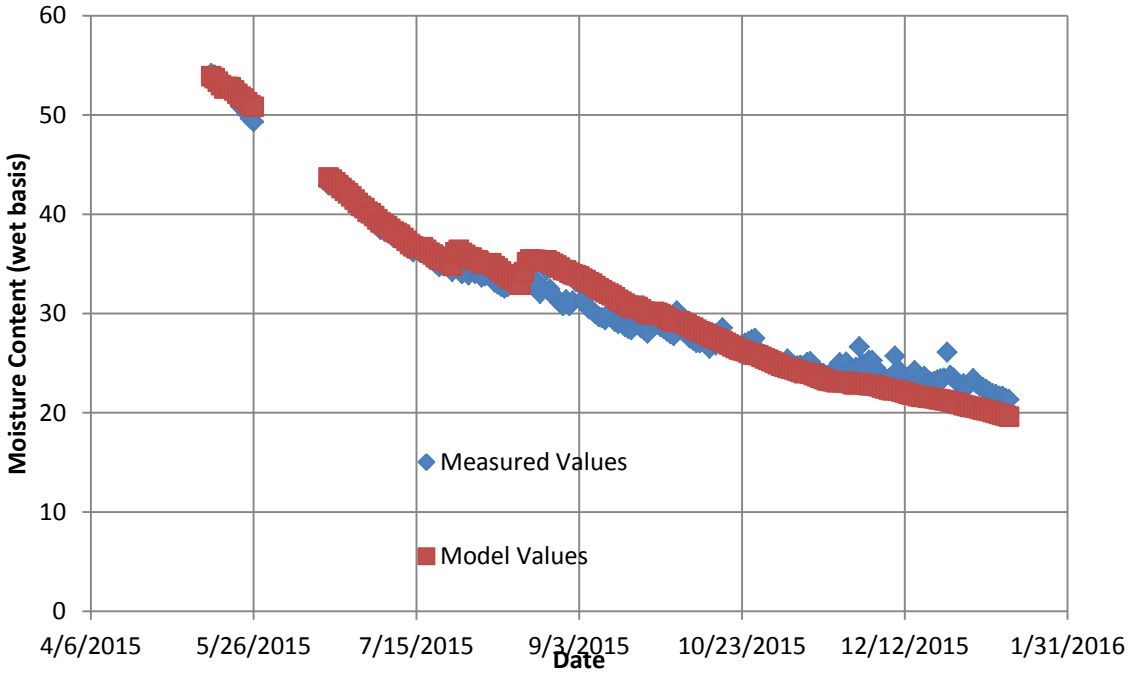

Figure C.32: Lalamilo Bulk moisture content: measured vs model prediction derived from Lalamilo Bulk

Using a, b, values from Different locations

Waiakea Log B using a,b,c from Lalamilo

a=	0.001375
b=	0.0014
c=	0

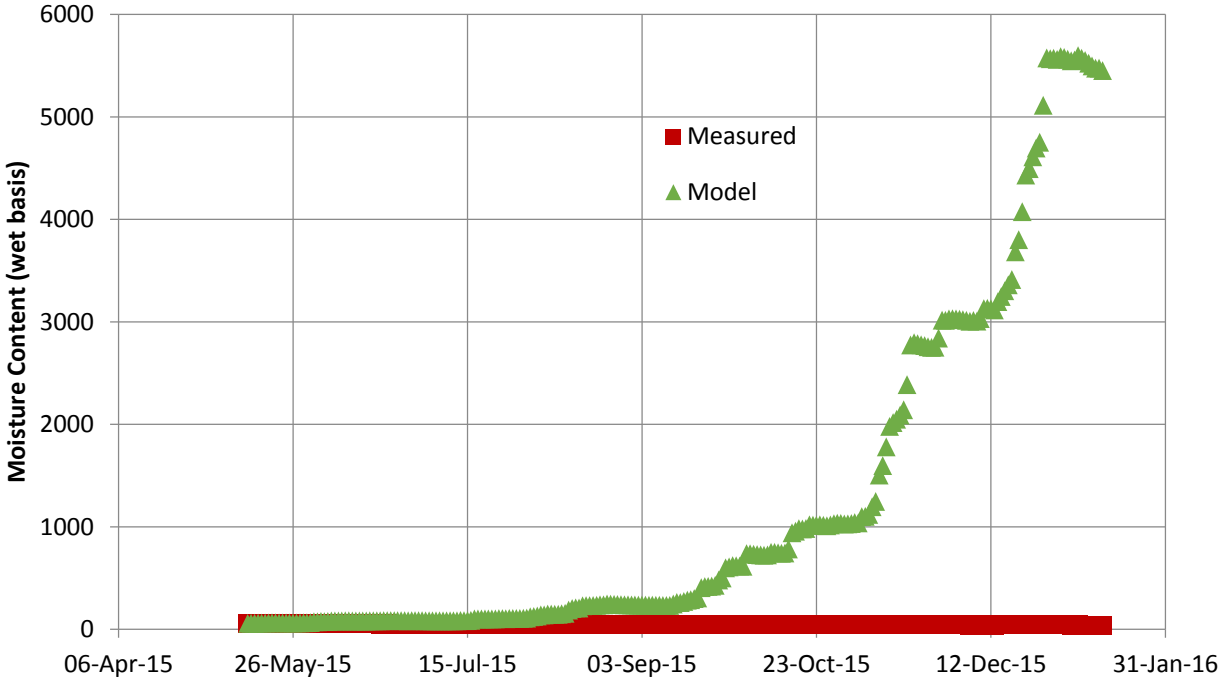

Figure C.33: Waiakea Log B moisture content: measured vs model prediction derived from Lalamilo Log B

Waiakea Log D using a,b,c from Lalamilo

a=	0.001909
b=	0.002351
c=	0

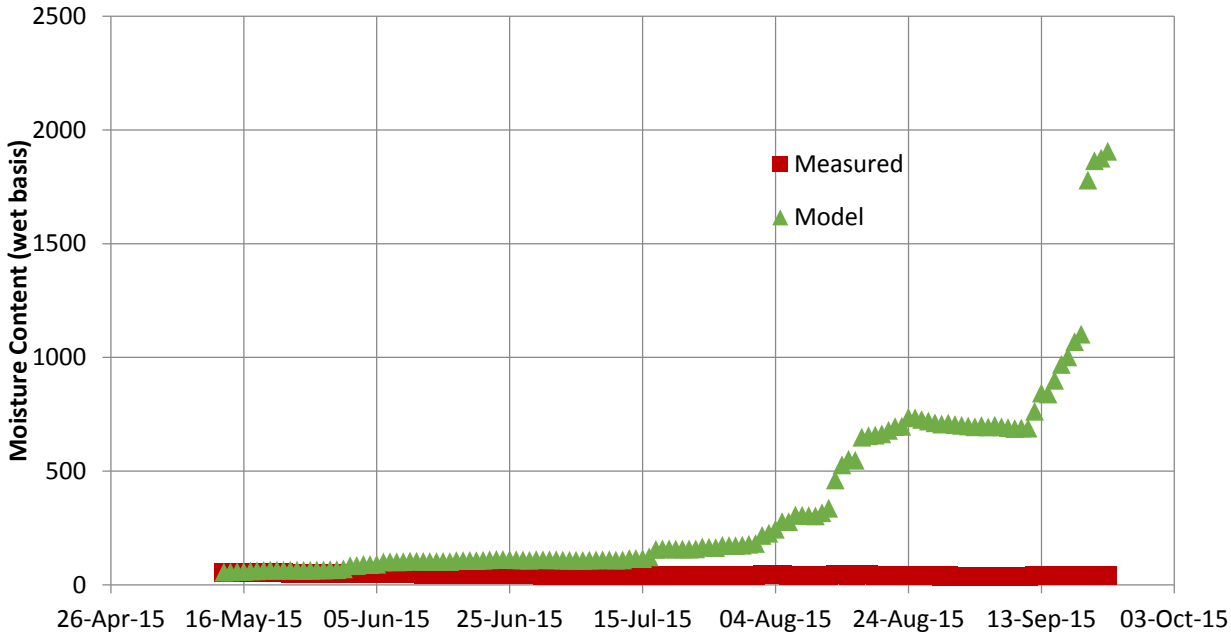

Figure C.34: Waiakea Log D moisture content: measured vs model prediction derived from Lalamilo Log D data

Waiakea Log F using a,b,c from Lalamilo

a=	0.00198
b=	0.002586
c=	0

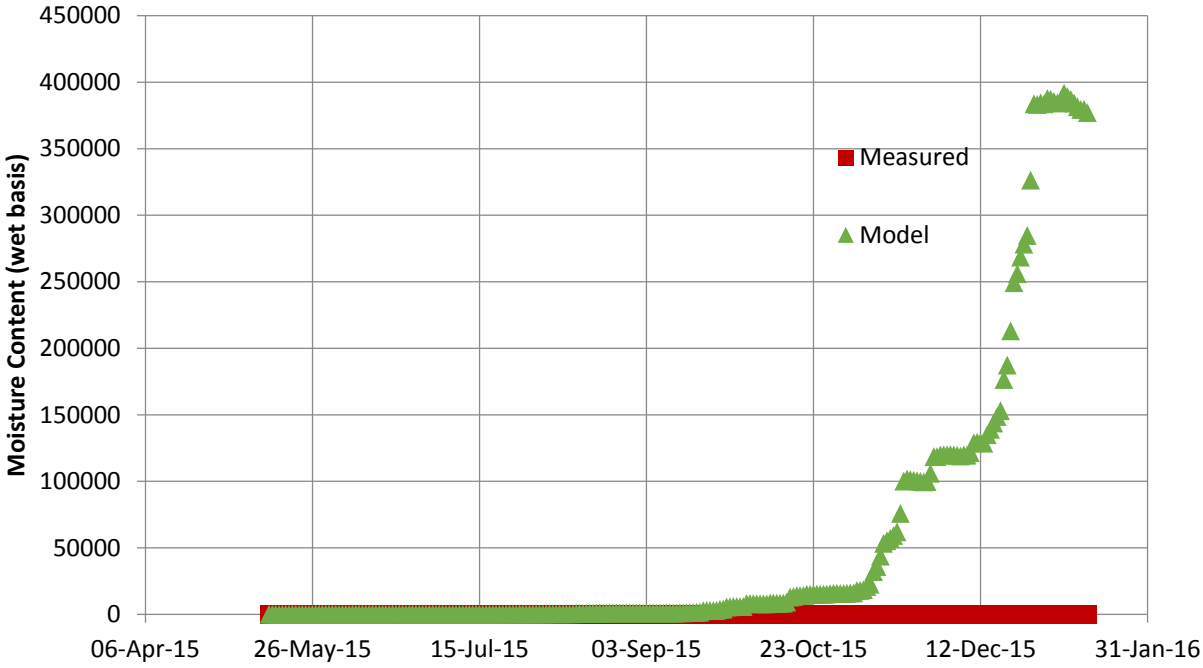

Figure C.35: Waiakea Log F moisture content: measured vs model prediction derived from Lalamilo Log F data

Waiakea Bulk using a,b,c from Lalamilo Bulk

a=	0.00122
b=	0.000153
c=	0

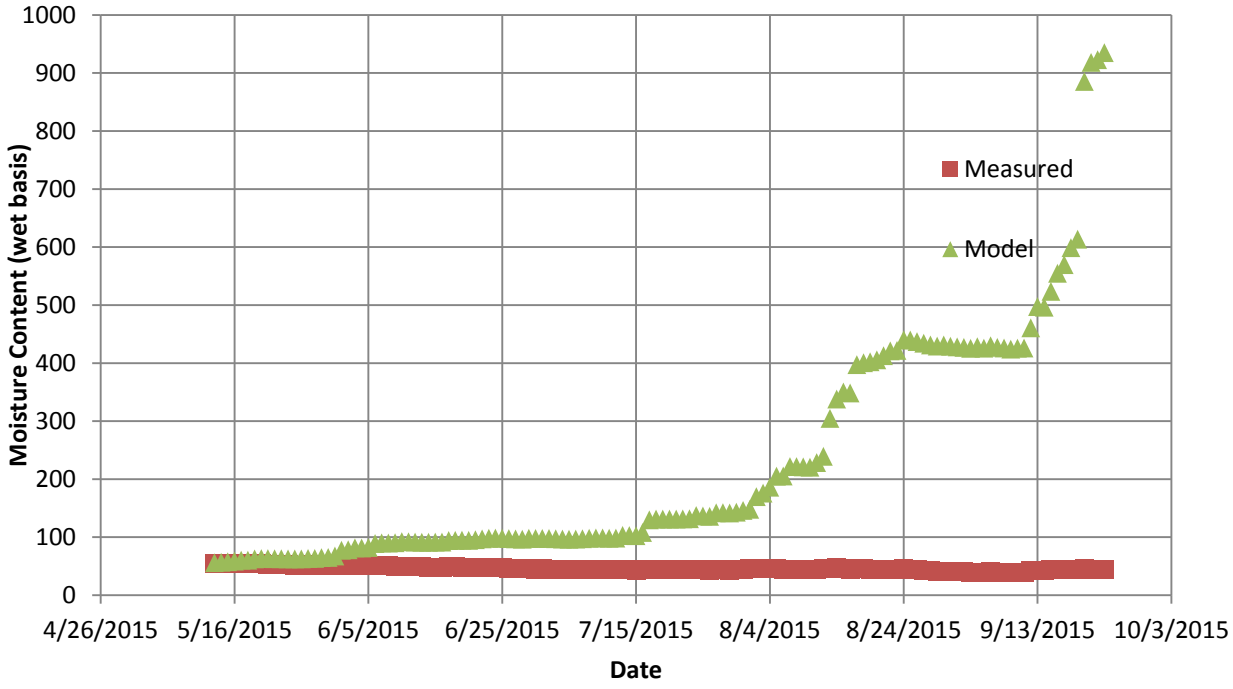

Figure C.36: Waiakea Bulk moisture content: measured vs model prediction derived from Lalamilo Bulk data.

Lalamilo Log B using Values from Waiakea

a=	0.000702
b=	7.198-05
c=	0

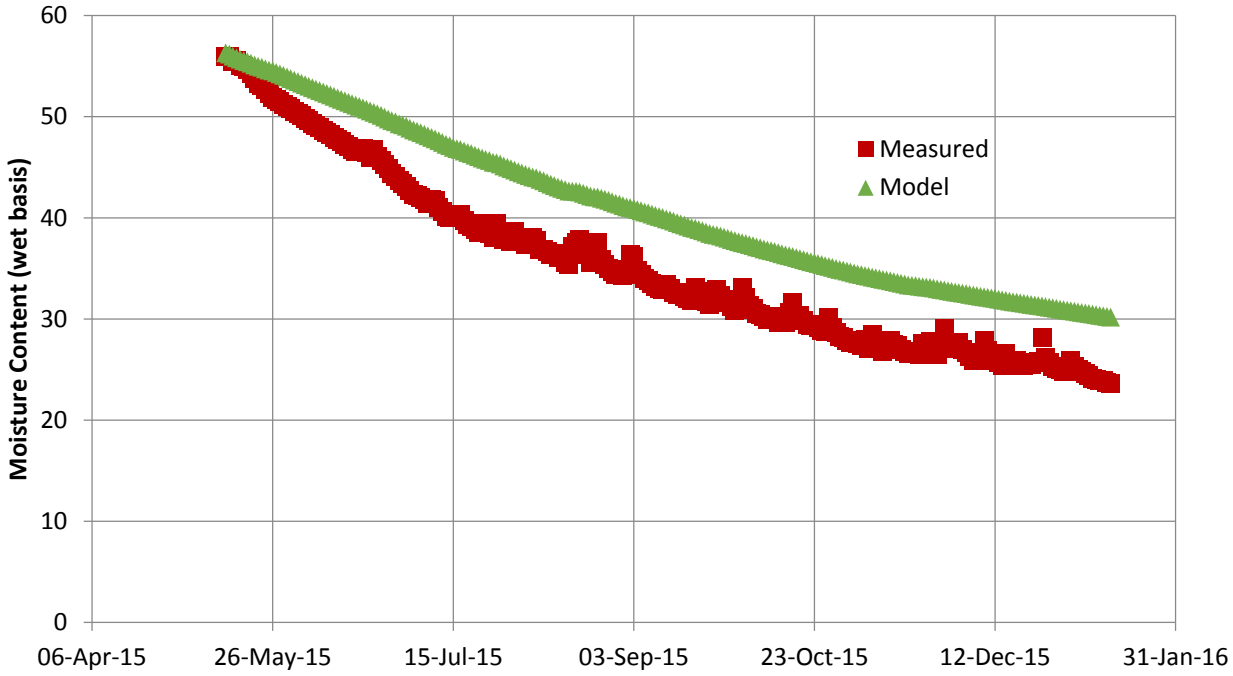

Figure C.37: Lalamilo Log B moisture content: measured vs model prediction derived from Waiakea Log B

Lalamilo Log D using Waiakea

a=	0.00151
b=	0.000204
c=	0

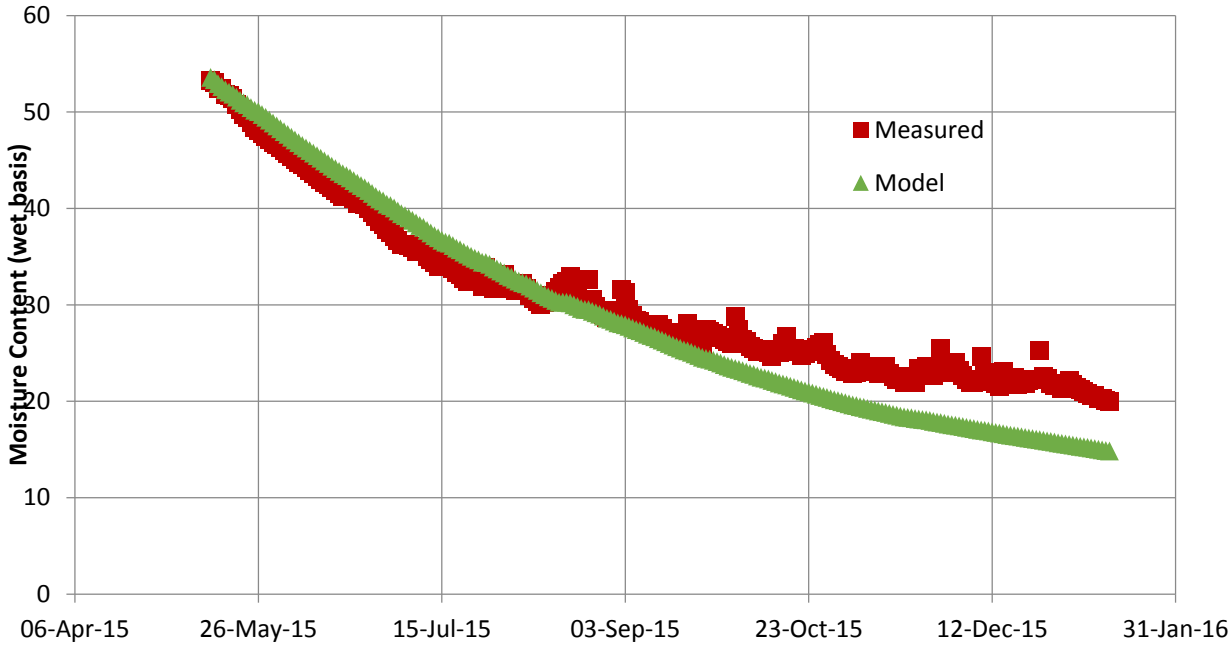

Figure C.38: Lalamilo Log D moisture content: measured vs model prediction derived from Waiakea Log D data

Lalamilo Log F using values from Waiakea

a=	0.00196
b=	0.000287
c=	0

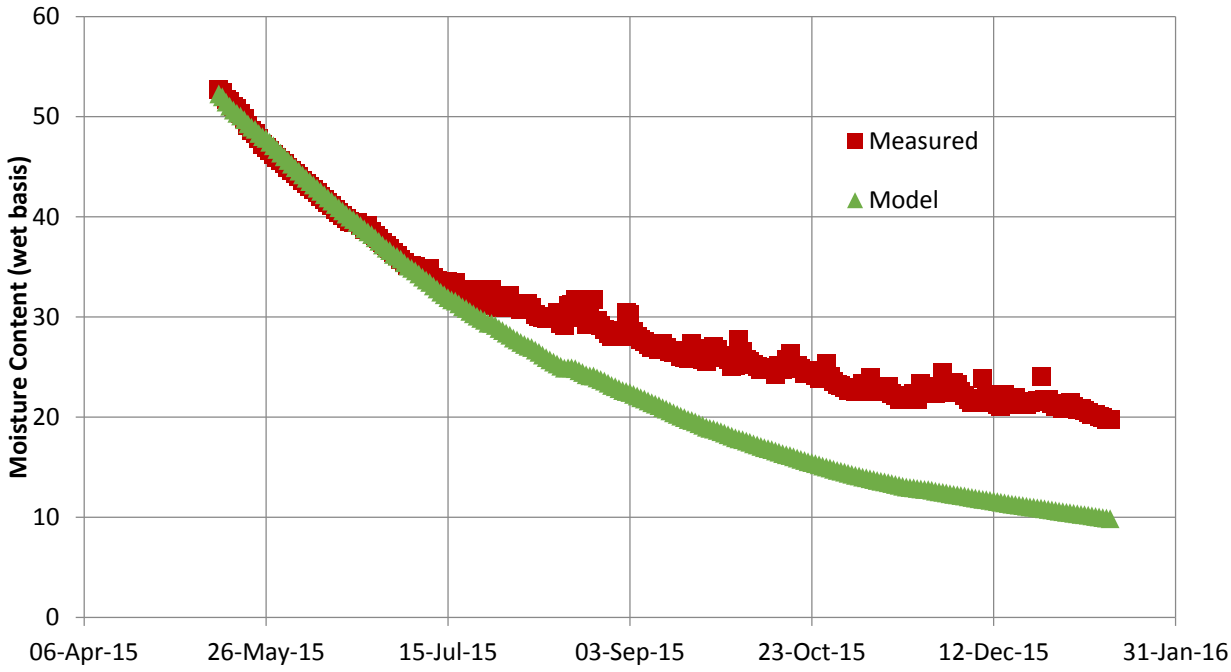

Figure C.39: Lalamilo Log F moisture content: measured vs model prediction derived from Waiakea Log F

Lalamilo Log F using values from Waiakea

a=	0.00122
b=	0.000158
c=	0

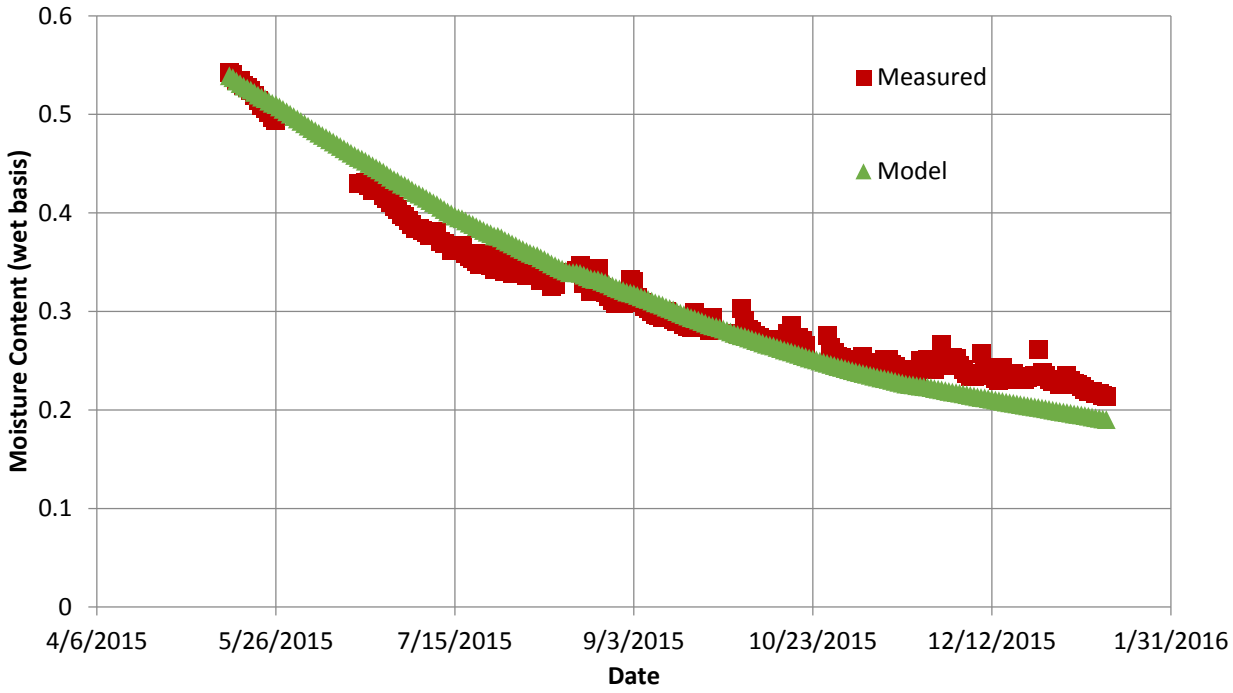

Figure C.40: Lalamilo Bulk moisture content: measured vs model prediction derived from Waiakea Bulk data